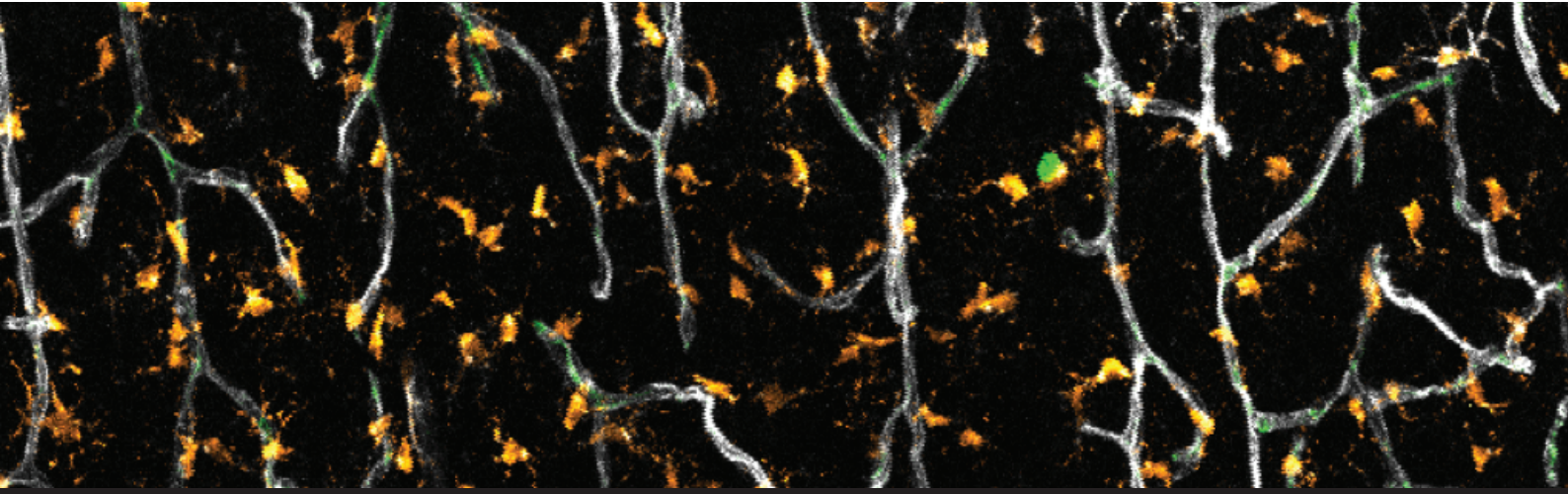

# The CD95/CD95L signaling system in developmental and tumor angiogenesis of the central nervous system

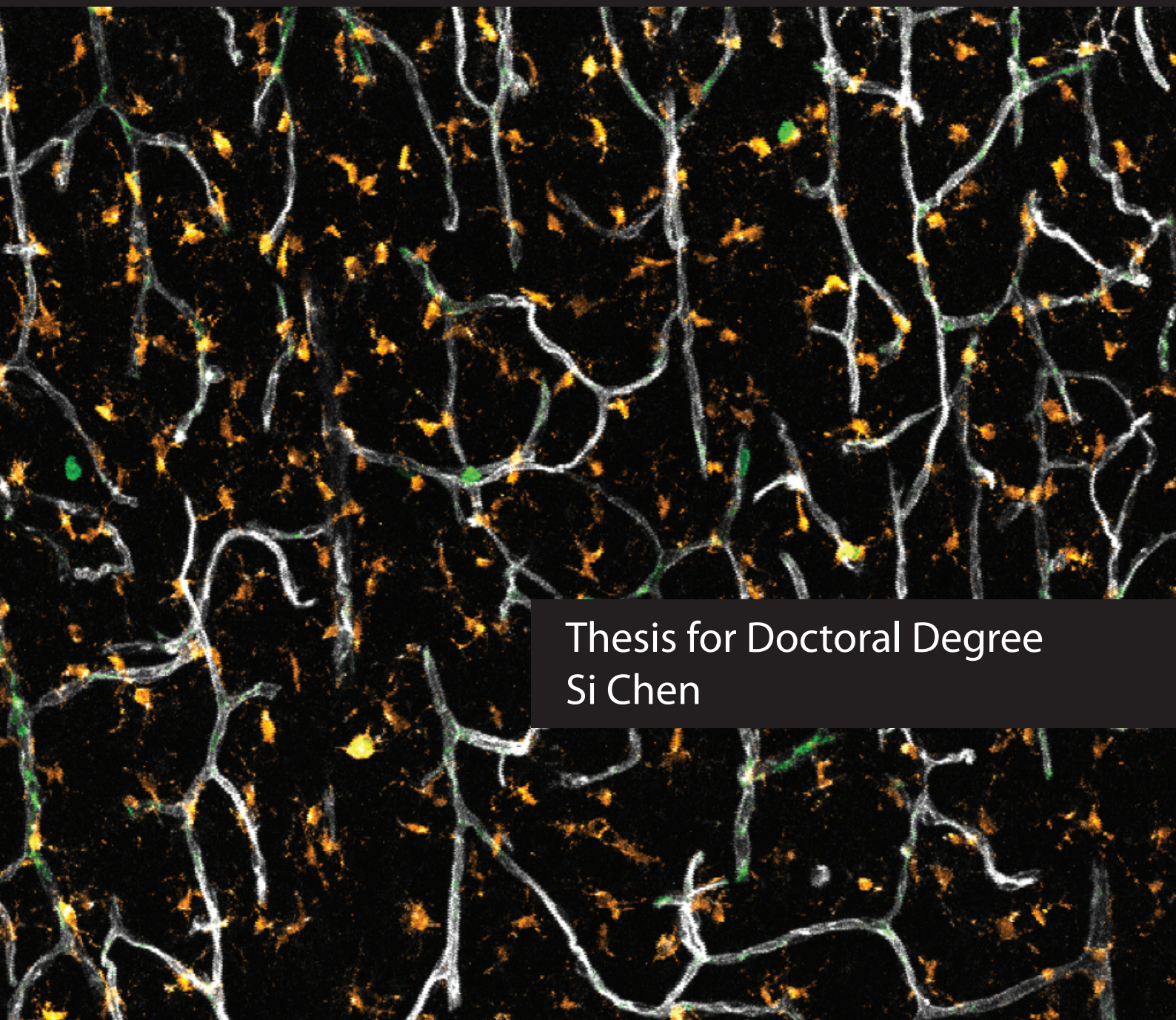

Thesis for Doctoral Degree

Si Chen

Dissertation
submitted to the
Combined Faculties for the Natural Sciences and for Mathematics
of the Ruperto-Carola University of Heidelberg, Germany
for the degree of
Doctor of Natural Sciences

presented by
Master of Science
**Si Chen**
Born in Shanghai, China
Oral examination: 16.02.2017

# The CD95/CD95L signaling system in developmental and tumor angiogenesis of the central nervous system

Referees:

Prof. Dr. Ana Martin-Villalba

Dr. Carmen Ruiz de Almodóvar

## Summary

During central nervous system (CNS) development, extensive reciprocal interactions exist between different cell types, including neural progenitors, neurons, endothelial cells, microglia and other glial cells that are crucial in driving proper development. Moreover, neurons and vessels share striking anatomical and molecular features and are presumably orchestrated by an overlapping repertoire of signaling systems.

Here, we identify an important neuron/vessel/glia-interaction essential for the correct formation of the neurovascular system in the CNS that involves the CD95 receptor and ligand system. Deletion of CD95 receptor in neurons, as shown before, and in endothelial cells result in aberrant branching and growth of both cell types in the postnatal CNS. Furthermore, we identify microglia as the main source of CD95L and microglial-specific deletion thereof impairs proper neurovascular development. CD95 promotes endothelial cell branching and proliferation by acting as a receptor tyrosine kinase that upon activation leads to recruitment of SFK and p85 which further elicit Akt and Erk signaling, two effectors that are crucial in regulating endothelial cell growth. These data highlight a coordinated neurovascular development instructed by microglial-derived CD95L and impact the importance of microglia for the establishment of the neurovascular network during CNS development.

In tumorigenesis, angiogenesis is reactivated and takes place extensively to support tumor cell growth. Glioblastoma multiforme (GBM), the most aggressive and deadly type of tumor in the brain, is characterized by a high level of angiogenesis. The CD95 receptor and ligand system also fosters tumor angiogenesis. However, this does not occur by direct activation of CD95 on endothelial cells, but rather results from CD95 activation on GBM cells. Activation of CD95 on GBM cells by CD95L leads to an increase in the release of pro-angiogenic factors that promote vessel growth in the tumor.

Together, our data demonstrate a novel role of CD95 in angiogenesis both during development and tumorigenesis and show a potential to target CD95 in neurovascular diseases or tumor angiogenesis.

## Zusammenfassung

Im Laufe der Entwicklung des zentralen Nervensystems (ZNS) finden umfangreiche wechselseitige Interaktionen zwischen verschiedenen Zelltypen, wie zum Beispiel neuralen Progenitorzellen, Neuronen, Endothelzellen, Mikroglia und andere gliale Zellen, statt, welche äußerst wichtig zur Entwicklung beitragen. Darüber hinaus teilen Neuronen und Blutgefäße auffällig ähnliche anatomische und molekulare Eigenschaften und werden vermutlich von einem überlappenden Repertoire an Signalsystemen orchestriert.

Hier identifizieren wir eine wichtige Neuron-Blutgefäß-Glia-Interaktion, die entscheidend zur korrekten Formation des neurovaskulären Systems in ZNS beiträgt und in der das CD95 Rezeptor und Ligand System wesentlich involviert ist. Deletion des CD95 Rezeptors in Neuronen, wie bereits gezeigt, und in Endothelzellen führt zur anomalen Verzweigung und Wachstum beider Zelltypen im post-natalen ZNS. Des Weiteren identifizieren wir Mikroglia als die zentrale Quelle von CD95L und Mikroglia-spezifische Deletion von CD95L beeinträchtigt die richtige Entwicklung des neurovaskulären Systems. CD95 fördert die Verzweigung und Proliferation von Endothelzellen durch seine Funktion als Rezeptortyrosinkinase, welche nach Aktivierung zur Rekrutierung von SFK und p85 führt, die Akt und Erk Signale auslösen, zwei Effektoren, die entscheidend in der Regulation von Endothelzellwachstum sind. Diese Daten heben eine koordinierte neurovaskuläre Entwicklung hervor, welche durch Mikroglia-abgeleiteten CD95L instruiert wird, und verdeutlichen die Wichtigkeit von Mikroglia in der Etablierung des neurovaskulären Netzwerks in der ZNS Entwicklung.

In der Tumorentwicklung wird Angiogenese reaktiviert und findet umfangreich statt, um Tumorzellwachstum zu unterstützen. Glioblastoma multiforme (GBM), der aggressivste und tödlichste Tumor im Gehirn, ist durch einen hohen Grad an Angiogenese charakterisiert. Das CD95 Rezeptor und Ligand System fördert auch die Tumorangiogenese. Allerdings erfolgt dies nicht durch direkte Aktivierung von CD95 auf Endothelzellen, sondern resultiert vielmehr von der CD95 Aktivierung auf GBM Zellen. Die Aktivierung von CD95 auf GBM Zellen durch CD95L führt zum

Anstieg von pro-angiogenen Faktoren, welche das Blutgefäßwachstum im Tumor vorantreiben.

Zusammenfassend legen unsere Daten eine neue Rolle von CD95 in der Angiogenese sowohl während der Entwicklung als auch der Tumorigenese dar und zeigen das Potential CD95 in neurovaskulären Krankheiten oder in der Tumorangiogenese zu targeten.

## Acknowledgements

The past four years have been stimulating, enriching and educational for me both professionally as well as personally. This is owing to a large part to the people around me during this time who have supported and motivated me throughout the pleasant and not-so-pleasant times. For this I would like to say a big thank you!

More specifically, I would first and foremost like to express my gratitude and appreciation to Ana. You have brought me to a lab that is diverse, fun and filled with smart people. Your advice and constructive criticism were invaluable throughout this research process. Although it has not been easy with the focus of my project during my PhD, you gave me the freedom to work on different subjects and pursue the projects that I mostly believed in.

I would also like to thank my collaborator and examiner Carmen and her group members Rosario and Nathalie who have contributed a lot to this project intellectually and experimentally. Moreover, I would like to thank the two students that I have supervised, Pieter and Oguzhan, who contributed to some of the work.

Moreover, I am grateful to my thesis committee members and examiners Frank Lyko, Francesca Peri and Eileen Furlong for their helpful discussions and advice.

A big thank you goes out to all of my office buddies who have become a valuable part of my life. All the trips we undertook, the good and bad times we went through and the laughter we shared have made life in the lab so much fun and will always remain the part of my memory that is going to make me smile.

Muchas gracias Enric for introducing me to the art of ischemia, Linda and Smarter in the first months of my PhD; the stimulating discussions about science, ethics, politics and other interesting topics, for take-it-easy Fridays spent with Atriviate, Geoguessr and Sporcle and of course for your hospitality that has led us twice to your home in Mallorca. Ευχαριστώ Georgios for bringing so much laughter and social life into the lab; the numerous Hibachi sessions, the great and delicious Greek trip, dangerous animals watching, retardigrade admiring, and yes I realize my hard drive is gonna die one day. Thank you also for reading and correcting my thesis. Of course thanks also to your significant other Andromachi who brought some very welcome female vibe and lots of delicious food into our group.

Thanks also to the RNA crew Wilson and Avni. Thanks Wilson for your many funny and at times disturbing jokes that made us laugh, the awesome Hongkong trip, and we will for sure miss the question “so early today?”. Maybe one day we will make something out of the HolyS idea. Thanks Avni for co-organizing presents with me every time it was needed, for discussing work, TV shows and many random topics and your critical mind that led me to think about caveats in my studies. 谢谢 Liang for advising me on many of the CD95 issues during my project as well as nice photography skills and food that you shared with us. Danke further goes to Damian, with you it was always a pleasure to discuss science and the academic system and I really look up to your perseverance and positivity despite many challenges you faced.
Furthermore, I am grateful to Sascha for your happy laughing that always brought good mood around, to Gülce for the discussions about CD95 and Sheng for the bioinformatics analyses and insights you have taught me.
A large thank you also goes to Suse, Klara, Steffi, Kathrin and Melanie who have regularly given me a helping hand in the lab, especially when things did not work out.
I am much indebted to my parents who have always given me the freedom to do what I liked and pursue my own goals. Thank you!
Last but not least I would like to thank a very special person that entered my life through the lab, Robert. Thank you for your support and patience when listening to my everyday concerns as well as your constant encouragement that has made me believe in myself more.

# Table of contents

## List of figures

## List of tables

## Abbreviations

| Abbreviation | Description |
|---|---|
| A | alanine mutant peptide |
| AMD | age-related macular degeneration |
| BBB | blood brain barrier |
| BCA | bicinchoninic acid assay |
| bHLH | basic helix loop helix |
| BSA | bovine serum albumin |
| CD95 | cluster of differentiation 95 |
| CNS | central nervous system |
| CRD | cysteine-rich domain |
| Ctrl | control |
| DAVID | Database for annotation, visualization and integrated discovery |
| DD | death domain |
| DG | dentate gyrus |
| DISC | death-inducing signaling complex |
| DNA | deoxyribonucleic acid |
| DTT | dithiothreitol |
| E | embryonic day |
| EC | endothelial cell |
| EMP | erythromyeloid progenitor |
| EMT | Epithelial-to-mesenchymal transition |
| eNOS | enodhelial nitric oxide synthase |
| Erk | extra-cellular signal regulated |
| FACS | fluorescence activated cell sorting |
| GBM | Glioblastoma multiforme |
| gld | generalized lymphoproliferative disease |
| GO | gene ontology |
| h | human |
| HBSS | Hank's balanced saltsolution |
| HRP | horse radish peroxidase |

| Abbreviation | Description |
|---|---|
| HS | high sensitivity |
| HUVEC | human umbilical vein endothelial cells |
| IsoB4 | isolectin B4 |
| i.p. | intraperitoneal |
| i.v. | intraveneous |
| IHC | immunohistochemistry |
| INVP | intraneural vascular plexus |
| IP | immunoprecipitation |
| KO | knockout |
| lpr | lymphoproliferation |
| m | mouse |
| MFI | median fluorescence intensity |
| MMP | matrix metalloproteases |
| MRL | Murphy Roths Large |
| n.s. | not significant |
| NVU | neurovascular unit |
| OPL | outer plexiform retinal layer |
| P | postnatal day |
| PBS | phosphate buffered saline |
| PCA | principal component analysis |
| PCR | polymerase chain reaction |
| PDX | patient-derived xenograft |
| PFA | paraformaldehyde |
| pH3 | phospho-histone 3 |
| PNVP | perineural vascular plexus |
| PSD95 | post synaptic density protein 95 |
| px | pixels |
| pY | phosphorylated tyrosine CD95 peptide |
| RG | radial glia |
| RNA | ribonucleic acid |
| ROI | region of interest |

| Abbreviation | Description |
|---|---|
| RT | room temperature |
| s.c. | subcutaneous |
| SCID | severe combined immune deficiency |
| Scr | scrambled peptide |
| SD | standard deviation |
| SDS-PAGE | sodium dodecyl sulphate – polyacrylamide gel electrophoresis |
| SFK | src-family kinases |
| siCD95 | siRNA targeting CD95 |
| siScr | scrambled siRNA |
| TAM | tamoxifen |
| TUNEL | TdT-mediated dUTP-biotin nick end labeling |
| VEGF | vascular endothelial growth factor |
| VGCC | voltage-gated calcium channel |
| Y | wildtpe CD95 peptide |

# 1. INTRODUCTION

## 1.1 The cellular diversity of the central nervous system

The human brain is a profoundly complex organ with immense capabilities, some of which we utilize – as in this thesis - to understand its structure and function. Within the brain, 86 billions neurons of thousands of different subtypes can fire via 100-500 trillion synaptic connections to enable the cognitive capabilities of thought, speech, emotion etc. – often all at the same time (Azevedo et al., 2009; Drachman, 2005).

Many different cell types in the brain support its functionality and have co-evolved with neurons to create a balanced system. Cells of neural origin such as neurons, glial cells, ependymal cells as well as non-neural origin as endothelial cells, pericytes and microglia arise concurrently during development and support each other during and beyond developmental stages. Neurons are often regarded as the central, working cell type of the brain. However, without the other cell types the brain is not capable of functioning. In fact, it is estimated that a similar number of supporting cells and neurons exists in the human brain (Azevedo et al., 2009).

The study of the brain's structure and function requires manipulations that can obviously only be conducted in animal models. Here, we utilize the mouse, the most commonly used mammalian model, to elucidate the cellular interactions during CNS development.

The mouse brain differs from that of humans in several aspects, although many cellular and molecular processes are highly conserved. The most obvious difference is the lyssencephalic nature of the mouse brain that lacks cortical folding. This also results in a smaller number of neurons that amounts to 71 million in the mouse brain. Interestingly, mice also have more neurons than glial cells (Azevedo et al., 2009).

In the next chapters, the development of the mouse central nervous system will be introduced, specifically focusing on the generation of neurons, vessels and microglia – the central cell types relevant for this thesis work.

## 1.2 Developmental neurogenesis in the mammalian brain

The development of neurons undergoes several stages and is a prolonged process that starts at mid-embryonic age and lasts until approx. four weeks after birth. First, neural stem cells are generated and give rise to neurons that through migration reach their

final destination in the brain. Second, neurons extend axons and dendrites in shapes characteristic for each neuronal type that serve as senders and receivers of information, respectively. And lastly, synapses are formed between neurons to build the complex neural circuitry, a process that is driven by neuronal activity to establish a mature pattern of connectivity (McAllister, 2000). The generation of neurons in the cortex follows a stereotypic process that has been analysed in detail and is thus often used as a model to study neurogenesis. In the following, the two first steps of neuron development relevant for this thesis will be further elucidated.

### 1.2.1 Generation of cortical neurons from radial glia

During early embryonic development, the CNS arises from the ectoderm at gestational day 7.5 to 9.5 (E7.5 to E9.5) with the formation of the neural plate and subsequently the neural tube. Neuroepithelial cells within the neural tube proliferate through symmetric division to generate a large pool of cells from which the neural cells arise later on (Stiles and Jernigan, 2010) (Figure 1.1).

The generation of neurons – neurogenesis - begins at E9.5-E10.5 with the transition of neuroepithelial cells to radial glial cells (RG) that establish the ventricular zone (VZ). These cells with astroglial characteristics in terms of marker expression (e.g. Glast, BLBP, nestin) are multipotent embryonic neural stem cells that give rise to neurons, astrocytes and oligodendrocytes (Götz and Barde, 2005; Kriegstein and Alvarez-Buylla, 2009). Newborn neurons subsequently migrate along the radial process of RG towards the cortical plate where they find their final position (Kriegstein and Alvarez-Buylla, 2009) (Figure 1.1). Where this final position is and which type of neurons they become is controlled by a combination of spatial and temporal cues.

Spatial control of neuronal diversity is imposed in the manner that different domains of the developing forebrain contain different combinations of diffusible morphogens to which radial glia respond with the activation of a specific genetic program, resulting in the production of specific types of neurons. This patterning is already established early in development starting at E9.5 with the secretion of FGFs, SHH, WNTs and BMPs at specific signaling centers of the neural tube. Patterning by these factors results in regional-specific expression of a combination of homeodomain and

basic helix-loop-helix (bHLH) transcription factors, such as Pax6, Emx1, Gsx1/2, Fezf2, Mash1, Nkx2.1 etc., the levels of which define a specification towards a certain neuronal subtype (Iwata and Hevner, 2009; Paridaen and Huttner, 2014).

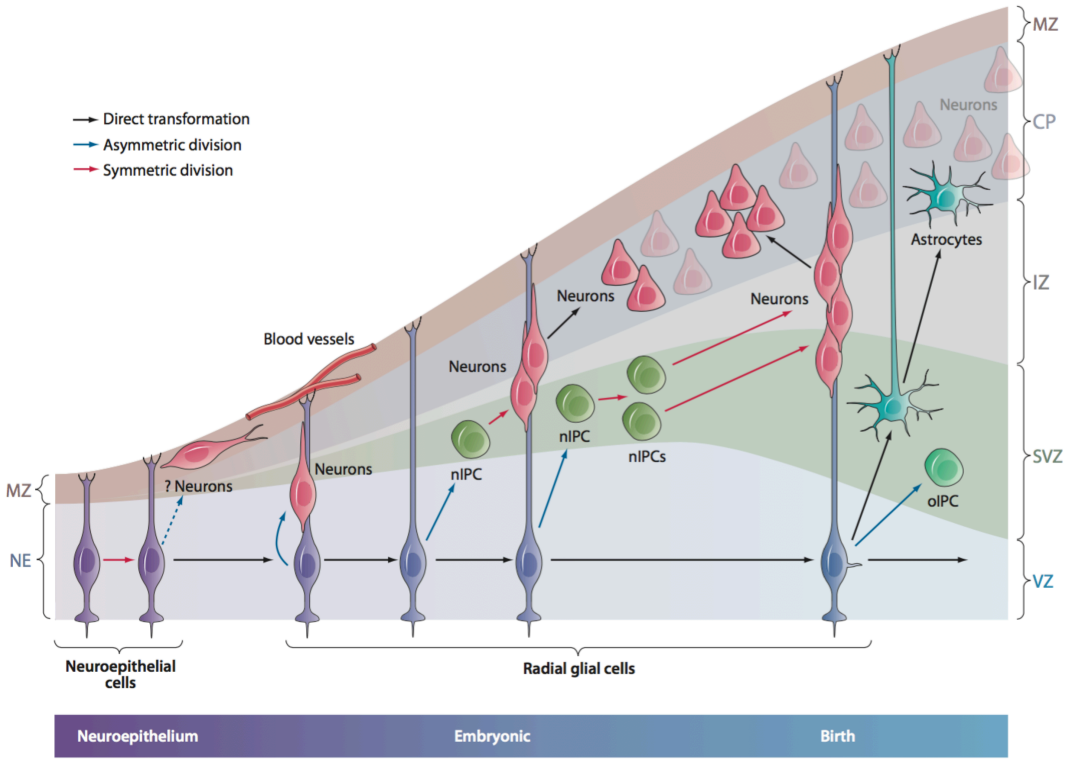


**Figure 1.1: Radial glia cells give rise to cortical neurons and glial cells.** During early development neuroepithelial cells give rise to radial glial cells that either directly differentiate into neurons or through intermediate progenitor cells (nIPCs). Close to birth, radial glial cells also differentiate into oligodendrocytes through an intermediate stage (oIPCs) or detach from the ventricle to become astrocytes. IPC, intermediate progenitor cell; MA, mantle; MZ, marginal zone; NE, neuroepithelium; nIPC, neurogenic progenitor cell; oIPC, oligodendrocytic progenitor cell; RG, radial glia; SVZ, subventricular zone; VZ, ventricular zone. (adapted from (Kriegstein and Alvarez-Buylla, 2009)).

The cortex is organized in six layers (layer I-VI) and the different layers are generated in a temporal sequence where the early-born neurons populate the deep cortical layers, while late-born neurons migrate through already established layers to be sequentially added to more superficial layers in an inside-out fashion (Greig et al., 2013). The timing also determines the neuronal type being generated. The first neurons being born form the preplate and differentiate to Caja-Retzius and subplate neurons. The next wave of neurons are born E11.5 and mainly become layer VI corticothalamic projection neurons. This is followed by layer V subcerebral projection neurons born at

around E13.5 and layer IV granule neurons born one day later. Moreover, callosal projection neurons populate the cortex with the ones born at E12.5 localizing to deep layers while those that are born between E14.5 and E16.5 migrate to the superficial cortical layers II/III (Greig et al., 2013; Kriegstein and Alvarez-Buylla, 2009).

At E16.5, when neurogenesis is mostly finished, RG cells switch from a neurogenic to a gliogenic fate. First, astrocytes are being generated, peaking at E18.5-19.5, followed by oligodendrocytes, the majority of which are born postnatally (Greig et al., 2013; Kriegstein and Alvarez-Buylla, 2009) (Figure 1.1).

### 1.2.2 Axon and dendrite formation

Directly after birth, post-mitotic neurons assume a bipolar morphology and undergo axo-dendritic polarization to eventually develop into polarized cells with a single long axon and many short highly branched dendrites (Cheng and Poo, 2012). In cortical principal neurons and cerebellar granule cells, the leading process of the migrating neuron becomes the dendrite, while the trailing process develops into the axon (Cheng and Poo, 2012; Hatanaka and Murakami, 2002). Axons and dendrites differ in their function, structure and morphology. Axons act as the information output compartment whereas dendrites represent the information input compartment of neurons. Whereas dendrites have specialized structures of main excitatory synaptic sites including spines, axons do not. Moreover, while axons have unidirectional plus-end-distal microtubules, dendrites possess both plus- and minus-end-distal microtubules that influence the transport of organelles and molecules. Axons and dendrites serve the core functions of neurons of signal transduction and synaptic transmission, thus their correct formation and targeting is highly important.

The establishment of neuronal polarity is regulated by several signaling pathways, including the PI3K-mediated activation of AKT/Gsk3β and Cdc42/Par3/6 signaling as well as cAMP-induced PKA/LKB1/Sad kinase signaling (Kim et al., 2011). Interestingly, global inhibition of Gsk3β results in multiple axon formation, while overexpression of the phosphorylation dead form Gsk3β-Ser9Ala inhibits axon formation (Jiang et al., 2005; Yoshimura et al., 2005).

After specification of the axon/dendrite identity, dendrites further undergo five critical stages of morphogenesis: 1) guidance; 2) branching; 3) dendritic tiling and

self-avoidance; 4) differentiation and 5) pruning (Puram and Bonni, 2013) (Figure 1.2). During the guidance stage, dendrites follow guidance cues to move away from the soma and toward their target field while growing and increasing in length and diameter. In order to cover their complete target field, dendrites need to branch and they do so several times, forming extensive secondary and tertiary branching. This occurs mainly by interstitial branching, with new branches extending from the side of existing dendrite shafts as filopodia before becoming stable branches. The extent of dendritic branching is controlled by dendritic tiling mechanisms whereby non-redundant coverage by dendrites of the same neuronal type is ensured through growth inhibition upon contact with neighboring cells of the same type. Moreover, self-avoidance mechanisms limit dendrite growth and secure that dendritic branches of the same neuron do not crossover each other, but rather spread out evenly within distinct territories. Once neurons have formed dendrites, these differentiate and develop specialized structures called spines that are the site of synapses. Dendrite maturation further involves pruning whereby branches are retracted and eliminated to ensure that only the correctly innervated ones remain (Puram and Bonni, 2013).

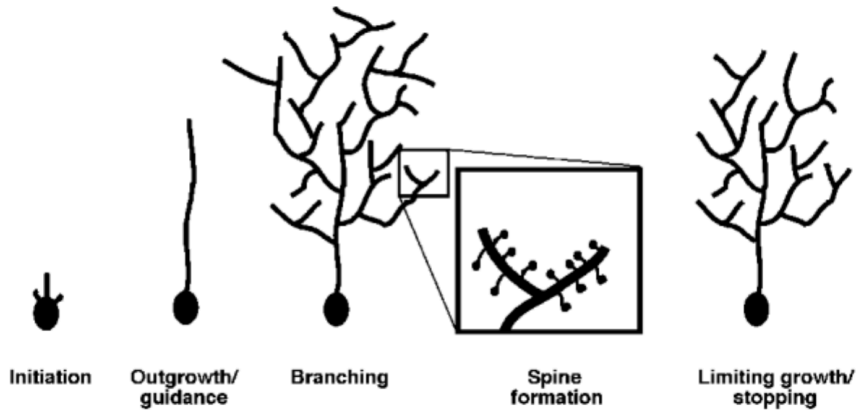


**Figure 1.2: Process of dendritic development.** Neuron branching of dendrites starts with initiation, followed by outgrowth and guidance through guidance molecules and continues with branching, spine formation and growth stop. (adapted from (Scott and Luo, 2001))

On a molecular level, these processes are regulated by numerous cell-intrinsic and cell-extrinsic cues. Cell-intrinsic cues comprise of transcription factor activity, cytoskeletal molecules, motor proteins and microtubule regulators as well as cell cycle-regulated ubiquitin ligases. These factors allow a cell-specific interpretation of environmental cues that can be different depending on neuronal cell type, thus

generating diversity in dendrite morphology. Transcription factors can be expressed in different types of neurons to execute different functions in a cell-type specific fashion. Cux1 and Cux2 for example specifically promote dendrite branching in layer II-III pyramidal neurons by suppressing p27Kip1 (Cubelos et al., 2010; Li et al., 2010). Of the cytoskeleton regulators the Rho family GTPases are crucial for dendrite dynamics through cell structural changes. The GTPase RhoA reduces dendrite length by regulating myosin light chain and actomyosin contractility (Nakayama et al., 2000; Winter et al., 2001). In contrast, Rac1 and Cdc42 of the same family promote dendrite arborization (Scott et al., 2010). Another imported regulator of dendritic growth is the cell cycle-regulated ubiquitin ligase Cdc20-APC that triggers polyubiquitylation and degradation of the transcriptional regulator Id1, resulting in increased dendrite growth and elaboration (Kim et al., 2009; Puram and Bonni, 2013).

Cell-extrinsic cues that regulate dendrite morphogenesis include many secreted molecules, contact-mediated regulators and neuronal activity. Several secreted molecules act as guidance for dendritic targeting, such as Slits, Ephrin A7 and Wnt5 that repel dendrite branches, whereas netrins and semaphorins attract branching. Neurotrophins such as NGF, BDNF, NT-3/4 are another class of secreted molecules that promote dendrite growth and arborization, partially through activity-dependent pathways via inactivating phosphorylation Gsk3β at Ser9 (Rui et al., 1AD).

Contact-mediated regulators are especially important for dendrite tiling and self-avoidance. The cell adhesion molecule DSCAM is expressed in thousands of different isoforms on different dendrites of a neuron and has been shown to induce self-avoidance in Drosophila neurons through isoform specific homophilic binding to individual dendrites (Wojtowicz et al., 2004).

Neuronal activity is another key factor in regulating dendrite development. It induces calcium transients within the cell that activates CaMKs which can positively or negatively affect dendrite complexity depending on context (Valnegri et al., 2015). Calcium signals induced by voltage-gated calcium channels (VGCC) for example can activate the protease calpain that promotes dendrite pruning (Kanamori et al., 2013).

Axons and dendrites share many mechanisms of growth. Secreted guidance molecules both steer axons and dendrites toward the correct direction. However, how dendrite and axon growth are differentially regulated is generally not well studied. Two principles of regulation have been proposed with one involving mechanisms that regulate either axon-specific or dendrite-specific growth, termed "dedicated mechanisms", and the other involving mechanisms that direct dendritic and axonal development in opposite manners, termed "bimodal mechanisms" (Wang et al., 2014). The bHLH transcription factor NeuroD is one example of a dendrite-dedicated regulator. It promotes specifically dendritic growth and arborization, but not axonal morphogenesis (Gaudillière et al., 2004). Conversely, the small GTPase Rac1 inhibits axonal outgrowth and elongation, but does not affect dendrite branching (Luo et al., 1996). The secreted molecule Sema3A of the semaphorin family act as bimodal regulator with opposite effects on axons and dendrites. Sema3A promotes dendrite initiation, targeting and growth but suppresses axonal formation by inhibiting cAMP activity that is important for axon initiation and enhancing cGMP activity that supports dendritic growth. Similarly, Sema3A also serves as a chemoattractant for cortical dendrites while acting as a chemorepellent for cortical axons (Polleux et al., 2000; Shelly et al., 2011a; 2011b).

### 1.3 Vascular development in the CNS

The vertebrate CNS is made up of the brain, spinal cord and retina and its vascularization during development is crucial to supply newly born neurons with oxygen and nutrients, long before they form axons and dendrites to build a neuronal network (Ruhrberg and Bautch, 2013). In spite of the brain only representing 2% of the body mass, it utilizes almost 25% of the entire body's energy, thus making it highly dependent on metabolic supply from blood vessels (Lacoste et al., 2014). It is estimated that the human brain encompasses up to 100 billion vessels, which would mean that each neuron is supplied by a vessel (Quaegebeur et al., 2011).

In contrast to non-CNS vessels, the CNS endothelium is equipped with a tightly regulated neurovascular unit (NVU) that is composed of endothelial cells lining the blood vessels, perivascular cells (i.e. pericytes and vascular smooth muscle cells) and vascular astrocytes interacting with each other to form the blood-brain barrier (BBB).

The CNS vasculature is also distinct to other tissues in that the endothelial cells are thinner, the pericyte coverage is higher and the communication with the surrounding parenchymal cells is more pronounced (Quaegebeur et al., 2011).

Vascularization of the early CNS, similar to all other embryonic tissues, is established by the process of vasculogenesis – the *de novo* generation of new blood vessels through differentiation of mesoderm-derived angioblasts. The definitive CNS, however, is vascularized exclusively through angiogenesis – the sprouting of new blood vessels from pre-existing ones (Flamme et al., 1997). In the following the cellular and molecular mechanisms regarding CNS vascularization will be introduced.

### 1.3.1 Vascularization of the mouse brain

Early in CNS development at E7.5-8.5 when the neural tube is established, angioblasts are recruited by the neuroepithelium to form a perineural vascular plexus (PNVP) in the hindbrain via vasculogenesis (Hogan, 2004). From this first vascular plexus, new capillaries sprout via angiogenesis from E9.5 on in a caudal to cranial direction, attracted by pro-angiogenic factors, to form the intraneural vessel plexus (INVP) (Vallon et al., 2014). Both the establishment of the PNVP and the INVP depend heavily on Vegf-A expression from the neuroepithelium (Breier et al., 1992). Neuroectodermal deletion of VEGF-A using the Nestin-cre VEGF-$A^{fl/fl}$ mice results in complete failure of the forebrain to be vascularized due to migratory arrest of endothelial cells at the periphery of the early CNS and ultimately leads to developmental retardation and neural tissue death (Raab et al., 2004). The periventricular areas are especially high in VEGF-A expression, attracting extensive branching and arborization of capillary sprouts from the pial surface to form a temporary periventricular vascular plexus around the ventricular spaces and spinal cords central canal (Arnold and Betsholtz, 2013; Breier et al., 1992; Greenberg and Jin, 2005; Vasudevan and Bhide, 2014).

The first cortical vessels are formed this way beginning form E12.5 when endothelial cells migrate from the pial surface towards the ventricle to establish the first loop-structured dense plexus. This is followed by a second plexus beneath the developing cortical plate at E14.5 which is interconnected to the first plexus via a few penetrating branches. At E15.5 tangential vessels to the pial surface develop in the intermediate

zone. At E18.5 the ventricular plexus looses much of its definition and a complex vascular network forms (Stubbs et al., 2009) (Figure 1.3).

After birth, angiogenesis decreases, however, it has been shown using two-photon time-lapse microscopy in living mice that during the early postnatal period extensive microvascular remodeling takes place. Endothelial cell proliferation as well as vessel branching continue and peak at around P10, dropping thereafter and stabilizing by P25. Unlike in earlier developmental stages, endothelial sprouts in postnatal brain often contain only one tip cell and span rather short distances between nearby microvessels (Harb et al., 2012).

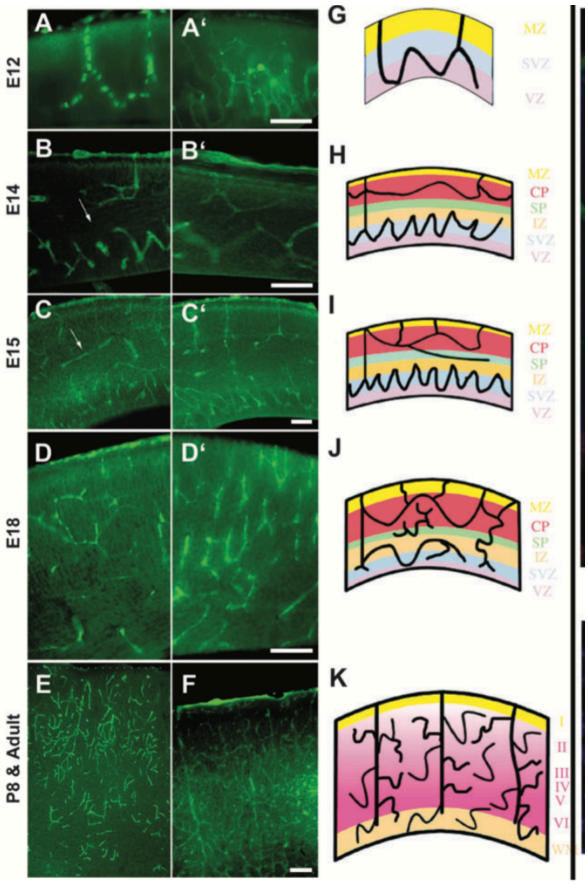


**Figure 1.3: Development of vessels in the somatosensory cortex.** Staining of vessels by Isolectin B4 from development stage E12 to adulthood and schematic drawings thereof. Vessels start entering the cortex at E12 and form two plexi at E14 that further branch to cover the majority of the cortex. MZ: marginal zone, CP: cortical plate, SP: subplate, IZ: intermediate zone, SVZ: subventricular zone, VZ: ventricular zone, I-VI represent cortical layers in the adult. Scale: 100 µm (adapted from (Stubbs et al., 2009))

During adulthood, endothelial cells are mostly quiescent during homeostasis with little microvascular formation and elimination being maintained (Harb et al., 2012). Interestingly, however, the brain is capable of increasing its microvascular density in response to neuronal activity and hypoxia (Black et al., 1990; Harik et al., 1996).

### 1.3.2 Vascularization of the mouse retina

The retina and the optic nerve are extensions of the brain and develop as exvaginations of the forebrain neuroectoderm (Fruttiger, 2007; Mancuso et al., 2008). In contrast to the vasculature of the cortex, the vasculature within the mouse retina develops completely postnatally. Before birth, the retina is avascular, only supplied by two extra-retinal vasculatures, the choroidal vessels around the optic cup that nurture the outer retina, and the hyaloid vessels in the vitreous humor that supply the inner retina and lens (Mancuso et al., 2008; Ruhrberg and Bautch, 2013).

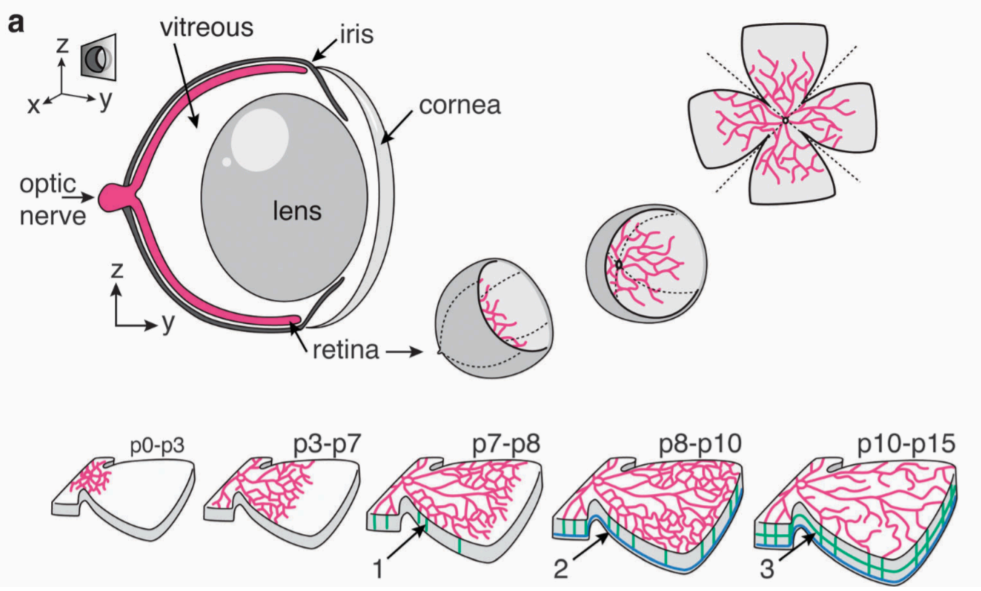


**Figure 1.4: Development of blood vessels in the retina.** Blood vessels in the retina develop postnatally starting at the optic nerve in the central retina. The first superficial layer of vessels (1) cover the retina completely by P8 after which the deep layer is formed through vertical sprouting from P8-P10 (2). Lastly, an intermediate layer of vessels is formed between the superficial and deep layer until P15 (3). (adapted from (Milde et al., 2013))

In the first eight days after birth, the hyaloid vessels regress and new vessels extend radially from the central retina to the periphery through endothelial cell proliferation, sprouting and migration, ultimately leading to the formation of the primary vascular plexus in the retina (Gerhardt et al., 2003; Pitulescu et al., 2010). The endothelial cells are mainly guided by astrocytes and Mueller glia that release large amounts of VEGF-A (Gerhardt et al., 2003). Beginning from P7, the primary superficial plexus sprouts vertically into deeper layers of the retina, first generating the deep vascular plexus in the outer plexiform retinal layer (OPL) from P8-P10 and subsequently the intermediate vascular plexus at P10-15 (Arnold and Betsholtz, 2013; Milde et al.,

2013). Following this, vascular remodeling and differentiation into arteries and veins takes place until a mature vascular network is formed at six weeks after birth (Arnold and Betsholtz, 2013) (Figure 1.4).

Due to the stereotypical vessel growth, the retina represents an ideal system to study angiogenesis *in vivo* and has been utilized to characterize many mechanisms of angiogenesis.

### 1.3.3 Cellular and Molecular determinants of CNS vascularization

The process of angiogenesis is governed by sprouting tip cells that spearhead new vessel formation and by proliferating stalk cells that extend sprouts and form the vessel lumen. Sprouting tip cells subsequently anastomose with neighboring tip cells to form vascular loops, followed by blood perfusion and vessel maturation (Herbert and Stainier, 2011; Potente et al., 2011). The process of sprouting, extension, branching and anastomosis repeats until a full vascular network is established (Figure 1.5).

The initiation of angiogenesis occurs upon pro-angiogenic factor stimulation and liberation of endothelial cells from the basement membrane (Potente et al., 2011). Tip cells are enriched in matrix metalloproteases (MMPs) such as MT-MMP1 that break down basement membrane and free endothelial cells, allowing them to extend plasma membrane protrusions called filopodia toward guidance cues (Arroyo and Iruela-Arispe, 2010; Eble and Niland, 2009; Wang et al., 2014).

The tip/stalk cell identity is mainly established by DLL4/Notch and VEGF-A signaling that acts as a branching pattern generator (Potente et al., 2011). During this process, the guidance cue VEGF-A induces Notch ligand DLL4 expression in tip cells that results in Notch activation in neighboring cells. These cells establish a stalk cell phenotype through Notch-induced downregulation of VEGF receptor (including VEGFR2, VEGFR3 and NRP1) and parallel upregulation of anti-angiogenic factors such as sFlt1 and Jagged1 (Eilken and Adams, 2010; Moya et al., 2012; Phng and Gerhardt, 2009; Potente et al., 2011). Notch thus acts as a suppressor of the tip cell phenotype and promoter of stalk cell specification.

Once tip and stalk cell identities are established, tip cells must be guided correctly for proper vascular patterning. To this end, tip cell filopodia function as sensors for

attractive and repulsive cues. Similar to axonal growth cones of neurons, tip cells express guidance receptors such as ROBO, UNC5B, NRP, Plexin-D1 and Ephrin receptors that can respond to the guidance cues Slit, Semaphorin and Ephrin ligands (Carmeliet and Tessier-Lavigne, 2005; Potente et al., 2011). The molecular mechanisms that regulate tip cell filopodia are just beginning to be unraveled. VEGF-A for instance activates VEGFR2 in tip cells to induces PI3K, followed by Rac/Rho and Grb2 that result in Cdc42 activation, leading to stimulation of actin reorganization, filopodia formation and cell migration (De Smet et al., 2009; Matsumoto and Mugishima, 2006). Moreover, it has been shown in the mouse retina that VEGFR2-expressing neurons regulate directionality of angiogenesis by titrating VEGF-A (Okabe et al., 2014).

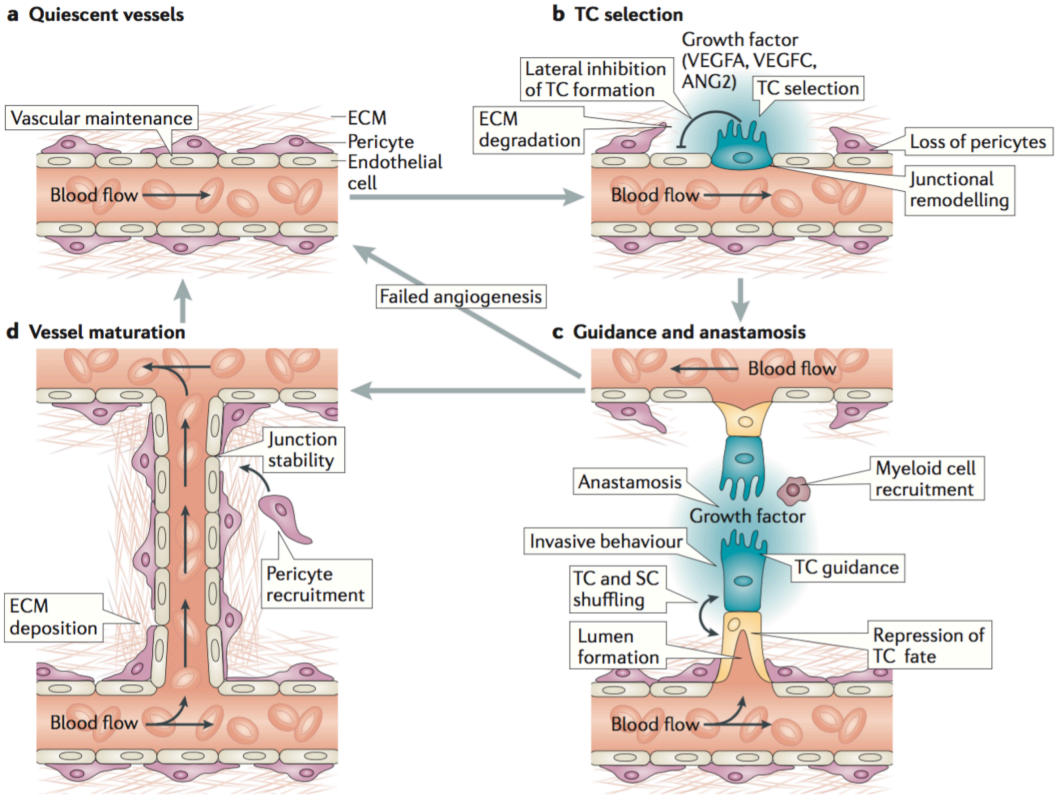


**Figure 1.5: Cellular and molecular mechanisms of angiogenesis.** a) In homeostasis during adulthood, endothelial cells are normally quiescent. b) Upon angiogenic stimulation through growth factors such as VEGF that is secreted by the neuroepithelium during development, extracellular matrix (ECM) degradation becomes activated and loss of pericytes is induced. Furthermore, tip cells (TC) are selected through VEGFR2 and neighboring cells are inhibited in TC fate through lateral inhibition by DLL4-Notch signaling. c) TC sprouting is guided by different growth factors and are followed by stalk cells (SC) which form the vessel lumen. When TC contact other TCs, the process of anastomosis is initiated which is supported by associated myeloid cells. d) After new vessels are established vessels become perfused and are stabilized by pericytes that are recruited through PDGF-B and ECM deposition. (adapted from (Herbert and Stainier, 2011))

While tip cells are finding the orientation, stalk cells proliferate via VEGF-A induced MAP kinase activation and start to form a lumen by coalescence of intracellular vacuoles and joining of vacuoles from adjacent stalk cells in a process called cell hollowing (Potente et al., 2011; Strilic et al., 2009; Zeeb et al., 2010).

The next step in the angiogenic process is anastomosis where tip cells fuse with adjacent tip cells to form new vessel circuits. Microglia have shown to facilitate this process by bridging between tip cell filopodia (Fantin et al., 2013). The new vessel connection is then strengthened by the adherens junction molecules VE-cadherin and N-cadherin, the buildup of extracellular matrix into the basement membrane and the recruitment of supporting vascular smooth muscle cells (pericytes or mural cells depending on context) through endothelial cell-derived PDGFB (Cavallaro and Dejana, 2011; Lindahl et al., 1997; Potente et al., 2011). With this, new vessels enter the maturation state, where the hierarchically branched network is remodeled and adapted to tissue needs (Jain, 2003). Also the start of blood perfusion contributes to this by decreasing VEGF expression, thus shifting endothelial cells towards quiescence, and by determining arterio-venous differentiation (Potente et al., 2011).

VEGF-A signaling through its receptor VEGFR2 and NRP-1 is the major pathway regulating vasculogenesis and angiogenesis in the CNS, however, many other factors have been identified to induce angiogenesis in endothelial cell-autonomous or -non-autonomous ways. Endothelial cell-specific deletion of the VEGFR2 and its co-receptor NRP1/2, TGFBR1/2 (Robson et al., 2010; Sridurongrit et al., 2008), β–catenin (Stenman et al., 2008) or the orphan G-protein coupled receptor GPR124 (Kuhnert et al., 2010) all lead to defects in proper CNS angiogenesis and embryonic lethality (Vallon et al., 2014). Similarly, neuroepithelium-specific deletion of genes such as VEGF-A, WNT7a/b (Daneman et al., 2009; Stenman et al., 2008), ID1/3 and the integrins $\alpha_v$ and $\beta_8$ (McCarty, 2004; Proctor, 2005) result in angiogenic failure and CNS hemorrhage (Vallon et al., 2014).

### 1.3.4 Concurrent development of vessels and neurons – the neurovascular link

The Belgian anatomist Andreas Versalius aleady noticed five centuries ago that nerves and vessels run parallely and form highly branched and complex networks through sterotypical patterning during development (Adams and Eichmann, 2010; Lacoste et

al., 2014). Particularly in the periphery, blood vessels and nerves spread to all edges of the body and are often aligned (Eichmann and Thomas, 2013). The morphogenesis of neurons and vessels shares striking anatomical, cellular and molecular features and is orchestrated by an overlapping repertoire of extracellular signals (Segura et al., 2009).

Developing neurons use growth cones at axonal terminals for guidance during neuronal network formation (Tessier-Lavigne and Goodman, 1996) and similarly, blood vessels use endothelial tip cells for guidance during sprouting angiogenesis (Gerhardt et al., 2003). Both systems are governed by the a gradient of guidance molecules that has initially been discovered as axon guidance cues but have been recently coined "angioneurins" due to their acitivty in vessels as well as in neurons (Zacchigna et al., 2007). Four main families of guidanance cues have been identified: ephrins, semaphorins, netrins and slits. These ligands bind to their respective receptors: Eph family receptor, NRP/Plexin-D1, UNC5B and ROBO4 and act as attractive or repulsive cues (Adams and Eichmann, 2010).

Beside the classical guidance cues, the blood vessel growth factor VEGF-A has also been shown to influence nervous system development in that it promotes axonal growth (Silverman et al., 1999; Sondell et al., 1999) as well as axon guidance in the visual system (Erskine et al., 2011) and at the floor plate of the spinal cord (Ruiz de Almodovar et al., 2010).

In addition, neurons and vessels influence each other extensively during development. Starting from E10.5, the neuroepithelium drives the initial ingression and the stabilization and pruning of blood vessels (Daneman et al., 2009; Hogan, 2004). Later in the embryonic cortex, radial glia neural progenitors stabilize the vascular network via modulation of Wnt signaling (Ma et al., 2012). In turn, vessels are positioned in the neural progenitor niche and promote neurogenesis, neuronal migration and neurite outgrowth (Shen et al., 2004; Stubbs et al., 2009). In the peripheral nervous system, sympathetic axons follow neurotrophic factors released by arteries to reach their destination (Damon et al., 2007; Makita et al., 2008).

The neural and vascular system thus not only utilizes the same molecules to grow but also support each other's development.

## 1.4 Glioblastoma and tumor vascularization

Brain tumors are a rare tumor entity with less than 2% of all tumors diagnosed each year (Jemal et al., 2009). However, the most common type in the adulat that accounts for nearly 40% of all primary brain tumors – glioblastoma multiforme (GBM) – is one of the most deadly tumors with a 5-year survival rate of only 5% and a median survival of only 15 months, despite of multimodal therapy (Behin et al., 2003; Furnari et al., 2007; Stupp et al., 2005). One hallmark of GBM is extensive microvascular proliferation (Brem et al., 1972; Louis et al., 2016) and in fact, GBM is one of the most vascularized tumors. Tumor cells need vessels for nutrients and oxygen, and similar to neural progenitors during development, glioma stem cells seek proximity of vessels as they support their growth and proliferation (Calabrese et al., 2007).

Tumor growth depends heavily on blood vessels, as Judah Folkman postulated in the early 70's: "Solid tumors can grow to visibility only if they can vascularize themselves." (Folkman, 1971; 1972). Studies have in fact shown that tumors need to turn on the "angiogenic switch", upon which the balance of pro- and angiogenic activity in homeostasis is tipped towards pro-angiogenic factor release, in order to grow beyond 1-2 mm in diameter (Fidler et al., 2002; Vallon et al., 2014).

Vascularization within a tumor follows similar mechanisms as during development with the tumor hijacking molecular determinants of normal angiogenic processes. In GBM, sprouting angiogenesis is initiated by angiopoietin-mediated disruption of pre-existing vessels, followed by ECM breakdown and acquisition of tip/stalk cell identity (Hardee and Zagzag, 2012).

VEGF-A, the master regulator of angiogenesis, also plays a crucial role in tumor angiogenesis. Tumor cells strongly upregulate expression of VEGF-A, promoted by hypoxia, acidosis and oncogenes (Ras, Src) (Carmeliet and Jain, 2000; Fukumura et al., 2001). Moreover, chemokines including IL-8 and CXCL12 (Li and Ransohoff, 2009; Salmaggi et al., 2003; Schmidt et al., 1999) and growth factors such as PDGF and FGF (Carmeliet and Jain, 2011) drive angiogenesis in GBM.

Due to the constant exposure to VEGF-A and other pro-angiogenic molecules released by tumor cells and the tumor niche (e.g. myeloid cells) (Brandenburg et al., 2015; Osterberg et al., 2016), tumor vessels can not mature properly and are highly abnormal, characterized by high permeability and leakiness, disorganization,

tortuosity and low pericyte coverage (Guo et al., 2010; Winkler et al., 2004). Moreover, in the brain, the BBB is impaired and vessels exhibit pores as large as 550 nm in diameter (Hobbs et al., 1998). The consequence of this is a high interstitial fluid pressure and edema, which can cause severe complications in the patient.

Due to the high impact of angiogenesis in brain tumor progression, angiogenesis inhibitors have been developed as a treatment option for GBM. The most prominent one is the VEGF-A neutralizing antibody bevacizumab. The major benefit from bevacizumab is vessel normalization that is associated with reduced vascular permeability and edema (Vredenburgh et al., 2007). However, the success of bevacizumab is dampened by the fact that it only increases progression-free survival by 3-4 months in combination with radiotherapy and temozolomide chemotherapy, but not overall survival (Chinot et al., 2014; Gilbert et al., 2014). Patient relapse represents a big problem, moreover, VEGF-A inhibition has been shown to increase the invasive phenotype of GBM (Paez-Ribes et al., 2009).

Beside angiogenesis, other mechanisms of neovascularization in GBM include vasculogenesis, vascular co-option, vascular mimicry and GBM to endothelial cell transdifferentation (Hardee and Zagzag, 2012). Vascular co-option is an early mechanism that involves tumor cells attaching to pre-existing vessels (Holash et al., 1999; Zagzag et al., 2000). Later, tumor cells can establish functional vessel-like networks, also incorporating into endothelial networks, in a process called vascular mimicry (Yue, 2005). Although still controversial, it has also been shown that GBM cells can transdifferentiate into endothelial cells that integrate into functional vessesl (Ricci-Vitiani et al., 2010; Soda et al., 2013; Wang et al., 2010).

## 1.5 Microglia during the development of the central nervous system

Microglia were discovered in the brain by a student of Ramon y Cajal – Pio del Rio Hortega in 1932 (Kettenmann et al., 2011). Initially described as the resident immune cells of the brain, it is now recognized that microglia have manifold functions beyond immune modulation such as regulation of development, maintenance of neural homeostasis and response to injury followed by regulation of repair (Nayak et al., 2014). Microglia in a resting state have a highly ramified morphology that enables dynamic monitoring of their environment and direct communication with neurons,

astrocytes and blood vessels (Davalos et al., 2005; Nimmerjahn et al., 2005; Stence et al., 2001; Wake et al., 2009). In response to a pathological insult, microglia respond by transforming into an activated amoeboid phenotype to orchestrate an innate immune response (Casano and Peri, 2015).

Microglia make up 5-15% of all glial cells in the human brain (Lyck et al., 2009; Pelvig et al., 2008) and their ontogeny is highly conserved amongst vertebrates (Pont-Lezica et al., 2011), making them likely to play an important role in maintaining CNS health. Furthermore, they secrete a plethora of neuroactive molecules (Lucin and Wyss-Coray, 2009) and express receptors for all known neurotransmitters (Kettenmann et al., 2011) which theoretically enables them to sense and react to neuronal activity. Indeed, a lack of microglia, for instance in Hoxb8 mice, can lead to compromised brain function, learning skills and individual behavior as seen by excessive compulsive grooming (Chen et al., 2010b).

In the following, the origin and development of microglia will be highlighted and the function of microglia during development will be described, specifically focusing on its role in neuronal and vessel development of the CNS.

### 1.5.1 The origin and development of microglia

The lineage and origin of microglia had been a long-standing debate. Initially, it was thought that microglia, like other macrophages, are of hematopoietic origin and exclusively derive from circulating monocytes due to similar marker expression (Nayak et al., 2014).

A recent series of publications however refuted this model and proved that microglia are distinct from bone marrow-derived monocytes/macrophages and instead derive from the embryonic yolk sac during primitive hematopoiesis.

First indications of this were found in the avian system, where chimeras between chick embryos and quail yolk sacs showed establishment of primitive myeloid cells invading the brain rudiment independently of blood supply (Cuadros et al., 1993). Moreover, in non-irradiated parabiotic mice, microglia were maintained by self-renewal without the need of bone marrow progenitors (Ajami et al., 2007). More convincing evidence was presented by Ginhoux et al. in a fate mapping study in which $Runx1^{+}$ progenitors of the yolk sac were shown to give rise to primitive macrophages

that populate the brain (Ginhoux et al., 2010). This was further confirmed by Schulz et al. who showed that deletion of Myb, a transcription factor essential for hematopoiesis, led to deficiency in hematopoietically derived monocytes/macrophages but did not affect numbers of microglia in the CNS (Schulz et al., 2012). Additional FACS approaches in the last few years have identified that microglia derive from $CD45^{-}cKit^{+}$ and Tie2+ erythromyeloid progenitors (EMP) that convert to $CD45^{+}cKit^{-}Cx3cr1^{+}$ microglia (Kierdorf et al., 2013; Perdiguero et al., 2015).

These cells invade the brain rudiment at E8.5, surround the neuroepithelium at E9.5 and start to colonize the CNS parenchyma at E10.5 after entering the neuroepithelium (Ginhoux et al., 2010). Once in the neuroepithelium, microglia proliferate rapidly and populate the brain from dorsal to ventral and rostral to caudal (Arnold and Betsholtz, 2013). The number of microglia rises steadily from E8.5 onwards, with 58% of microglia being $PCNA^{+}$ at E16.5 and the majority (95%) of all microglia actually being generated within the first two weeks after birth (Alliot et al., 1999). During this period, microglia differentiate from cells of an amoeboid to a more branched morphology and become completely ramified throughout the brain by P28 (Herbomel et al., 2001; Orłowski et al., 2003; Sorokin et al., 1992). Also during adulthood, microglia are normally maintained through local self-renewal. Only under certain pathological conditions such as inflammation (Ajami et al., 2007) or irradiation (Kierdorf et al., 2013; Mildner et al., 2007) does infiltration of blood-derived monocytes and bone marrow-derived cells into the CNS occur.

Which route microglia take to enter the brain is still controversial. It has been shown that microglia colonization of the brain occurs with embryonic vascularization (Ajami et al., 2007). Moreover, Ncx-/- mice that have a defective sodium calcium exchanger and therefore lack functioning blood circulation do not have microglia in the brain at E10.5 (Ginhoux et al., 2010). However, despite the vascular system being the primary route for transport, microglia also appear in regions of the developing CNS devoid of blood vessels and in the embryonic retina, microglia arrive well before post-natal retinal angiogenesis occurs (Ginhoux et al., 2010; Koushik et al., 2001; Rigato et al., 2011). It is thus likely that ventricles or para-meninges also serve as routes of entry (Cuadros and Navascués, 1998). In avian studies for instance, microglia have been shown to cross the pial membranes and the roof plate independently of blood vessels

(Cuadros et al., 1993; Kurz and Christ, 1998). Neuronal cell death-induced nucleotide release has further shown to guide microglia into the brain and mediate their distribution (Casano et al., 2016).

### 1.5.2 Function of microglia during CNS development

Although microglia are distributed throughout the brain during homeostasis, there are certain locations where they are found more frequently. These include areas of cell death, close to developing blood vessels, areas containing developing axon fascicles and near radial glial cells (Pont-Lezica et al., 2011). The proximity of microglia to these locations correlates with functions that they perform during development. In fact, interaction of microglia with other cell types in the brain is indispensible for normal development (Figure 1.6).

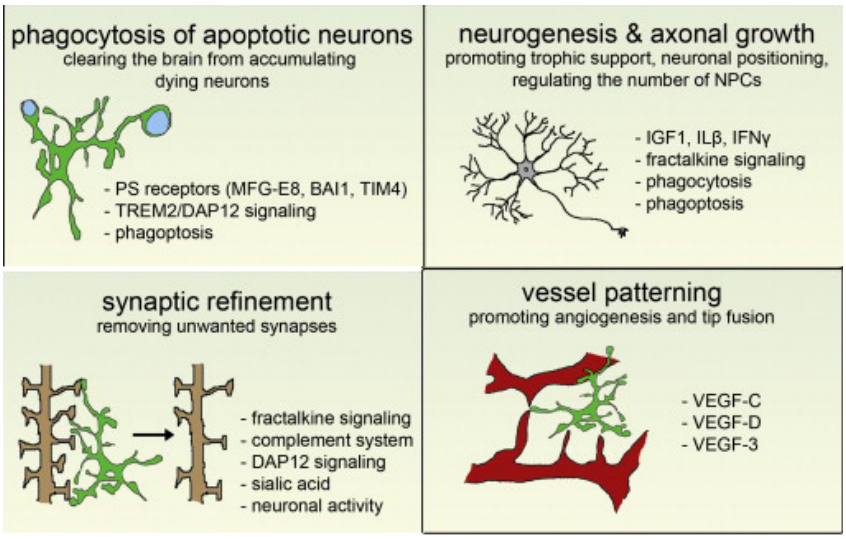


**Figure 1.6: The role of microglia during CNS development.** Microglia support different processes during CNS development, including the take up of apoptotic neurons, support of neurogenesis and axonal growth, refinement of synapses as well as patterning of vessels. Theses processes are regulated by various signaling pathways. (modified from (Casano and Peri, 2015))

#### *1.5.2.1 Role of microglia in neuronal development*

##### 1.5.2.1.1 Neuronal death

Traditionally, microglia have been mainly attributed the role of phagocyting apoptotic neurons (Bessis et al., 2007; Desbarats et al., 2003; Kuida et al., 1998; la Rosa and de Pablo, 2000; Oppenheim, 1991; Schlegelmilch et al., 2011; Zuliani et al., 2006). Approximately half of all immature neurons that are generated during development

undergo apoptosis (Kuida et al., 1998; la Rosa and de Pablo, 2000; Oppenheim, 1991). These dead cells have to be removed and microglia play a central role in this clearing process (Ashwell, 1990; Calderó et al., 2009; Sierra et al., 2010). Interestingly, the arrival of microglia in the brain parenchyma correlates with the presence of apoptotic cells (Cuadros et al., 1993; Dalmau et al., 1997; Rigato et al., 2011; Wakselman et al., 2008). *In vivo* imaging of zebrafish embryos has shown that microglia engulf apoptotic neurons by extending their processes and encapsuling them (Peri and Nüsslein-Volhard, 2008). Microglia sense and are recruited to dying neurons through factors released by them such as chemotactic signals including ATP (Davalos et al., 2005) or the ligand fractalkine (Cx3cl1) that activates MFG-E8 in microglia to bind phosphatidilserine exposed to the cell surface of apoptotic neurons (Hanayama et al., 2002). The phagocytic functions of microglia do not only keep the brain clear of dying cells during development but also contributes during adulthood to maintain healthy neural networks (Nayak et al., 2014).

**1.5.2.1.2 Neuronal survival and neurite formation**

The generation of neurons and microglia occur concomitantly in the developing brain, thus it is not far-fetched to assume that they interact to affect each other's development. In fact, microglia secrete a plethora of trophic factors such as bFgf, Egf, Pdgf, Ngf, Bdnf (Araujo and Cotman, 1992; Nakajima et al., 2001; Yamagata et al., 1995) that can potentially support neuronal function. Conditioned medium from low-density cultures of microglia has for instance been shown to promote neuronal survival as well as increase neurite outgrowth *in vitro* (Chamak et al., 1994; Morgan et al., 2004; Nagata et al., 1993; Zhang and Fedoroff, 1996). Moreover, Csf1, an important factor for microglia proliferation and development, can also act as a neurotrophic factor to enhance neurite outgrowth (Michaelson et al., 1996).

One recent study by Ueno *et al.* further confirmed a crucial role of microglia in regulating neuronal survival *in vivo*. Ablation of microglia during postnatal development was shown to critically reduce survival of layer V cortical neurons. This neuro-supportive effect acted through fractaline (Cx3cl1) and IGF-1 release, as downregulation or deletion of Cx3cr1 or Igf1 led to layer V neuron death (Ueno et al.,

2013). Notably, microglia seem to only affect neuronal survival in a specific cortical layer, the reason of which is so far unknown.

#### 1.5.2.1.3 Synaptogenesis

Beside its association with dying neurons, microglia are also often found being lined up along developing axon fibers throughout development in different species (Cuadros et al., 1993; Herbomel et al., 2001; Innocenti et al., 1983; Ueno et al., 2013; Verney et al., 2010). This specific localization allows them to regulate neurons in yet another way, namely through synaptic pruning. In mice, synaptic pruning takes place during postnatal stages for remodeling of synapses and is crucial for the establishment of a functional, mature neuronal network (Arnold and Betsholtz, 2013). Microglia establish transient connections with neuronal synapses (Wake et al., 2009) and during synaptic maturation pre- and postsynaptic proteins have been found within phagocytic compartments of microglia, especially in the cerebral cortex, hippocampus and thalamus of postnatal mice (Paolicelli et al., 2011; Schafer et al., 2012; Tremblay et al., 2010). The engulfment of synapses by microglia is partially regulated by fractalkine signaling, with mice deficient in Cx3cr1 that have a transient decrease of microglia during early postnatal days exhibiting reduced synaptic pruning and less mature synapses 2-3 days after birth. This also results in deficiency in functional brain connectivity on an electrophysiological and behavioral level, apparent through reduced social interaction and increased repetitive behaviors (Paolicelli et al., 2011; Zhan et al., 2014). Moreover, the complement system is involved in microglial synaptic pruning. The complement factor C1q on neurons can activate C3 receptors (CR3) on microglia, leading to synaptic complement activation and subsequent phagocytosis and synaptic elimination (Lui et al., 2016; Stevens et al., 2007).

Through synaptic remodeling, microglia are directly involved in neuronal plasticity and can also affect synaptic structure in response external stimuli. In the juvenile mouse visual cortex, light deprivation has shown to result in increased association of microglia to dendritic spines and axon terminals, accompanied by the generation of phagocytic structures (Tremblay et al., 2010).

Beyond synaptic elimination, microglia also affect synaptic strength by releasing TNFα (Zhong et al., 2010) and by enhancing AMPA-type glutamate receptors on hippocampal neurons (Beattie et al., 2002).

#### *1.5.2.2 Role of microglia in neurogenesis*

Microglia are located closely to radial glia in different regions of the CNS, such as the hippocampus (Dalmau et al., 1997), retina (Santos et al., 2008; Sánchez-López et al., 2004) and the spinal cord where more than half of microglia are in contact with radial glia (Rigato et al., 2011). In vitro, microglia have been shown to direct migration and differentiation of embryonic cortical neural precursor cells (Aarum et al., 2003), regulate the size of the neural precursor pool (Cunningham et al., 2013) and facilitate differentiation of basal forebrain progenitors into cholinergic neurons (Jonakait et al., 2000). Moreover, *in vivo*, microglia can enhance neurogenesis and oligodendrogenesis in the early postnatal subventricular zone via the release of cytokines (Shigemoto-Mogami 2014). In the adult brain, microglia have shown to regulate adult hippocampal neurogenesis through apoptosis-coupled phagocytosis of new-born neurons (Sierra et al., 2010).

#### 1.5.2.3 Role of microglia in CNS angiogenesis

Microglia arrive in the brain at around the same time as the first endothelial cells and in the retina well before vascularization occurs in the first postnatal days. With their location in close proximity to the vasculature during CNS development (Checchin et al., 2006; Cuadros et al., 1993; 1992; Dalmau et al., 1997; Fantin et al., 2010; Herbomel et al., 2001; Monier et al., 2007; Rigato et al., 2011), microglia are in a prime position to interact with vessels and influence their development.

In fact, some parenchymal microglia have end-feet that are in direct contact with the basal lamina of microvessels (Lassmann et al., 1991) – termed juxtavascular microglia – and it has been shown that upon traumatic injury they migrate along the surface of blood vessels (Grossmann et al., 2002). In the retina, microglia are already present during postnatal angiogenesis, and are distributed as single cells with a regular density in front of the growing vascular plexus (Rymo et al., 2011).

Several laboratories have studied the function of microglia in vessel development after their depletion using either genetic models such as the $Csf1^{op/op}$ (homozygous inactivating mutation of Csf-1 gene) or $Pu.1^{-/-}$ mice that both lack microglia, or chemical/pharmacological ablation with clodronate liposomes or Csf1-antagonists. These experiments consistently showed an abnormally sparser vascular network accompanied by a reduction of vessel branches both in the developing brain and retina in absence of microglia (Checchin et al., 2006; Fantin et al., 2010; Kubota et al., 2009; Rymo et al., 2011). Microglia deletion did not, however, affect the number of tip cells, filopodia or the ingression of vessels (Fantin et al., 2010; Kubota et al., 2009).

Interestingly, in the hindbrain and retina, microglia processes associate closely with endothelial tip cells, especially between neighboring tip cells, and actively bridge vascular sprouts. This has been shown to promote endothelial tip cell fusion and anastomosis (Checchin et al., 2006; Fantin et al., 2010; Rymo et al., 2011). Also the time of microglia association with vessels in early development correlates with vessel growth. When the SVP is formed between E10.5 and E11.5 with the major phase of vascular networking, the number of microglia also peaks (Fantin et al., 2010). Consistent with this observation, hindbrain microglia numbers correlates with the number of vessel branch points (Fantin et al., 2010).

A model of aortic ring culture showed oriented migration of microglia towards the ring followed by an increased vessel branching. This effect was also achieved using microglia conditioned medium, indicating that soluble factors secreted by microglia can promote vessel sprouting (Rymo et al., 2011). Which factors microglia release and which mechanisms come into play to promote vessel growth, however, remains to be discovered. Due to phenotypic differences of vessel defects in mice lacking Vegf-A, it can be excluded that this is the factor regulating microglia-mediated angiogenesis (Fantin et al., 2010)

### 1.6 The CD95/CD95L signaling system

CD95 (also called Fas or Apo-1) is a type I transmembrane receptor of the tumor necrosis factor receptor (TNFR) superfamily. Receptors of this family sense the extracellular environment and communicate changes thereof through a variety of

intracellular effectors. Structurally, they are characterized by up to six well-conserved cysteine-rich domains (CRDs) at the N-terminal extracellular side that are responsible for specific receptor-ligand interaction (Locksley et al., 2001).

CD95 further belongs to the death receptor subfamily, which is defined by an 80 amino acid death domain (DD) in the cytoplasmic part (Bodmer et al., 2002). As the name of this subfamily indicates, CD95 was initially discovered to induce apoptotic cell death upon activation. However, an increasing amount of reports suggest that CD95 also has non-apoptotic and, paradoxically, even reverse roles in eliciting migration, invasion, inflammation and proliferation (Brint et al., 2013) (Figure 1.7). The functional details and the differential outcomes of CD95/CD95L signaling will be described in the following sections.

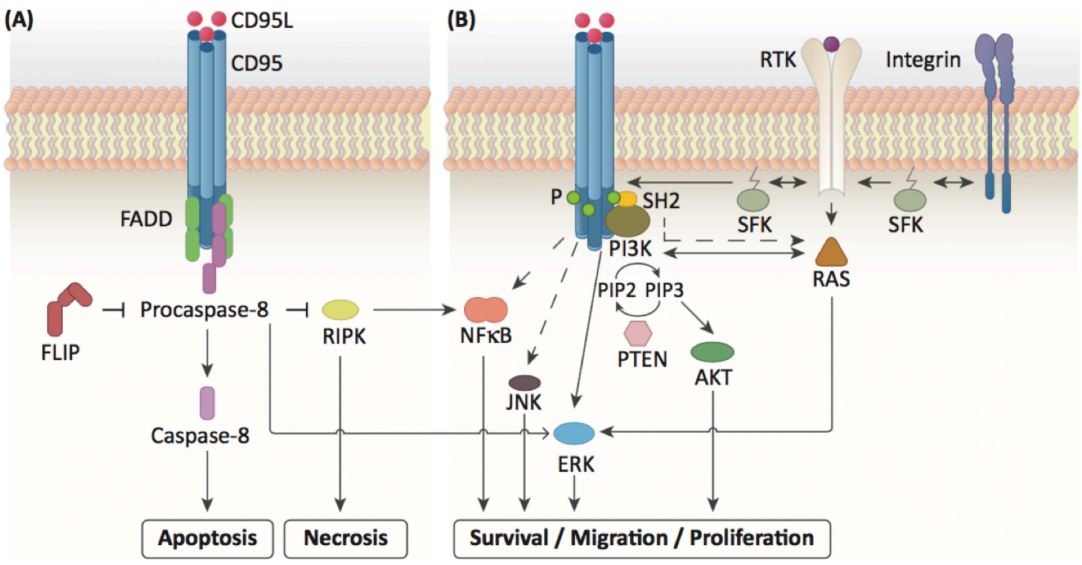


**Figure 1.7: The CD95 signaling system.** A) CD95 can activate apoptosis through FADD binding to its death domain, followed by recruitment of procaspase-8 and its autoproteolytic cleavage to caspase-8. Necroptosis can also be induced through inhibition of RIPK. B) CD95 can activate multiple non-apoptotic pathways through recruitment of SFKs and other SH2 adaptors such as p85 of PI3K to its phosphorylated death domain. This induces several downstream pathways including NFkB, JNK, Erk and Akt that ultimately lead to cell survival, migration or proliferation. Crosstalk between the apoptotic and non-apoptotic pathways exist, e.g. pro-caspase 8 can lead to activation of Erk. (adapted from (Martin-Villalba et al., 2013))

The CD95 receptor is activated through binding of its cognate ligand CD95L (or FasL). CD95L is a type II transmembrane protein of the TNF superfamily of cytokines. Similar to other family members, the ligand trimerizes through well-

conserved internal residues and exposes a less-conserved external surface that allows receptor-specific binding (Locksley et al., 2001). Binding of trimerized CD95L induces trimerization of the CD95 receptor and triggers downstream signaling. CD95L is normally membrane-bound, but can be cleaved by metalloproteases to generate a soluble form (Kayagaki et al., 1995; Tanaka et al., 1998).

### 1.6.1 Apoptotic function of CD95

CD95 was the first death receptor identified and was discovered as a cell surface molecule expressed on human lymphocytes that triggers apoptosis upon stimulation with agonistic antibodies (Trauth et al., 1989; Yonehara et al., 1989). Extensive studies of the signaling pathway elicited by CD95 activation has led to a detailed picture of how CD95 mediates apoptosis.

The first step is the binding of trimerized CD95L to CD95 which leads to clustering of the receptor on the cell membrane and the stabilization of an open confirmation of its intracellular DD. This allows the recruitment of the DD-containing protein FADD (Fas associated protein with death domain) which binds to CD95's DD through homotypic interactions via its own DD (Scott et al., 2009). FADD possess a death effector domain (DED) to which procaspase-8 is recruited. Once the number of procaspase-8 exceeds the number of FADD at the receptor, the caspase-activating chain can cluster and together with the regulator c-FLIP the death-inducing-singaling complex (DISC) is formed (Dickens et al., 2012; Peter and Krammer, 2003; Schleich et al., 2012). Subsequently, caspase-8 is activated through self-cleavage and triggers caspase-3 either directly or indirectly via the mitochondrial apoptotic pathway, eventually resulting in apoptotic cell death (Kischkel et al., 1995) (Figure 1.7).

CD95-mediated cell death has been implicated in many processes both during homeostasis and disease. Particular the immune system depends on CD95/CD95L signaling for proper functioning. For instance, CD95L has been shown to be responsible for the perforin-independent cytotoxic activity of killer T cells (Berke, 1995; Lowin et al., 1994). Moreover, immunological tolerance in immune privileged sites has been suggested to be induced through CD95L-induced cell death of inflammatory cells (Griffith et al., 1996; Nagata, 1997). In mice with reduced

expression of CD95 (*lpr* ~ lymphoproliferation) or non-functional CD95L (*gld* ~ generalized lymphoproliferative disease), which have been extensively used as animal models for CD95/CD95L, lymphadenopathy and a systemic lupus erythematosus like autoimmune disease develops. This is caused by the lack of activation-induced cell death in T-cells and the resulting accumulation of aberrant T-cells (Alderson et al., 1995; Brunner et al., 1995; Takahashi et al., 1994; Watanabe-Fukunaga et al., 1992).
In cancer, CD95L on cytotoxic T-cells and NK cells have shown to kill cancer cells expressing CD95. However, CD95L expression on tumor cells has also suggested to be the mechanism for tumor immune evasion by inducing death of $CD95^+$ infiltrating cytotoxic immune cells, known as the "tumor strikes back" effect (Peter et al., 2015).

### 1.6.2 Non-apoptotic functions of CD95

In the recent past, it became slowly clear that in a context-dependent manner, CD95 can also transmit non-apoptotic cellular functions, such as cell proliferation, migration and inflammation.
First indications of a apoptosis-independent function of CD95 already appeared as early as 1993, where proliferation was found to be stimulated in CD3-activated T-cells (Alderson et al., 1993; Desbarats et al., 1999) and fibroblasts (Freiberg et al., 1997).
Further evidence for the non-apoptotic role of CD95 came from the cancer field where realization dawned that many different types of cancer cells are resistant to CD95-induced apoptosis. Stimulation of cancer cells with CD95 - once thought to be a good therapeutic approach to treat tumors through inducing apoptosis - led to the activation of signaling pathways such as Erk1/2, NfκB that increased motility and invasiveness of the tumor cells (Barnhart et al., 2004). Moreover, CD95 has shown to support tumor growth in various cancers via JNK and Jun pathways (Chen et al., 2010a) (Figure 1.7).
Outside of the cancer field, CD95 has also exhibited non-apoptotic functions. Although highly liver toxic under homeostatic conditions (Ogasawara et al., 1993), CD95 can accelerate liver regeneration after partial hepatectomy (Desbarats and Newell, 2000), possibly due to activation of EGFR and Erk in quiescent hepatic stellate cells (Reinehr et al., 2008).

The non-apoptotic functions of CD95 seem to be also mediated via the DD. Within CD95's DD lies a modified immunoreceptor tyrosine-based activatory/inhibitory-like motif (ITAM/ITIM) consisting of the amino acid sequence YXXL that has been suggested to recruit alternative players. The tyrosine-residue (Y) within the motif is susceptible to phosphorylation through members of the Src-family kinase (SFK) thereby providing a platform for binding of SH2 domain containing proteins and leading to activation of various non-apoptotic pathways (Sancho-Martinez and Martin-Villalba, 2009; Schlottmann et al., 1996).

### 1.6.3 Regulation of the pro- and anti-death decision via CD95

With CD95 seemingly signaling for opposite functions it is obvious to ask how the switch between life and death is regulated. The mechanisms of this molecular switch are not fully elucidated and seem to be highly context-dependent. The most likely scenario is a concomitant activation of both apoptotic and non-apoptotic signaling components upon CD95 activation, where the balance of apoptosis-inhibiting factors and the availability of cell-growth-promoting kinases eventually determine the ultimate outcome.

Three main levels of regulation can be found for the molecular switch CD95: 1) extracellular level, 2) DISC level and 3) mitochondria level (Yurchenko et al., 2012).

On the extracellular level, it has been suggested that the membrane-bound form of CD95L is responsible for apoptosis while soluble CD95L drives other cellular functions (O' Reilly et al., 2009), although this theory is still controversial. Moreover, low concentrations of CD95L could result in survival signaling (Lavrik et al., 2007).

At the level of the DISC, reduced expression of FADD or caspase-8 can lead to decreased apoptotic induction (Tourneur L, Oncogene, 2003 Fulda S, Oncogene 2001). Furthermore, the protein cFLIP (cellular FLICE inhibitory protein) can inhibit the interaction of caspase-8 with the DISC, thus preventing execution of apoptosis (Irmler et al., 1997; Lavrik and Krammer, 2011). In apoptosis-resistant glioma cell lines, it has further been shown that FADD association with CD95 can be inhibited by the adaptor protein TRIP6 that directly binds to the intracellular domain of CD95. TRIP6 leads to activation of NfκB or phosphorylation by src family kinases (SFK) to induce migration (Lai et al., 2010).

At the mitochondria, deregulation of anti-apoptotic proteins such as the Bcl2 family proteins or XIAPs can tip the balance between life and death as well (Igney and Krammer, 2002).

### 1.6.4 CD95 in the central nervous system

The relevance of the CD95/CD95L signaling system in the nervous system has received little attention for many years due to the more obvious immune system-related defects of the *lpr* and *gld* mutant mice. In the late 90s however, first studies showed wide expression of CD95 in the developing brain of rodents. CD95 was mainly found in cells of the ventricular/subventricular zone (VZ/SVZ), hippocampus, cerebellum and cortex. Expression begins at E14.5-E15.5, peaks at early postnatal stages and declines thereafter (Cheema et al., 1999; Park et al., 1998). After the completion of neural development, CD95 expression is reduced to an almost undetectable level, except for the neurogenic regions of the SVZ and dentate gyrus (DG), where CD95 activation has been suggested to increase neural stem cell survival and differentiation through c-src/PI3K/Akt (Corsini et al., 2009).

CD95L seemed to follow a similar expression pattern as CD95 during development (French et al., 1996; Shin et al., 2002; Zuliani et al., 2006), however, ligand expression has been shown to be primarily present in neuroglial cells, including microglia, within white matter regions (Shin et al., 2002).

Early studies related CD95 expression to the apoptosis of immature neurons (Cheema et al., 1999; Le-Niculescu et al., 1999) – however, these studies were conducted *in vitro* and might not reflect the actual situation in the brain. In fact, CD95 has been shown to promote neuronal growth in several studies. First, adult *lpr* mice with the Murphy Roths Large (MRL) background – called MRL have also been shown to have abnormal neuronal morphology with reduction of dendrites and atrophy of dendritic spines in pyramidal neurons of the parietal cortex and hippocampus (Sakić et al., 1998). Second, activation of CD95 in developing or regenerating neurons after sciatic nerve injury enhances neurite outgrowth through Erk activation and subsequent expression of p35, a neuron-specific activator of Cdk5 (Desbarats et al., 2003). Thirdly, *lpr* or *gld* mice display abnormal branching of hippocampal neurons with less complex dendritic trees than wildtype mice. The CD95-induced neuronal

branching seemed to be caspase-independent and required dephosphorylation of Tau that promotes assembly and stabilization of microtubules (Ruan et al., 2008; Zuliani et al., 2006). Lastly, the cytoplasmic membrane proximal domain of CD95 was found to recruit the adaptor protein ezrin, which in turn activates the small GTPase Rac1 to induce neurite growth in cortical neurons (Ruan et al., 2008).

### 1.6.5 CD95 in brain tumors

Many types of tumors in the brain such as gliomas, oligodendrogliomas and ependymomas express CD95, and in gliomas, expression positively correlates with the degree of malignancy (Frankel et al., 1999; Gratas et al., 1997; Kleber et al., 2008; Riffkin et al., 2001; Tachibana et al., 1996). CD95L is also expressed in gliomas, preferentially at the tumor/host interface and close to vessels within the tumor (Kleber et al., 2008). Interestingly CD95L has shown to be highly epxressed in microglia of brain with glioma transplants (Badie et al., 2001).

Similar to other tumor cells, glioma cells are resistant to apoptosis-induction by CD95 (Barnhart et al., 2004; Kleber et al., 2008; Weller et al., 1994). Instead, CD95 acts as a key driver of basal invasion by recruiting the src-family kinase (SFK) Yes and activating PI3K and Akt to induce the expression of matrix-metalloproteases MMP-2 and MMP-9 (Kleber et al., 2008). Moreover, a new form of cell death called "death induced by CD95 or CD95L elimination" has been described for the requirement of CD95/CD95L for cancer cell survival, including glioma cells. Elimination of either receptor or ligand leads to death that resembles a necrotic form of mitotic catastrophe (Hadji et al., 2014). CD95 activation on glioma cells can also result in the induction of the chemokines MCP-1, IL-8 and IL-6 through the Erk pathway that together form a tumor-promoting inflammatory environment (Choi et al., 2001; 2002). Another study conducted by our lab has shown that CD95 expression further associates with glioblastoma stemness and epithelial to mesenchymal transition (EMT), features required for tumor maintenance (Drachsler et al., 2016).

The tumor growth-promoting effect of CD95 has led to the development of a therapeutic approach to treat grade IV glioblastoma. A fusion protein consisting of the extracellular domain of the CD95 receptor and the Fc domain of IgG, called APG101, has been designed as a decoy to block CD95L. Phase II clinical trial has so

far shown promising results with an increased percentage of patients reaching six months of progression free survival using APG101 in combination with radiotherapy (Bendszus et al., 2012).

### 1.6.6 CD95 in angiogenesis

Endothelial cells widely express CD95, and similar to other systems, both pro-apoptotic as well as non-apoptotic functions have been described for CD95 in endothelial cells, either resulting in inhibition or promotion of angiogenic processes.

Generally, endothelial cells are resistant to CD95L-induced apoptosis (Aoudjit and Vuori, 2001; Richardson et al., 1994; Sata and Walsh, 1998; Sata et al., 2000; Suhara et al., 2001; Takemura et al., 2004). This resistance has been explained by PI3K/Akt activation upon CD95L stimulation that promotes survival and concomitant upregulation of the regulator c-FLIP which blocks caspase-8 activity and thus apoptosis-induction (Aoudjit and Vuori, 2001; Suhara et al., 2001; Takemura et al., 2004). Consistently, it has been shown that CD95L-induced Akt phosphorylation mediates endothelial nitric oxide synthase (eNOS) expression that regulates vascular tone and proliferation. In absence of CD95, *lpr* mice exhibit hypertension with endothelial dysfunction (Takemura et al., 2004).

Further, CD95 can also actively promote angiogenesis. Local stimulation of CD95 *in vivo* using an agonistic CD95 antibody triggers inflammation and pronounced neoangiogeenesis independent of apoptosis (Biancone et al., 1997). This might be elicited indirectly through CD95-induced inflammation, however, evidence of direct stimulation of angiogenesis comes from a study that shows increased secretion of VEGF by human umbilical vein endothelial cells (HUVECs) after exposure to CD95L (Marx et al., 1999).

Under certain conditions, CD95 has been reported to activate apoptosis in endothelial cells, for instance under hypoxia, after detachment and after stimulation with TNFα or VEGF (Aoudjit and Vuori, 2001; Cardier et al., 1999; Sata and Walsh, 1998).

Furthermore, a number of studies following the traditional path of thought of CD95, implicates it in apoptosis during angiogenic processes *in vivo*, especially in different models of retinopathy. The main problem in retinopathies is the overgrowth of vessels that can eventually lead to blindness. In *lpr* and *gld* mice, exacerbated vessel growth

was observed in models of age-related macular degeneration (AMD) and retinopathy of prematurity, supposedly owing to a lack of apoptosis in endothelial cells (Barreiro et al., 2003; Davies et al., 2003; Kaplan et al., 1999). In AMD, CD95L expressed on retinal pigment epithelial cells was shown to be responsible for apoptosis activation in CD95-expressing endothelial cells beneath the retina (Kaplan et al., 1999).

During development, CD95 on endothelial cells has been reported to be responsible for pruning of the vasculature by CD95L expressing T-leukocytes that induce endothelial-cell apoptosis (Ishida et al., 2003). Moreover, it has been suggested that endogenous angiogenesis inhibitors like thrombospondin 1 (TSP1) and pigment epithelium-derived factor (PEDF) act through upregulation of CD95L on endothelial cells to induce their apoptosis (Volpert et al., 2002).

Unlike the receptor, CD95L is only expressed at low levels or is completely absent in endothelial cells *in vivo* (Cardier et al., 1999; Motz et al., 2014), although expression in cultured HUVECs has also been shown (Sata and Walsh, 1998; Sata et al., 2000). In the vasculature of various tumors however, CD95L seems to be upregulated on endothelial cells by factors released by tumor cells, and contributes to tumor immune evasion through apoptosis-induction of cytotoxic T-cells (Motz et al., 2014).

## 1.7 Aims of the study

In this dissertation the role of CD95 in developmental regulation of the neurovascular system as well as in brain tumor angiogenesis is examined.

CD95 has been reported to be expressed by endothelial cells and neurons in the CNS. However, functional studies thereof in the two systems have been often contradicting. Previous studies in our laboratory have uncovered that CD95 promotes neuronal branching during CNS development in a neuron-specific manner. As the vascular and nervous system are highly dependent on each other and are often co-regulated by the same set of molecules, we hypothesized that CD95 may act as an angioneurin to promote both endothelial cell as well as neuronal complexity during development.

As a first aim, we studied the effect of endothelial-specific deletion of CD95 on vessel growth. As we discovered that the ligand for the CD95 receptor – CD95L – is mainly expressed by microglia, we further analysed the phenotype of mice containing a deletion of CD95L in microglia.

A second aim of the study was to identify the molecular mechanisms governing CD95's function in vessel development. Interaction partners and potential downstream effectors of CD95 were examined to decipher how CD95 may promote vessel growth.

Developmental mechanisms of growth are often exploited by cancers and we further hypothesized that CD95 may also play a role during tumor angiogenesis in the brain. Thus, we studied the effect of CD95 stimulation as well as deletion on angiogenesis in glioblastoma, one of the most vascularized tumors.

# 2. MATERIALS AND METHODS

## 2.1 Materials

### 2.1.1 Chemicals and Reagents

**Table 2.1**: List of chemicals, reagents and kits

| Chemical/Reagent/Kit | Manufacturer |
|---|---|
| β-mercaptoethanol | Sigma |
| Accutase | Sigma |
| Agarose | Sigma |
| Agilent high-sensitivity DNA kit | Agilent |
| Amerham Hyperfilm ECL | GE Healthcare |
| B27 supplement | Invitrogen |
| BCA kit | Thermo Fisher Scientific |
| BD PharmLyse Lysing buffer | BD Biosciences |
| bFGF | Relia tech |
| Bovine serum albumin (BSA) | Sigma |
| Brain tissue dissociation kit (P) | Miltenyi Biotec |
| Calcein AM | Life technologies |
| CD95L-T4 | Apogenix GmbH |
| Collagenase/Dispase | Roche |
| ColorPlus Prestained Protein Ladder Broad Range | NEB |
| cOmplete protease inhibitor cocktail tablets | Roche |
| C tubes | Miltenyi Biotec |
| DeadEnd Fluorometric TUNEL System | Promega |
| dNTP mix (10 mM) | Fermentas |
| Dulbecco's Modified Eagles Medium (DMEM) | Invitrogen |
| Dithiothreitol (DTT) | Thermo Fisher Scientific |
| Dynabeads M-280 Streptavidin | Thermo Fisher Scientific |
| Enhanced chemoluminescence substrate (ECL) | Perkin Elmer |
| EGF | Promocell |
| EGM-2 Bullet kit | Lonza |

| Chemical/Reagent/Kit | Manufacturer |
|---|---|
| ERCC Spike-In mix | Ambion |
| Ethanol | Riedel de Haen |
| Eukitt Mounting Medium | Sgima |
| FASER kit – APC | Miltenyi Biotec |
| FD Rapid GolgiStain Kit | FD Neurotechnologies |
| Fetal calf serum (FCS) | Biochrom |
| Fluoromount-G | Southern Biotech |
| 2% gelatin | Sigma |
| GoTaq Flexi Green DNA polymerase | Promega |
| Glutamine | Life Technologies |
| Glycerol | Sigma |
| Glycine | Sigma |
| Hank's Balanced Salt Solution (HBSS) | Invitrogen |
| Heparin Cell Culture Grade | Sigma |
| Hoechst 33342 | Biotrend |
| Human Angiogenesis Antibody Array | R&D Systems |
| Hydrochloric acid (HCl) | VWR |
| Isoflurane | Baxter |
| Ketavet (100mg/ml) | Pfizer |
| 4x Laemlli Buffer | Bio-Rad |
| Lipofectamin 2000 | Invitrogen |
| L-Glutamine (100x) | Invitrogen |
| LY294002 | Cell Signaling |
| MangoTaq DNA polymerase | Bioline |
| Matrigel | BD Biosciences |
| Matrigel (growth-factor reduced) | BD Biosciences |
| mirVana miRNA Extraction kit | Ambion |
| Mix-n-Stain CF488A Antibody Labelling kit | Biotium |
| Nitrocelulose transfer membrane | Bio-Rad |
| Neural Tissue Dissociation kit | Miltenyi Biotec |
| Neurobasal A Medium | Invitrogen |

| Chemical/Reagent/Kit | Manufacturer |
|---|---|
| NEB-Next Library Preparation kit | NEB |
| PD98095 | Cell Signaling |
| Oligonucleotide primers | MWG |
| ON-TARGET plus Non-targeting pool | Dharmacon |
| On-TARGET plus Human FAS SMARTpool | Dharmacon |
| Opti-Mem | Gibco |
| 4% Paraformaldehyde (PFA) in phosphate buffer | Roth |
| 1 x PBS (without $Mg^{2+}$ and $Ca^{2+}$) | PAA |
| PCR $H_2O$ | Braun |
| Penicillin/Streptomycin | Invitrogen |
| Pierce Co-Immunoprecipitation Kit | Thermo Fisher Scientific |
| Pierce IP Lysis Buffer | Thermo Fisher Scientific |
| PhosSTOP | Roche |
| Potassium chloride (KCl) | AppliChem |
| Potassium phosphate monobasic ($KH_2PO_4$) | Gerbu |
| QuantiTect Primer Assay, Fas, mouse | Qiagen |
| Qubit dsDNA high-sensitivity (HS) kit | Life Technologies |
| RNAlater | Ambion |
| Rnase-free Dnase set | Qiagen |
| Rnase-free $H_2O$ | Ambion |
| RNaseZAP | Sigma |
| Rompun (2%) | Bayer |
| Skim milk powder | Roth |
| SMARTer Ultra Low RNA Kit for Illumina Sequencing – HA | Clontech |
| Sodium azide (NaN3) | Merck |
| Sodium citrate tribasic dehydrate | Sigma |
| Sodium chloride (NaCl) | Sigma |
| Sodium choloride 0.9% sterile (NaCl) | Braun |
| Sodium dihydrogen phosphate ($NaH_2PO_4$) | Sigma |
| Sodium dodecyl sulphate (SDS) | Sigma |

| Chemical/Reagent/Kit | Manufacturer |
|---|---|
| Sodium hydrogen phosphate ($Na_2HPO_4$) | Sigma |
| Sodium hydroxide (NaOH) | Sigma |
| Sunflower Oil | Sigma |
| SuperFrost slides | Roth |
| Sucrose | Sigma |
| SYBR Green Master Mix | Life technologies |
| Tamoxifen | Sigma |
| TGX Gels (Mini-Protean or Criterion, 4-20%, 10%, 12%) | Bio-Rad |
| Tools for mouse surgery | Fine Science Tools |
| Trans-Blot Turbo Transfer Buffer | Bio-Rad |
| Tris base | Sigma |
| Triton X-100 | Sigma |
| Trypsin-EDTA (0.05%) | Invitrogen |
| Tween-20 | Sigma |
| Western Bloting Filter Paper | Bio-Rad |
| Xylene | Sigma |

### 2.1.2 Solutions and Media

**Table 2.2**: List of solutions and media

| **Solutions** | **Composition** |
|---|---|
| **Histology and Immunofluorescence** | |
| Blocking buffer for IHC | Triton X-100, 0.3%<br>FCS 5%<br>Dissolve in PBS |
| FACS staining buffer | PBS 1x<br>FCS 5% |
| PBS (20x) | 160 g/L NaCl<br>23 g/L $Na_2HPO_4$<br>4 g/L KCl |

| | |
|---|---|
| | 4 g/L $KH_2PO_4$<br>Fill up to 1L with H2O and adjust pH to 7.4 |
| **Solutions** | **Composition** |
| Perfusion solution | 5.71 mg/ml Ketavet<br>2.8 mg/ml Rompun<br>in NaCl 0.9% |
| 0.1 M Phosphate buffer | 69 ml 0.2 M Monobasic Stock ($NaH_2PO_4$, 13.9 g/500ml)<br>231 ml 0.2M dibasic stock solution ($Na_2HPO_4$, $7H_2O$, 53.65 g/L)<br>Fill up to 600 ml (pH7.3) |
| 30% sucrose buffer | 30g sucrose in 100ml Millipore $H_2O$ |
| Citric acid buffer for antigen retrieval | 10 mM sodium citrate tribasic dehydrate<br>0.05% Tween-20<br>Dissolve in VE-$H_2O$ and ajust to pH 6.0 |
| Tamoxifen (TAM) | Tamoxifen 10 mg/ml<br>In a 9:1 mixture of sunflower oil and EtOH |

| **Cell culture** | |
|---|---|
| Endothelial cell medium | EBM2 |
| Neurobasal A medium | 500 ml Neurobasal A medium<br>10 ml B27 Supplement (50x)<br>5ml L-Glutamine (200mM)<br>5ml Penicillin/Streptomycin (10 000 units/ml and 10 000 µg/ml)<br>2 µg/ml Heparin<br>20 ng/ml bFGF<br>20 ng/ml EGF |

| **Western blot** | |
|---|---|
| PBS-Tween | Tween-20 0.1% |

| | |
|---|---|
| | Dissolve in PBS |
| Running buffer | 10 g/l Tris Base<br>30.28 g/l glycine<br>150 g/l SDS |

### 2.1.3 Antibodies

**Table 2.3**: List of antibodies

| **Antibodies for flow cytometry** | | | | | |
|---|---|---|---|---|---|
| **Antibody** | **Clone** | **Isotype** | **Conjugate** | **Dilution** | **Manufacturer** |
| CD11b | M1/70 | Rat IgG2b | FITC | 1:200 | eBioscience |
| CD31 | 390 | Rag igG2a | PE/FITC | 1:100 | eBioscience |
| CD45 | 30-F11 | Rag IgG2b | APC-Cy7 | 1:200 | BD |
| CD95 | Jo2 | Hamster IgG2, λ2 | PE-Cy7 | 1:100 | BD |
| CD95L | MFL3 | Hamster IgG | APC | 1:100 | BD |
| Prom1 (CD133) | 13A4 | Rat IgG1 | PerCP-eFluor710 | 1:75 | eBioscience |
| PSD95 | 7E3-1B8 | Mouse IgG1 | Alexa 488 (conjugated with Mix-n-Stain kit) | 1:100 | Life technologies |
| O4 | O4 | Mouse IgM | PE | 1:25 | Miltenyi Biotec |
| Glast | ACSA-1 | Mouse IgG2a | PE | 1:30 | Miltenyi Biotec |

| **Primary antibodies for immunohistochemistry** | | | | | |
|---|---|---|---|---|---|
| **Antibody** | **Clone** | **Isotype** | **Conjugate** | **Dilution** | **Manufacturer** |
| CD31 | Poly-clonal | Rabbit IgG | - | 1:100 | Abcam (a28364) |

| Antibody | Clone | Isotype | Conjugate | Dilution | Manufacturer |
|---|---|---|---|---|---|
| Collagen IV | Poly-clonal | Rabbit | - | 1:100 | Novotec |
| Iba1 | Poly-clonal | Rabbit IgG | - | 1:100 | Wako |
| Iba1 | Poly-clonal | Goat IgG | - | 1:100 | Abcam (ab107159) |
| IsolectinB4 | - | - | Alexa647/ Alexa568 | 1:100 | Life technologies |
| pH3 | 3H10 | Mouse IgG1 | - | 1:1000 | Millipore |
| pH3 | Poly-clonal | Rabbit | - | 1:100 | Cell Signaling |
| Ki67 | SP6 | Rabbit | | 1:100 | Novus Biologicals |

**Secondary antibodies for immunohistochemistry**

| Antibody | Clone | Isotype | Conjugate | Dilution | Manufacturer |
|---|---|---|---|---|---|
| Mouse | Poly-clonal | Goat IgG1/ Donkey IgG | Alexa488 | 1:400 | Life technologies |
| Rabbit | Poly-clonal | Goat IgG1/ Donkey IgG | Alexa555 | 1:400 | Life technologies |
| Goat | Poly-clonal | Donkey IgG | Alexa488 | 1:400 | Life technologies |

**Primary antibodies for immunoprecipitation and Western blot**

| Antibody | Clone | Isotype | Conjugate | Dilution | Manufacturer |
|---|---|---|---|---|---|
| Akt | Poly-clonal | Rabbit | - | 1:1000 | Cell signaling (#9272) |
| Apo1 | | Rabbit | - | 10 ug | Apogenix |
| CD95 | 7C10 | Rat IgG2a | - | 1:500 | Acris |

| Antibody | Clone | Isotype | Conjugate | Dilution | Manufacturer |
|---|---|---|---|---|---|
| Erk(1/2) | Poly-clonal | Rabbit | - | 1:1000 | Cell signaling (#9102) |
| Gapdh | Fl-335 | Rabbit IgG | - | 1:2000 | Santa Cruz |
| IRS1 | Poly-clonal | Rabbit | - | 1:1000 | Santa Cruz |
| p85 | Poly-clonal | Rabbit IgG | - | 1:1000 | Millipore (06-195) |
| Phospho-Erk(1/2) | Poly-clonal | Rabbit | - | 1:1000 | Cell signaling (#9101) |
| phospho-Akt (Ser473) | Poly-clonal | Rabbit | - | 1:1000 | Cell signaling (#9271) |
| SFK | Poly-clonal | Rabbit | - | 1:1000 | Cell Signaling (#2108) |

**Secondary antibodies for Western blot**

| Antibody | Clone | Isotype | Conjugate | Dilution | Manufacturer |
|---|---|---|---|---|---|
| Rabbit | Poly-clonal | IgG | HRP | 1:5000 | Jackson Immuno-Research |
| Rat | Poly-clonal | IgG | HRP | 1:5000 | Jackson Immuno-Research |

### 2.1.4 Peptides

**Table 2.4**: List of peptides

| Species | Name | Amino acid sequence |
|---|---|---|
| Human | Scrambled control (hScr) | SS-Biotin-SGSG-LKDKHTE(p)YKAGKILD |
| | Alanine mutant | SS-Biotin-SGSG-HGKKEAADTLIKDLK |

| | | |
|---|---|---|
| | (hA) | |
| | Wildtpe CD95 (hY) | SS-Biotin-SGSG-HGKKEAYDTLIKDLK |
| | Phosphorylated CD95 (hpY) | SS-Biotin-SGSG-HGKKEA(p)YDTLIKDLK (with hydrolytically stable phosphotyrosine analogue F(CF2PO3)) |
| Mouse | Scrambled control (mScr) | SS-Biotin-SGSG-KA(p)YHKDDSKLGLGQI |
| | Alanine mutant (mA) | SS-Biotin-SGSG-HGKSDAAQDLIKGLK |
| | Wildtpe CD95 (mY) | SS-Biotin-SGSG-HGKSDAYQDLIKGLK |
| | Phosphorylated CD95 (mpY) | SS-Biotin-SGSG-HGKSDA(p)YQDLIKGLK (with hydrolytically stable phosphotyrosine analogue F(CF2PO3)) |

The peptides were synthesized by PSL GmbH, Heidelberg

### 2.1.5 Primers

**Table 2.5**: List of primers for genotyping

| **Name** | **Nucleotide sequence (5' – 3')** |
|---|---|
| CD95 forward | GGCTTTGGAAAGGAATTTCCTCCTAAGAAG |
| CD95 reverse | TGCAGTTGCTGAGATGAACCATTTTCTCTG |
| CD95L forward | GAA CAC AGA CCT ACA CAG AAG TCA CAT C |
| CD95L reverse | TGCAGTTGCTGAGATGAACCATTTTCTCTG |
| LysM Cre forward | CCCAGAAATGCCAGATTACG |
| LysM Cre reverse | CTTGGGCTGCCAGAATTTCTC |
| Cdh5-CreERT2 forward | GCC TGC ATT ACC GGT CGA TGC AAC GA |
| Cdh5-CreERT2 Reverse | GTG GCA GAT GGC GCG GCA ACA CCA TT |

## 2.2 Methods

### 2.2.1 Animal Experiments

#### *2.2.1.1 Animals*

Experimental mice were housed in the animal facilities of the German Cancer Research Center (DKFZ, Heidelberg, Germany) at a twelve-hour dark/light cycle under standard conditions and had ad libitum access to food and water.

All animal experiments were performed in accordance with institutional guidelines of the German Cancer Research Center and were approved by the Regierungspräsidium Karlsruhe, Germany (G309/14).

C57BL/6J mice were purchased from Charles River or bred in house at the DKFZ Center for Preclinical Research core facility.

$CD95^{fl/fl}$ mice (carrying a loxP-flanked CD95 gene) were a kind gift from K. Rajewsky. Cdh5-(PAC)-$CreER^{T2}$ mice were a kind gift from R. Adams (Sorensen et al., 2009). $CD95L^{fl/fl}$ mice were a kind gift from M. Lévi-Strauss (Karray et al., 2004). LysM-Cre mice were purchased from Jackson Laboratories (Bar Harbor, Maine).

$CD95^{fl/fl}$ mice were crossed with the Cdh5-(PAC)-$CreER^{T2}$ line to generate $CD95^{fl/fl}$;Cdh5-(PAC)-$CreER^{T2}$ mice. Newborn $CD95^{fl/fl}$;Cdh5-(PAC)-$CreER^{T2}$ pups were intragastrically injected with 50 µg of tamoxifen in 50 µl sunflower oil/10% ethanol at postnatal days P1, P2, P3 and P5. Tamoxifen-induced cre negative littermates were used as controls. For tumor implantation, adult mice (8-10 weeks) were injected with 250mg/kg tamoxifen in 100 µl sunflower oil/10% ethanol once per day for 5 days.

$CD95L^{fl/fl}$ mice were crossed with the LysM-Cre line to generate $CD95L^{fl/fl}$;LysM-Cre mice. Cre negative littermates were used as controls.

Fox Chase SCID® Beige mice for transplantation experiments were purchased from Charles River.

**Table 6**: List of experimental mice

| Short name | Full name | Description | Reference |
|---|---|---|---|
| C57BL/6J | | Wildtype mice | |
| Cdh5-(PAC)-CreER$^{T2}$ | B6-Tg(Cdh5-cre/ERT2)1Rha Fastm1Cgn | Tamoxifen-inducible Cre recombinase under the control of endothelial-cell specific promoter Cdh5 | Sorensen et al., 2009 |
| CD95$^{fl/fl}$ | B6-Fastm1Cgn | Mice harboring loxP-flanked exon IX of CD95 that codes for its death domain | Hao et al., 2004 |
| CD95L$^{fl/fl}$ | B6-Fasltm1Lest | Mice harboring loxP-flanked CD95L gene | Karray et al., 2004 |
| Fox Chase SCID Beige | CB17.Cg-Prkdcscid Lyst bg /Crl | Immune-deficient mice lacking T- and B-cells and with defective natural killer cells | |
| LysM-Cre | B6.129P2-Lyz2tm1(cre)Ifo/J | Cre recombinase under the control of macrophage-specific promoter LysM | Clausen et al., 1999 |

#### *2.2.1.2 Orthotopic injection of SMA560 cells*

10,000 SMA560 cells in 2 µl were injected into the striatum of CD95$^{fl/fl}$ or CD95$^{fl/fl}$;Cdh5-CreER$^{T2}$ mice at the coordinates x=0, y=2, z=3 from the bregma using a stereotact.

#### *2.2.1.3 Xenografting and treatment with CD95L beads*

SCID beige mice (8 -10 weeks old, female) were subcutaneously transplanted with 10,000 GBM cells in 100 µl matrigel. Tumor size was measured every week with a caliper and after establishment of tumors, mice were intravenously injected with 2x10$^6$

CD95L-coated beads through the tail vein. Two weeks later animals were sacrificed and tumors were retrieved after transcardial perfusion.

#### *2.2.1.4 Perfusion*

Mice were anesthetized by intraperitoneal injection of 800 µl perfusion solution. After the thoracic cavity was opened, the heart was exposed and transcardial perfusion was performed with 10 ml of HBSS. For immunohistochemistry, the mice were additionally perfused with 10 ml of 4% PFA.

### 2.2.2 Cell and Tissue Biology

#### *2.2.2.1 Culture of human umbilical vein endothelial cells (HUVECs) and bEnd.3cells*

HUVECs (Lonza) were maintained in endothelial basal medium-2 (EBM-2, Lonza) supplemented with EGM-2 SingleQuot Kit Supplements and Growth Factors (Lonza) on 0.1% gelatin-coated flasks. bEnd.3 cells were are gift of Carmen Ruiz de Almodovars lab and were maintained in DMEM supplemented with 1x glutamine and 1x penicillin/streptomycin. Cells were kept in 5% $CO_2$ at 37˚C and HUVECs were used up to passage 6 for experiments.

For CD95L stimulation, HUVECs were starved on endothelial basal medium-2 with 0.1% FCS and bEnd.3 cells in DMEM with 0.1% FCS for 12 hours and subsequently treated with 40 ng/ml CD95L-T4 (Kleber et al., 2008) for 5, 10, 15, 20 or 30 min.

For treatment with LY294002 (Cell Signaling) and PD98095 (Cell Signaling), cells were pretreated with different concentrations of the inhibitors for 1 hour, after which inhibitors were removed and replace by medium with CD95L-T4.

#### *2.2.2.2 Endothelial tube formation assay*

The endothelial tube formation assay was performed according to Arnaoutova et al. (Arnaoutova et al., 2009). 80 µl of growth factor reduced matrigel was plated in each well of a 96-well plate and allowed to gel at 37˚C for 30 min. 15000 HUVECS in EBM-2 supplemented with 35 ng/ul bFGF were seeded per well and the formation of endeothelial tubes was assessed after 12 hours. For visualization, tubes were stained with the live cell dye Calcein AM (8 µg/ml) before imaging. Experiments were performed in triplicates.

For CD95L stimulation, HUVECs were stimulated for 4 hours on control- or CD95L (CD95L-T4) coated lipid membranes prior to plating on matrigel. For siRNA experiments, knockdown was allowed to occur for 48 hrs and cells were then plated on matrigel.

#### *2.2.2.3 siRNA-mediated knockdown in HUVECs*

For siRNA-mediated knockdown of endothelial cells, 100 000 HUVECs were plated in one well of a 6-well-plate. On the next day, 50 nM siRNA targeted against CD95 (On-TARGET plus Human FAS SMARTpool, Dharmacon, GAACAUGGAAUCAUCAAGG, UGGAAGGCCUGCAUCAUGA, UGAGGAAGACUGUUACUAC, GCGUAUGACACAUUGAUUA) was transfected using Lipofectamine 2000 according to manufacturer's protocol. Briefly, 150 µl Optimem and 9 µl Lipofectamin 2000 were mixed and added to a mixture of 150 µl Optimem and 4 µl siRNA, which was then put dropwise onto one well of HUVECs. Non-targeting scrambled siRNA (ON-TARGET plus Non-targeting pool, Dharmacon) was used as a control. siRNA knockdown was performed for 48 hours before the experiment.

#### *2.2.2.4 CD95L supported membrane and beads preparation* (conducted by Gülce Sila Gülcüler)

The model of membrane bounded CD95 ligand was prepared by the deposition of planar lipid membranes on solid substrates as previously described (Kaindl et al., 2012). The desired bilayers were made from stock solutions of DOPC (Avanti) containing 0.8 mol% of biotin-DOPE (Avanti) resulting in 8.7nm lateral distance (<*d*>) of CD95L molecules (<*d*> = ($Area_{\text{Lipids}}$ /($Molar\ fraction_{\text{biotin-DOPE}}$)$^{1/2}$) and only DOPC as control bilayers. The lipids were mixed in a chloroform solution, first dried under a stream of nitrogen, and then kept in a vacuum chamber at 25°C for 12 hrs. Afterwards, they are hydrated in distilled water to a final concentration of ~1mg/ml. This resulted in multilamellar vesicles that were rendered unilamellar (SUVs) by pulsed sonication with a tip sonicator (Misonix, New York, USA) for 30 min at 1.0 W. The debris from the sonication tip and SUVs were separated by ultracentrifugation for 10 min and then stored at 4°C. The glass slides from Menzel

(Braunschweig, Germany) were cleaned by RCA protocol (Kern and Puotinen, 1970). Afterwards, they were intensively rinsed with water, dried at 70 ˚C, and stored in a vacuum chamber. The bottomless plastic fluidic channels (µ-slide I) (Ibidi) were bonded with glass slides by using Polydimethylsiloxane (Sylgard184, Dow Corning Co., USA). Supported membranes were prepared by deposition of SUV suspensions onto the cleaned bonded chambers. After 1 h incubation, the chambers were intensively rinsed with de-ionized water to remove the remaining vesicles. Subsequently, the supported membranes were incubated with 1 µg/ml neutravidin (Invitrogen) for 15 min and thoroughly washed with de-ionized water. In the next step, the membranes were incubated with aqueous CD95L-T4-biotin (20 nM) (Apogenix) solution for 1hr at room temperature. Finally, the samples were carefully washed with PBS and it was replaced by pre-warmed cell culture medium. The supported membranes were kept at 37˚C prior to the cell experiments.

The prepared lipid vesicles as above were also used to form supported lipid monolayer on porous silica microspheres NUCLEOSIL® standard C18 phases, nonpolar (Macherey-Nagel). The lipid vesicles were incubated with silica beads at 60˚C for 2hrs by rotation. The coated beads were centrifuged down and washed with PBS. CD95L functionalization on lipids was performed as described above by additional rotation for beads incubation.

#### *2.2.2.5 Culture of SMA560 cells*

SMA560 cells were were maintained in DMEM supplemented with 1x glutamine and 1x penicillin/streptomycin. Cells were kept in 5% $CO_2$ at 37˚C.

#### *2.2.2.6 Culture of patient-derived glioblastoma (GBM) cells*

Collection of patient samples was approved by the Ehtics committee of the Charite University Medicine, Campus Virchow-Klinikum, Berlin (EA3/023/06). The specimen was examined by a neuropathologist to confirm that the tumor met WHO critera for glioblastoma. The sample was dissociated using the Brain Tumor Dissociation Kit (P) and subsequently expanded in culture in Neurobasal medium supplemented with B27,heparin (2 µg/ml) and the growth factors EGF (20 ng/ml)and bFGF (20 ng/ml) at 5% $CO_2$ and 37˚C.

*2.2.2.7 Collection of conditioned medium from GBM cells*

For collection of conditioned medium 10 000 GBM cells were incubated on control- or CD95L-membranes for 4 hours in NBM without supplements and subsequently allowed to rest on one well of a 6 well plate for 24 hours in medium with 50% NBM with and 50% without supplements. 2 ml of conditioned medium was then collected and filtered through a 0.22 μm sterile filter. The conditioned medium was stored at -80˚C before usage for experiments.

*2.2.2.8 Flow cytometry*

For flow cytometry analysis of embryonic and postnatal brain, whole E14.5, P1 and P6 brains were retrieved and single cell suspensions were generated using the Neural Tissue Dissociation Kit (P). Subsequently, cells were washed in PBS with 10% FBS and stained with the following antibodies: PE-Cy7 conjugated anti-CD95 and APC-conjugated anti-CD95L with PercP-eFluor 710-conjugated CD133 and Alexa488-conjugated anti-PSD95 or with APC-Cy7-conjugated CD45, FITC-conjugated CD11b and PE-conjugated anti-CD31. For anti-Glast PE staining the Neural Dissosciation Kit (T) was utilized due to Glast sensitivity to papain. Anti-O4 PE staining was conducted in separate experiment. Both anti-O4 and anti-Glast staining were combined with anti-CD45 APC-Cy7 to exclude immune cells, anti CD95-PE-Cy7 and anti-CD95L APC. For CD95L staining, an amplification step was introduced (due to weak signal) using the FASER kit – APC. FACS was performed at a BD FACS Canto II machine. Unstained and fluorescence minus one controls were used for gating and compensation. At least 50000 single cells were recorded. Data were analysed using the FlowJo software. Median fluorescence intensity values were compared and normalized to unstained control.

For FACS analysis of cultured HUVECs, cells were detached from cell culture flasks with trypsin and washed twice with PBS. Blocking was performed with 10% FBS in PBS for 30min. Subsequently, HUVECs were stained with APC-conjugated anti-CD95 (Apogenix, 1 μg) and FITC-conjugated CD31 antibody for 1 hour. Unstained and single stained cells were used as controls. After washing three times with the blocking solution, cells were analysed on a BD FACS Canto II machine. Data were analysed with FlowJo.

*2.2.2.9 TUNEL staining*

For TUNEL staining, HUVECs on control- or CD95L-coated membranes were fixed for 15 min using 1% PFA, washed twice 5 min with PBS and stained using the DeadEnd™ Fluorometric TUNEL system kit (Promega) according to manufacturer's protocol. Cells were counterstained with Hoechst33342 (1:3000) and imaged on a Zeiss Cell Observer with a 63x objective.

*2.2.2.10 Immunohistochemistry of the brain*

For immunohistochemistry of the brain, pups were sacrificed, their brains extracted and fixed in 4% PFA overnight. 100 µm coronal sections were prepared using a vibratome. Sections were stored in PBS with 0.05% sodium azide until staining. For stainings, sections were incubated in PBS with 0.3% Triton X-100 and 5% fetal calf serum for one hour to block unspecific binding sites. For different analyses, sections were stained with anti-Iba1 antibody and anti-pH3 antibody diluted in blocking solution over night at 4°C with shaking. After washing the sections 3 times 5 min with PBS, secondary antibody staining was performed using the appropriate Alexa-fluorophore antibodies diluted in blocking buffer for 2 hour at room temperature. Furthermore, Alexa-647 conjugated IsoB4 was added to the secondary antibodies, as well as Hoechst33342 to stain for nuclei. Sections were then washed three times 5 min with PBS again, and in a last step with PB buffer. After mounting with Fluoromount-G, the sections were allowed to dry at room temperature for 30min and were stored in the dark at 4°C until imaging.

*2.2.2.11 Immunohistochemistry of the retina* (performed by Rosario Yerbes Cadenas and Nathalie Tisch)

Mice were sacrificed at P6, eyeballs were isolated and fixed in 4% PFA on ice for 2 hours. Retinas were isolated and blocked with 0.3% Triton X-100/1% bovine serum albumin in PBS for 2h at room temperature (RT). The retina vasculature was stained with Alexa568-conjugated Isolectin B4, anti-collagen IV antibody and anti-pH3 antibody diluted in blocking solution, overnight at 4°C and subsequently incubated with appropriate Alexa-labeled secondary antibodies for 2h at RT. Afterwards retinas were flat mounted and imaged.

*2.2.2.12 Golgi staining of the brain*

Mice were sacrificed at P3, brains were taken out and rinsed shortly with Millipore water. Subsequently, the brains were directly processed using the FD Rapid GolgiStain kit according to manufacturer's instructions with some modifications. Brains were first incubated in a 1:1 mixture of Solution A and B for 3 days at 37˚C. Subsequently, brains were transferred to 30% sucrose and incubated for 1 day at room temperature. The next day, brains were cut to 200 µm sections in 6% sucrose using a vibratome. After washing two times with Millipore $H_2O$, the sections were developed in a 2:1:1 mixture of Millipore $H_2O$, Solution C and D for 10 min. This was followed by 2 times 4 min washing of the sections with Millipore $H_2O$. Sections were then mounted with Fluoromount-G.

*2.2.2.13 Immunohistochemistry and vessel analysis of xenograft tumors*

Xenograft tumors were fixed overnight in 4% PFA and were subsequently paraffin embedded and cut into 5 µm sections on a microtome. Paraffin sections were cleared using xylene and dehydrated using 100%, 95%, 70% and 50% EtOH. Antigen-retrieval was performed in citric acid buffer for 20 min at 95˚C. After cooling down for 30 min, blocking was performed using PBS with 0.3% Triton X-100 and 5% FBS for 1 hour at room temperature. Sections were stained with primary antibody for anti-CD31 antibody at 4˚C over night and appropriate Alexa secondary antibody diluted in blocking buffer for 2 hours at room temperature. Dehydration was then performed using 50%, 70%, 95% and 100% ethanol. After clearing with Xylene, the sections were mounted using Eukitt.

**2.2.3 Microscopy analyses**

*2.2.3.1 Imaging and analysis of endothelial tubes*

Microscopy was performed on a Zeiss Cell Observer (Observer.Z1) with 4x objective. Images were subsequently cut into same sizes to remove the rim of the 96-well on the picture. Tubes were analyzed with the ImageJ plugin Angiogenesis Analyzer (http://image.bio.methods.free.fr/ImageJ/?Angiogenesis-Analyzer-for-ImageJ) using the Batch fluorescent mode. Data are expressed as mean±SD. Statistics were performed using unpaired two-tailed t-test.

*2.2.3.2 Imaging and analysis of vessels in the cortex*

Images of cortex vessels were obtained on a Leica SP5 confocal microscope at the DKFZ light microscopy core facility. Vessels were imaged in a blind manner with a 20x objective, and optical stacks (12 slices, 5 µm thick) of the same cortical region (somatosensory/motor cortex) of control and KO brains were acquired. At least 5 images of different sections per brain were taken. Vessel area and branching were analysed using the Fiji (ImageJ) software with a custom written macro (Appendix 5.1 I./II.). Briefly, background was first subtracted using the rollerball function and Gaussian blur was applied to smoothen the image. Next, vessels were segmented using the color threshold function. To measure the area of the image covered by vessels, the analyse particles function was used, with an exclusion size of 400 px. For branch analyses, thresholded images were used as input for the skeletonize and analyse skeleton 2D/3D functions that automatically detect branches and measure their length and branching points.

Cell proliferation analysis was conducted by counting pH3 and IsoB4 double positive cells, whereby excluding $IsoB4^+$ microglia either by morphology or additional Iba1 staining.

Data are expressed as mean± SD. Statistics were performed using unpaired two-tailed t-test.

*2.2.3.3 Imaging and analysis of vessels in the retina* (performed by Rosario Yerbes Cadenas and Nathalie Tisch)

Pictures were taken using a Zeiss LSM 510 confocal microscope (BZH, Heidelberg) and image analysis was accomplished manually with Fiji (ImageJ). The endothelial cell coverage (vessel area) was calculated as $IsoB4^+$ area per retina area. Branching and branching points were counted and normalized to total vessel area per retina. For the analysis of endothelial cell proliferation, $pH3^+/IsoB4^+$ endothelial cells were counted and normalized to vessel area. Vessel regression analysis was accomplished by counting $ColIV^+IsoB4^-$ structures (empty sleeves) and correlating them to retina vessel area. Data are expressed as mean± SD. Statistics were performed using unpaired two-tailed t-test.

*2.2.3.4 Imaging and analysis of Golgi-stained neurons*

Neurons were imaged in a blind fashion with a 40x objective on a Zeiss Cell Observer (DKFZ light microscopy core facility) using a color camera in brightfield mode. Stacks (1 µm) were imaged to cover whole single neurons. To assess neuron branching, branches were traced manually using ROIs in Fiji (ImageJ). At least 10 neurons per brain were traced. Data are expressed as mean± SD. Statistics were performed using unpaired two-tailed t-test.

*2.2.3.5 Imaging and analysis of tumor vessels*

Images were acquired at a Leica SP5 confocal microscope (DKFZ) with a 20x objective. At least two 2x2 tile scans per tumor were used for analysis. Vessel area was quantified using Fiji (ImageJ) with a macro (Appendix 5.1 I.) and normalized to the tissue area imaged. Data are expressed as mean± SD. Statistics were performed using unpaired two-tailed t-test.

*2.2.3.6 Imaging and analysis of tumor volume*

To assess intracranial glioblastoma tumor size, we utilized a stereological method. Tile scans of tumors were taken for every tenth section of the tumor stained with DAPI and imaged using the Zeiss Cell Observer with a 4x objective. The area covered by tumor cells was measured using Fiji (ImageJ). The measured area values were used to interpolate a function for the whole tumor and mathematical integration of the function resulted in the interpolated tumor volume. The calculations were conducted using a R script written by Frederik Ziebell (Appendix 5.2.1).

**2.2.4 Biochemical analyses**

*2.2.4.1 Protein extraction and concentration determination*

Cells were harvested, washed with chilled PBS and lysed in Pierce IP lysis buffer with cOmplete protease inhibitor cocktail and phosphate inhibitor cocktail for 20 min on ice. For protein isolation from tissue, the tissue was subsequently homogenized using the Minilys machine (Precellys). After centrifugation at 16000 x g for 10 min at 4˚C, the supernatant was taken and protein concentration was determined using the BCA

kit. Standardized concentrations of bovine serum albumin (BSA) was used for calibration.

#### *2.2.4.2 SDS-PAGE and Western blot*

Equal amount of protein from cel lysates were boiled for 5 min in Laemmli buffer with β-mercaptoethanol. Proteins were resolved by SDS–PAGE followed by Western blotting to nitrocellulose membranes using the Trans-Blot Turbo Transfer System (Bio-Rad). Membranes were blocked with 5% Skim Powder Milk in PBS-Tween for 1 h and then probed over night at 4˚C with the following antibodies dissolved either in 5% Milk or 5% BSA according to manufacturer's instructions: anti-CD95, anti-ERK 1/2, anti-phospho-ERK 1/2, anti-Akt, anti-phospho-Akt (Ser473), anti-p85 and anti-GAPDH (for concentrations see Table 3). Immunoreactive proteins were visualised with horse raddish peroxidase (HRP)-conjugated anti-rabbit or anti-rat antibodies by incubation for 1h at room temperature. The HRP signal was detected using ECL and membranes were developed using the ChemicDoc Touch imager (Bio-Rad). Quantification of Western blots were conducted in Fiji (ImageJ).

#### *2.2.4.3 Immunoprecipitation*

For immunoprecipitation, the Pierce co-immunoprecipitation kit was used according to manufacturer's instructions. First, 10 µg IgG and 10 µg anti-CD95 antibody (Apo-1) were each immobilized to one Pierce Spin Column. Next, HUVEC cells were lysed (see 2.2.4.1) and 1 mg of whole cell lysate was used as input. The lysate was then pre-cleared in a control agarose resin spin column. Afterwards, 500 µl of lysate was added to the IgG- and the antibody-bound columns and allowed to incubate under rotation overnight at 4˚C. After incubation, the columns were washed 5 times with IP lysis buffer. Finally, elution was performed using 60 µl elution buffer and eluates were subjected to SDS-PAGE and Western blot to analyse proteins bound to IgG and CD95. All stepes were performed at 4˚C

#### *2.2.4.4.Peptide pulldown assay*

The peptide pulldown assay was performed with DTT-cleavable, biotinylated peptides containing the YXXL motif present in the human or mouse CD95 death

domain as previously described with modifications (Letellier et al., 2010) (see peptide sequences in Table 4). A scrambled negative control was generated and subjected to Blast to confirm non-target in the human/mouse genome. Another negative control containing a mutant version of the YXXL motif with an non-phosphorylatable alanine instead of Y was also generated. A wildtype peptide with a non-modified Y291 (human) or Y283 (mouse) was used as bait. Furthermore, a phosphorylated CD95 peptide that contains a more stable phosho-mimic CD95-tyrosine 291 (human) or 283 (mouse) by using F2Pmp group instead of phosho-tyrosine (Meyer and Köhn, 2011) was also generated a bait. Cleavage site was introduced to the peptides with 15-mers bearing an N-terminal biotin on the tetrapeptide linker SGSG. Biotinylation was done using sulfo-NHS-SS-biotin (Pierce) that allows reductive cleavage of the 15-mer from the biotin group.

500 µg lysate of HUVEC cells or mouse brain tissue were incubated overnight at 4°C under rotation with 50 µM of either of the four biotinylated and DTT-cleavable peptide, human and mouse, respectively.

After incubation of the bait peptides with the lysate, 40 µl Dynabeads M-280 streptavidin were added and incubated for 1.5 h at 4°C under rotation. Beads were washed 5 times with lysis buffer in a magnetic rack and resuspended in 30 µl 4x Laemmli buffer. The first supernatant was taken as a flowthrough control. In order to cleave the bait peptides with bound proteins from the magnetic beads to reduce background binding, 50 mM DTT was added for 20 min at room temperature and supernatant was taken for SDS-PAGE and Western blotting as described with anti-p85 and anti-SFK.

#### *2.2.4.5. Human angiogenesis antibody array*

For the parallel determination of relative levels of angiogenesis-related proteins, 1 ml of conditioned medium from control- or CD95-membrane stimulated GBM cells was used as input for the human angiogenesis antibody array kit. The experiment was performed according to manufacturer's instructions. Briefly, the samples are mixed with a cocktail of biotinylated detection antibodies and subsequently incubated with an array membrane spotted in duplicate with capture antibodies for 55 angiogenesis-

related proteins. Captured proteins are visualized with chemilumniscence by exposure to Amerham Hyperfilm films in a Western blot developing machine.

### 2.2.5 Molecular biology

#### *2.2.5.1 RNA-seq sample preparation*

For RNA-seq of subcutaneous GBM tumors, SCID beige mice bearing tumors were sacrificed and perfused with sterile HBSS. Tumors were taken out and small pieces of the tumor (ca. 8 $cm^3$) were sampled. These were chopped into pieces <0.5 mm and dropped into RNAlater at 4°C until RNA isolation. mRNA was isolated from 3 control and 3 CD95L-treated xenograft tumors using the mirVana miRNA Isolation Kit, following the instructions for mRNA isolation. For homogenization of the tissue, small downers were used.

RNA was quantified and analysed on a Bioanalyzer High Sensitivity (HS) chip before including ERCC Spike-Ins at a 1:1000000 dilution.

Synthesis of full-length cDNA was performed from 10 ng mRNA using the SMARTer Ultra Low Input RNA for Illumina Sequencing – HV kit according to manufacturer's instructions. cDNA were produced with 13 PCR cycles and quantified in a Bioanalyzer HS chip.

This was followed by library preparation with the NEBNext Ultra DNA Library Prep Kit for Illumina to generate ca. 300 bp libraries. Libraries were quantified by Qubit, ran on a Bioanalyzer HS Chip, pooled and sequenced with 100 bp paired-end setting on an Illumina HiSeq 2000. Sequencing runs were performed at the DKFZ Genomics and Proteomics core facility and allocation of samples to lanes was arranged in a way to target a minimum of 30 million reads per sample.

### 2.2.6 Computational analyses

*2.2.6.1 Processing and analyses of RNA-seq data* (partially performed by Sheng Zhao)

In total, 6 samples were sequenced on Illumina Hiseq 2000. For each sample, around 36 million 100 bp, paired-end reads were retrieved.

*Read trimming and mapping*: Quality of raw reads was checked by FASTQC (http://www.bioinformatics.babraham.ac.uk/projects/fastqc/). Before alignment, adapter sequences in raw reads were trimmed by Btrim64

(http://graphics.med.yale.edu/trim) (Kong, 2011). Trimmed reads were mapped to human genome (ENSEMBL Release 82) using STAR_2.4.2a (Dobin et al., 2012). Genome mapping results were visualized by using Integrative Genome Viewer (www.broadinstitute.org/igv/).

*RNA-seq data quality metrics*: RNA-seq data quality metrics of each cell, including total reads, uniquely mapped reads and transcriptome mapped rate was calculated by picard-tools-1.136 (https://broadinstitute.github.io/picard/) (Figure 3.18).

*Gene Expression Matrices*: Expression level of each gene was quantified in unites by transcript per million (TPM) using rsem-1.2.22 (Li and Dewey, 2011) with default parameters on bam files from STAR.

*Validation RNAseq data using ERCC spike-in controls*: We assessed the quality of RNAseq data by comparing the results with known quantities of 92 ERCC spike-in RNA transcripts. Briefly, 92 ERCC spike-in RNA transcripts were added to each sample when preparing library. Expression levels of 92 ERCC spike-in controls in these 6 samples were quantified in units of TPM by RSEM. TPM of 92 spike-in controls across these 6 samples were plotted against known inputs (copies per reaction) of each spike-in control. The levels of RNA spikes determined correlated strongly with the known input quantities (Figure 3.18).

*Differential expression and gene ontology analysis*: Differential expression was analysed using the DEseq package from Bioconductor (Appendix 5.2.2) (Love et al., 2014). As a cutoff adjusted $p<0.05$ and log2 fold change > 0.5 was used. Principal component analysis of the samples was performed using the sample to sample comparison function of DEseq (Appedix 5.2.3). Gene ontology analysis was performed using the DAVID function annotation tool (https://david.ncifcrf.gov/home.jsp) (Huang et al., 2008). Heatmap was generated using log2(TPM+1) values in R (Appendix 5.2.4).

### 2.2.7 Statistical analyses

Statistical analyses were performed using GraphPad Prism 6.0 (GraphPad) or R. Differences between two groups were evaluated by unpaired two-tailed student's T-test and between more than two groups by on-way ANOVA. All data are presented as mean ± standard deviation (SD). Statistical significance was determined by the p-

value of the statistical test and deemed as significant * $p<0.05$, strongly significant ** $p<0.01$ and highly significant *** $p<0.001$.

# 3. RESULTS

## 3.1 CD95 during developmental angiogenesis in the CNS

### 3.1.1. CD95 promotes angiogenesis *in vitro*

CD95 has previously been reported to be expressed in endothelial cells (Sata et al., 2000). We confirmed this by analyzing the protein expression of CD95 in human umbilical vein cord cells (HUVECs) by fluorescence activated cell analysis (FACS) as well as Western blotting of HUVEC lysates (Figure 3.1 A,B). With both approaches, we could detect high levels of CD95.

As the function of CD95 in endothelial cells is controversial and it has been shown to be both pro-apoptotic (Ishida et al., 2003; Kaplan et al., 1999) and pro-angiogenic (Biancone et al., 1997; Richardson et al., 1994; Sata et al., 2000), we set out to clarify its role.

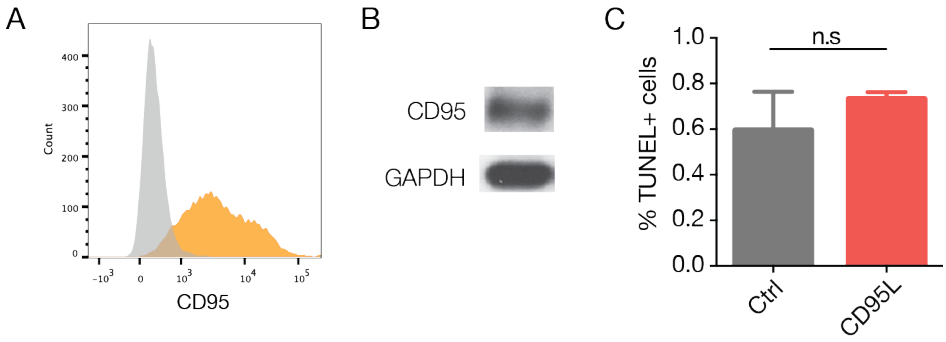


**Figure 3.1: HUVECs express CD95 and are resistant to CD95L-induced apoptosis.**
**A.** FACS analysis of HUVECs. Histogram shows unstained control (gray) and anti-CD95 PE-Cy7 stained HUVECs (orange). **B.** Western blot for CD95 and GAPDH of HUVEC lysate. **C.** Percentage of TUNEL⁺ HUVECs stimulated for four hours on control- or CD95L-coated membranes (n=3) n.s.: not significant, two-tailed unpaired Student's t-test.

We first tested whether endothelial cells would undergo apoptosis upon activation of CD95 by CD95L treatment. CD95L stimulation was conducted using membrane-coupled CD95L where trimerized CD95L via the foldon T4 (T4-CD95L) is bound by biotin/neutravidin crosslinkers to a lipid bilayer – so-called solid supported membranes. These CD95L membranes closely mimic CD95L concentration on cells (8.7 nm inter-ligand distance). Analysis of TUNEL⁺ HUVECs four hours after control-membrane or CD95L-membrane stimulation showed that in both cases only a small percentage of cells were TUNEL⁺ (Ctrl: 0.59% ± 0.12 vs. CD95L: 0.73% ±

0.02, p=0.45) (Figure 3.1 C). Consistent with previous reports of endothelial-resistance to CD95L-induced apoptosis (Richardson et al., 1994; Sata et al., 2000; Suhara et al., 2001), no significant difference was found when comparing control- to CD95L- treated cells (Figure 3.1 C), indicating that CD95L does not induce apoptosis in endothelial cells.

To further explore the functional relevance of CD95 receptor on endothelial cells, we subjected HUVECs to CD95L stimulation and subsequently tested their ability to form capillary-like tubes in matrigel. The tube formation assay has been widely used in the field of angiogenesis to assess factors influencing endothelial cell adhesion, migration and tubule formation (Arnaoutova et al., 2009) and is therefore well-suited as an initial screen.

After exposure to CD95L for four hours, HUVECs formed tubes with branches of significantly higher number (Ctrl: 53 ± 32 vs. CD95L: 113 ± 27, p=0.029) and length (Ctrl: 14598 µm ± 5571 vs. CD95L: 27488 µm ± 4270, p=0.017) compared to control. Consistent with this, the number of nodes and meshes increased significantly after CD95L treatment (nodes Ctrl: 116 ± 49 vs. CD95L: 236 ± 49 p=0.013; meshes Ctrl: 2 ± 1 vs. CD95L: 6 ± 2, p=0.002) (Figure 3.2 A-E).

Next, we also assessed the impact of CD95 loss on the angiogenic potential of the endothelial cells. For this, we performed siRNA-mediated knockdown of CD95 in HUVECs (Figure 3.2 K) and subsequently analysed their ability to form tubes in matrigel (Figure 3.2 F). A strong decrease in the number of tube branches (siScr: 42 ± 19 vs. siCD95: 11 ± 6, p=0.0002, n=2) as well as their length (siScr: 10425 ± 4206 vs. siCD95: 2666 ± 1514 µm, p<0.0001, n=2) could be observed after knockdown of CD95 with siRNA (siCD95) compared to scrambled control siRNA (siScr) (Figure 3.2 G-H). Moreover, the number of nodes and meshes that were formed was significantly reduced after siCD95 knockdown (nodes siScr: 139 ± 121 vs. siCD95: 13 ± 7, p=0.0065; meshes siScr: 5 ± 4 vs. siCD95 0 ± 0, p=0.0017, Figure 3.2 I-J).

The ability of CD95 activation to stimulate and its deletion to cause reduced endothelial tube formation *in vitro* thus suggests a pro-angiogenic role of CD95.

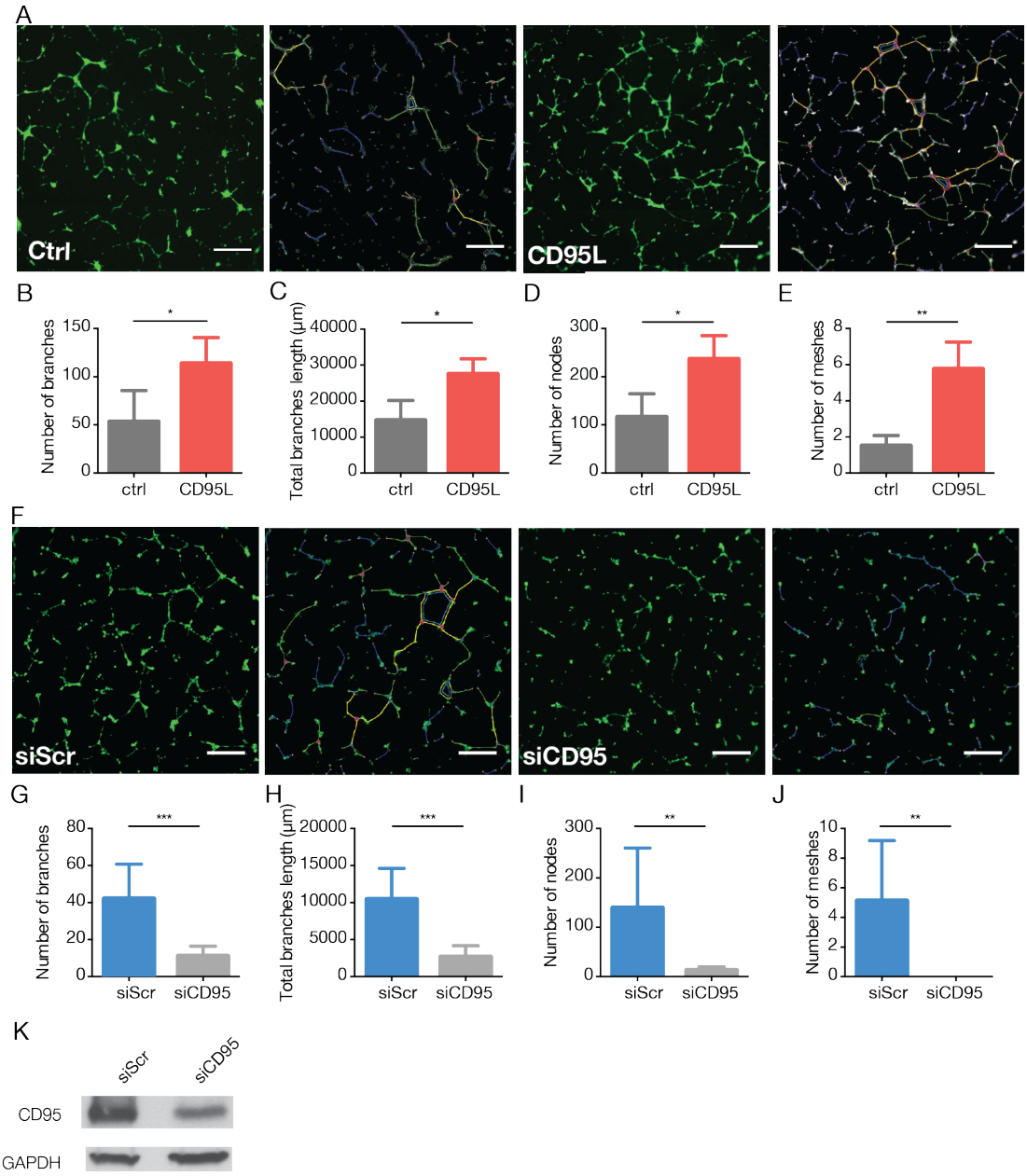


**Figure 3.2: CD95L treatment increases and CD95 knockdown decreases angiogenesis *in vitro*.**

**A.** Representative images and tracings of endothelial tubes formed in matrigel of HUVECs incubated four hours on control- or CD95-coated membranes. **B.-E.** Quantification of endothelial tubes for number of branches (B), total branches length (C), number of nodes (D) and number of meshes (E). (n=3) **F.** Representative images and tracings of endothelial tubes formed in matrigel of HUVECs transfected 48 hours with scrambled (siScr) or CD95 siRNA (siCD95). **G.-J.** Quantification of endothelial tubes for number of branches (G), total branch length (H), number of nodes (I) and number of meshes (J). **K.** Western blot for CD95 and GAPDH of HUVEC lysates transfected 48 hours with siScr or siCD95. (n=2) Scale bar=100 µm. Data are shown as mean±SD, *p<0.05, **p<0.01, **p<0.001 two-tailed unpaired Student's t-test.

### 3.1.2 CD95 is expressed in diverse cell types in the developing brain

To gain further knowledge on the role of CD95 *in vivo* in the developing brain, where CD95 has shown to be involved in neuronal branching before ((Zuliani et al., 2006) and unpublished data), we first assessed its expression in different cell populations at embryonic day 14.5 (E14.5) and postnatal day 1 (P1) by FACS.

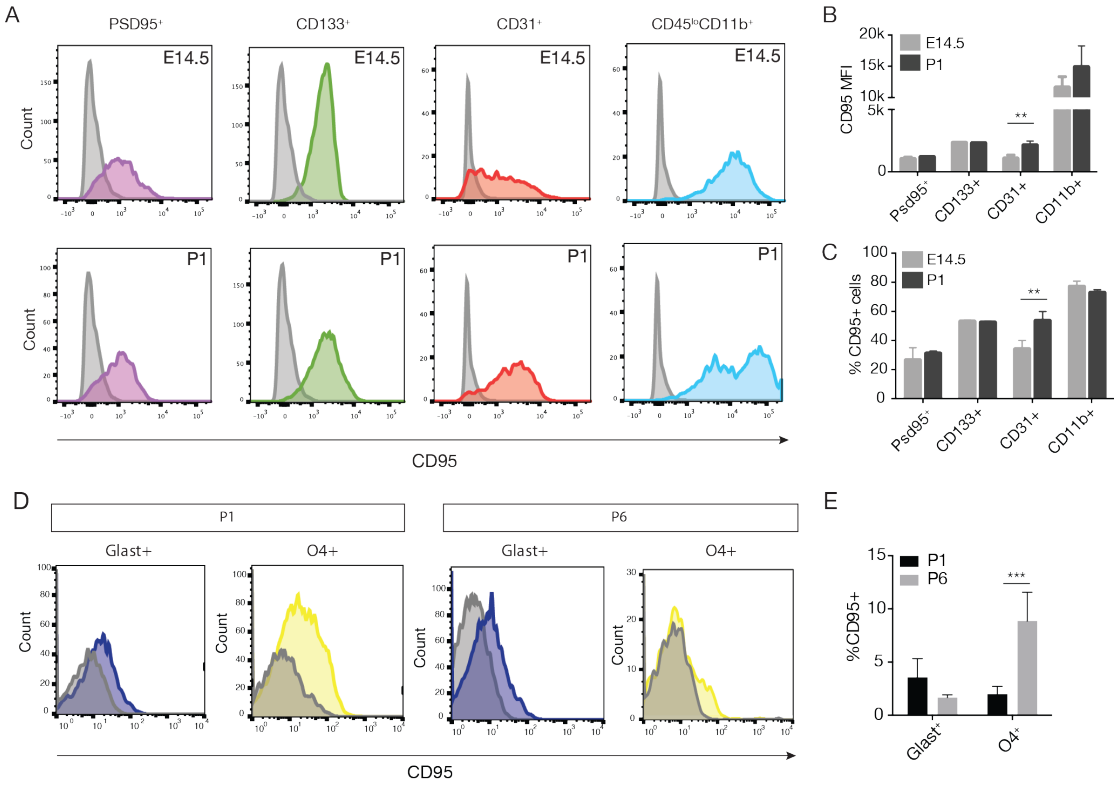


**Figure 3.3: CD95 is expressed in different cell types of the developing brain.**
**A.** FACS analysis of embryonic day 14.5 (E14.5) and postnatal day 1 (P1) brain cells labeled with the neuronal marker PSD95, the neural progenitor marker CD133, the endothelial marker CD31 and CD95. Representative FACS histograms for CD95 expression within the different cell populations at E14.5 (upper panel) and P1 (lower panel) (unstained control in grey). **B-C.** Median fluorescence intensity (MFI) (B) and percentage of CD95$^+$ cells (C) for each cell population at E14.5 and P1 (E14.5: n=4, P1: n=4). **D**. FACS analysis of P1 or P6 brain cells labeled with the astrocyte marker Glast, the oligodendroctye marker O4 and CD95. Representative FACS histograms for CD95. **E.** Percentage of CD95$^+$ cells for each cells population of D (P1: n=3, P6: n=4). Data are shown as mean±SD, *p<0.05, ****p<0.0001, unpaired two-tailed student's t-test.

Cells from whole brains were gated by the postsynaptic density protein PSD95 for neurons (Porter et al., 2005), CD133 for neural progenitors (Pfenninger et al., 2007) and CD31 for endothelial cells and CD95 expression was measured for all three

populations. All cell types expressed CD95, with microglia exhibiting the highest level and percentage of $CD95^+$ cells (median fluorescence intensity (MFI) E14.5: 11585.8 ± 1758.2 & P1: 14843.5 ± 3433.9, p=0.14; % $CD95^+$ E14.5: 76.9 % ± 4.0 & P1: 72.7% ± 2.3, p=0.12) (Figure 3.3 A-C). Neural progenitors also express CD95 (MFI: E14.5: 2304.8 ± 43.3 & P1: 2280.5 ± 39.9, p=0.44; % $CD95^+$ E14.5: 52.9% ± 1.1 & P1: 52.2% ± 1.1, p=0.41), as described previously by Corsini et al. (Corsini et al., 2009) (Figure 3.3 A-C). Consistent with previous data (Zuliani et al., 2006), CD95 was also expressed in neurons (MFI E14.5: 1011.3 ± 185.9 & P1: 1175.3 ± 45.9, p=0.14; % $CD95^+$ cells E14.5: 26.3% ± 8.8 & P1: 30.8% ± 1.8, p=0.35), although at lower levels and percentage as neural progenitors and endothelial cells (Figure 3.3 A-C). Interestingly, CD95 expression increased in endothelial cells from developmental age E14.5 to P1 (MFI E14.5 1058 ± 285.7 & P1 2107.8 ± 362.2, p=0.004; % $CD95^+$ cells E14.5: 33.8% ± 6.2 & P1 53.4% ± 6.5, p=0.005) (Figure 3.3 A-C), possibly implicating functional properties of CD95 in endothelial cells during development. As the glial populations in the brain are generated at about birth, their CD95 expression was assessed at P1 and P6. Astrocytes and oligodendrocytes were identified with the markers Glast and O4, respectively. Both glial populations express CD95 at a low, negligible level (% $CD95^+$ cells in $Glast^+$ population at P1: 3.6% ± 1.8, at P6: 1.7% ± 0.3, p=0.08; % $CD95^+$ cells in $O4^+$ population at P1: 2.0% ± 0.7, at P6: 8.8% ± 1.1, p=0.0005) (Figure 3.3 D-E).

### 3.1.3 CD95 regulates vessel growth and branching in the developing cortex and retina

*In vivo* functional analyses of CD95 during angiogenesis have mainly been performed with *lpr* and *gld* mice so far, which bear germline mutations in CD95 and CD95L, respectively, and therefore lead to ubiquitous expression of non-functional CD95 and CD95L (Ishida et al., 2003). As we have observed CD95 expression in multiple cell types of the brain, a global deletion may interfere with its function on all these cells and lead to secondary effects, thus masking its real effect in endothelial cells.

To more accurately address the function of CD95 during vessel development in the CNS, we generated conditional knockout animals for CD95 by crossing the endothelial cell-specific tamoxifen-inducible Cdh5-(PAC)-$CreER^{T2}$ mice (Sorensen

et al., 2009) with CD95$^{fl/fl}$ mice (Hao et al., 2004). Cre activity in the resulting CD95$^{fl/fl}$;Cdh5-CreER$^{T2}$ mice was induced in newborn pups by tamoxifen injections from P1-P3 and on P5 (Figure 3.4 A), according to Pitulescu & collegues that uses the same cre-driver for recombination in early postnatal mice (Pitulescu et al., 2010).

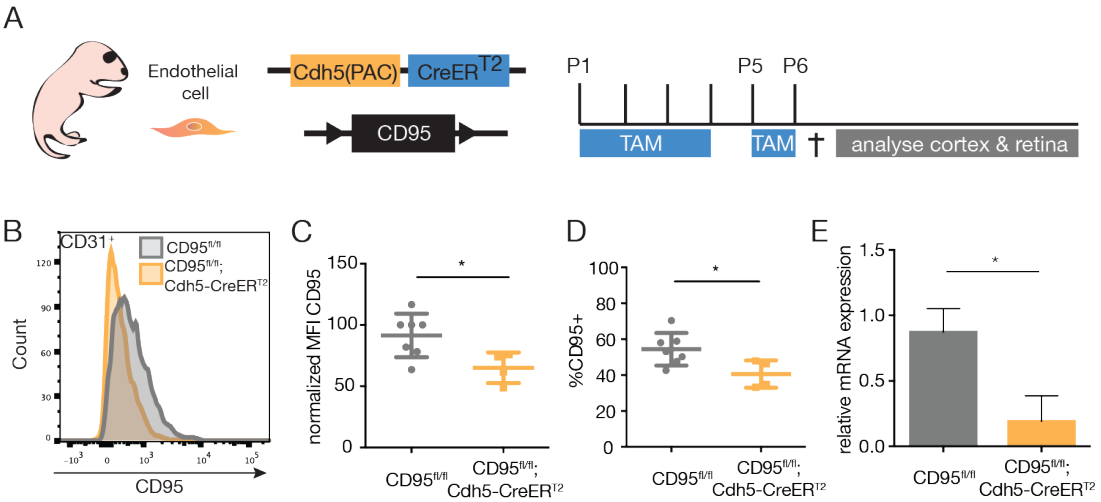


**Figure 3.4: Endothelial cell-specific deletion of CD95.**
**A.** Experimental scheme. CD95$^{fl/fl}$;Cdh5(PAC)-CreER$^{T2}$ mice were used to specifically delete CD95 in endothelial cells. Pups were subjected to tamoxifen (TAM) from P1-P3 and at P5, sacrificed at P6 and vessel morphology in the cortex and retina was analysed. **B.** FACS analysis of brains of CD95$^{fl/fl}$ and CD95$^{fl/fl}$;Cdh5-CreER$^{T2}$ mice for CD95 expression (Ctrl: n=7 vs. KO: n=4). FACS histogram of CD95 for cells gated on CD31$^+$ cells. **C-D.** Normalized MFI (C) and percentage of CD95$^+$ (D) endothelial cells in brains of CD95$^{fl/fl}$ and CD95$^{fl/fl}$;Cdh5-CreER$^{T2}$ mice. **E.** Relative mRNA levels of CD95 in endothelial cells isolated from P6 brains of CD95$^{fl/fl}$ and CD95$^{fl/fl}$;Cdh5-CreER$^{T2}$ mice analysed by qPCR (Ctrl: n=4 vs. KO: n=2). Data are shown as mean±SD, *p<0.05, unpaired two-tailed student's t-test.

The knockout efficiency was subsequently tested in P6 brains by FACS analysis of CD95 expression on CD31$^+$ endothelial cells. Although knockout was not complete, nMFI and percentage of CD95$^+$ cells were significantly reduced in tamoxifen-induced CD95$^{fl/fl}$;Cdh5-CreER$^{T2}$ pups as compared to CD95$^{fl/fl}$ controls (nMFI Ctrl: 91.5 ± 17.8 vs. KO: 65.0 ± 12.5, p=0.02; % CD95$^+$ Ctrl: 54.4 ± 9.1 vs KO: 40.5 ± 7.6, p=0.03) (Figure 3.4 B-D). Furthermore, expression level of CD95 mRNA in P6 brain endothelial cells was assessed by qPCR that consistently showed a strong decrease in CD95$^{fl/fl}$;Cdh5-CreER$^{T2}$ pups as compared to CD95$^{fl/fl}$ controls (Figure 3.4 E).

CD95$^{fl/fl}$;Cdh5-CreER$^{T2}$ mice were used to assess angiogenesis in the developing cortex and retina at P6, an age where continuous branching and proliferation is taking place (Harb et al., 2012).

For this purpose, blood vessels in the brain were stained with Isolectin B4 (IsoB4) and vessel morphology in the somatosensory and motor cortex was quantified.

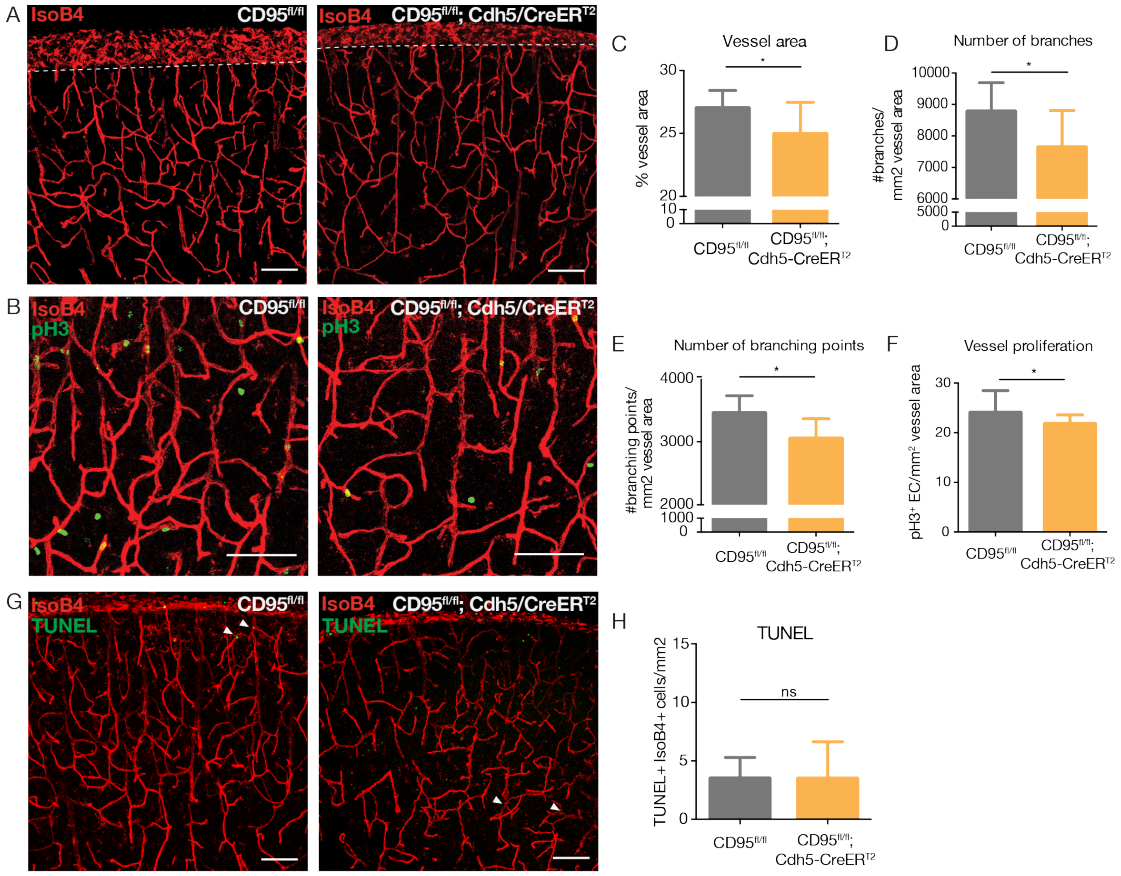


**Figure 3.5: Endothelial-specific CD95 deletion results in vessel defects in the cortex.**
**A.** Representative images of CD95$^{fl/fl}$ and CD95$^{fl/fl}$;Cdh5-CreER$^{T2}$ cortices stained with IsoB4. **B.** Co-staining of IsoB4 (red) and pH3 (green). **C-F** Quantification of the % area covered by endothelial cells (C), number of branches (D), number of branching points (E) and number of IsoB4$^{+}$/pH3$^{+}$ cells (F) for CD95$^{fl/fl}$ and CD95$^{fl/fl}$;Cdh5-CreER$^{T2}$ mice (Ctrl: n=12 vs. KO: n=5). **G.** Representative images of CD95$^{fl/fl}$ and CD95$^{fl/fl}$;Cdh5-CreER$^{T2}$ cortices stained with IsoB4 (red) and TUNEL (green). **H.** Quantification of TUNEL$^{+}$ and IsoB4$^{+}$ cells for CD95$^{fl/fl}$ and CD95$^{fl/fl}$;Cdh5-CreER$^{T2}$ mice (Ctrl: n= vs. KO: n=3). Scale bars = 100 µm. Data are shown as mean±SD. *p<0.05, unpaired two-tailed student's t-test.

Deletion of CD95 in endothelial cells in the cortex led to a significant decrease in the area that is covered by vessels (Ctrl: 27.0% ± 1.4 vs. KO: 24.9% ± 2.5, p=0.048), the number of vessel branches (Ctrl: 8768 ± 920 vs. KO: 7633 ± 1172 /mm$^2$ vessel area,

p=0.049) as well as the number of branching points (Ctrl: 3453 ± 279 vs. KO: 3049 ± 319/mm$^2$ vessel area, p=0.02) (Figure 3.5 A, C-E). Furthermore, endothelial-specific deletion of CD95 significantly diminished the number of proliferating endothelial cells stained with the mitosis marker phospho-histone H3 (pH3) (Ctrl: 24 ± 4 vs. KO: 21 ± 2, p=0.04 Figure 3.5 B, F). Notably, the number of apoptotic endothelial cells marked by TUNEL staining, of which not many were found at this age, did not differ between CD95 deleted and control mice (Ctrl: 4 ± 2 vs. KO: 4 ± 3, p=0.99, Figure 3.5 G-H).

In the retina, similar results could be obtained. Quantification of whole mount retinas stained with IsoB4 showed significant reduction in the area covered by blood vessels (Ctrl: 27.8% ± 3.4 vs. KO: 23.9% ± 3.2, p=0.0002) and in the vessel radial outgrowth from the optic nerve to the periphery (Ctrl: 71% ± 0.1 vs. KO: 66% ± 0.1, p=0.02) in CD95$^{fl/fl}$;Cdh5-CreER$^{T2}$ mice compared to CD95$^{fl/fl}$ controls (Figure 3.6 A, D-E), indicating impaired angiogenic front progression in the primary plexus during retinal vascularization. These defects were accompanied by a marked decrease in the number of branches (Ctrl: 2820 ± 183 vs. KO: 2627 ± 177 branches/mm$^2$ vessel area, p=0.0019) and branching points (Ctrl: 1684 ± 122 vs. KO: 1567 ± 112 branching points/mm$^2$ vessel area, p=0.0040, Figure 3.6 B, F-G).

To further explore the cause of the observed reduction of vessel outgrowth and branching, we analysed endothelial cell proliferation and vessel regression, two crucial aspects during the angiogenic process. Double immunostaining with pH3 and IsoB4 showed a significantly decreased number of proliferating endothelial cells in CD95$^{fl/fl}$;Cdh5-CreER$^{T2}$ mice compared CD95$^{fl/fl}$ control mice (Ctrl: 75 ± 22 vs. KO: 57 ± 17 pH3$^+$/IsoB4$^+$ cells/vessel area, p=0.02, Figure 3.6 B, H). Vessel regression was analyzed by counting collagen IV empty sleeves of basement membrane without endothelial cells. Quantification of the double immunostaining of IsoB4 and Collagen IV (ColIV) showed no difference in the number of empty sleeves between CD95$^{fl/fl}$ control and CD95$^{fl/fl}$;Cdh5-CreER$^{T2}$ retinas (Ctrl: 1.0 ± 0.3 vs. KO: 1.0 ± 0.4, ColIV$^+$/IsoB4$^-$ normalized to CD95-control, p=0.95, Figure 3.6 C, I), suggesting that the effect which CD95 has on vessel development was not due to enhanced pruning and retraction of previously formed vessels.

(Retina data are produced in collaboration with Rosario Yerbes Cadenas.)

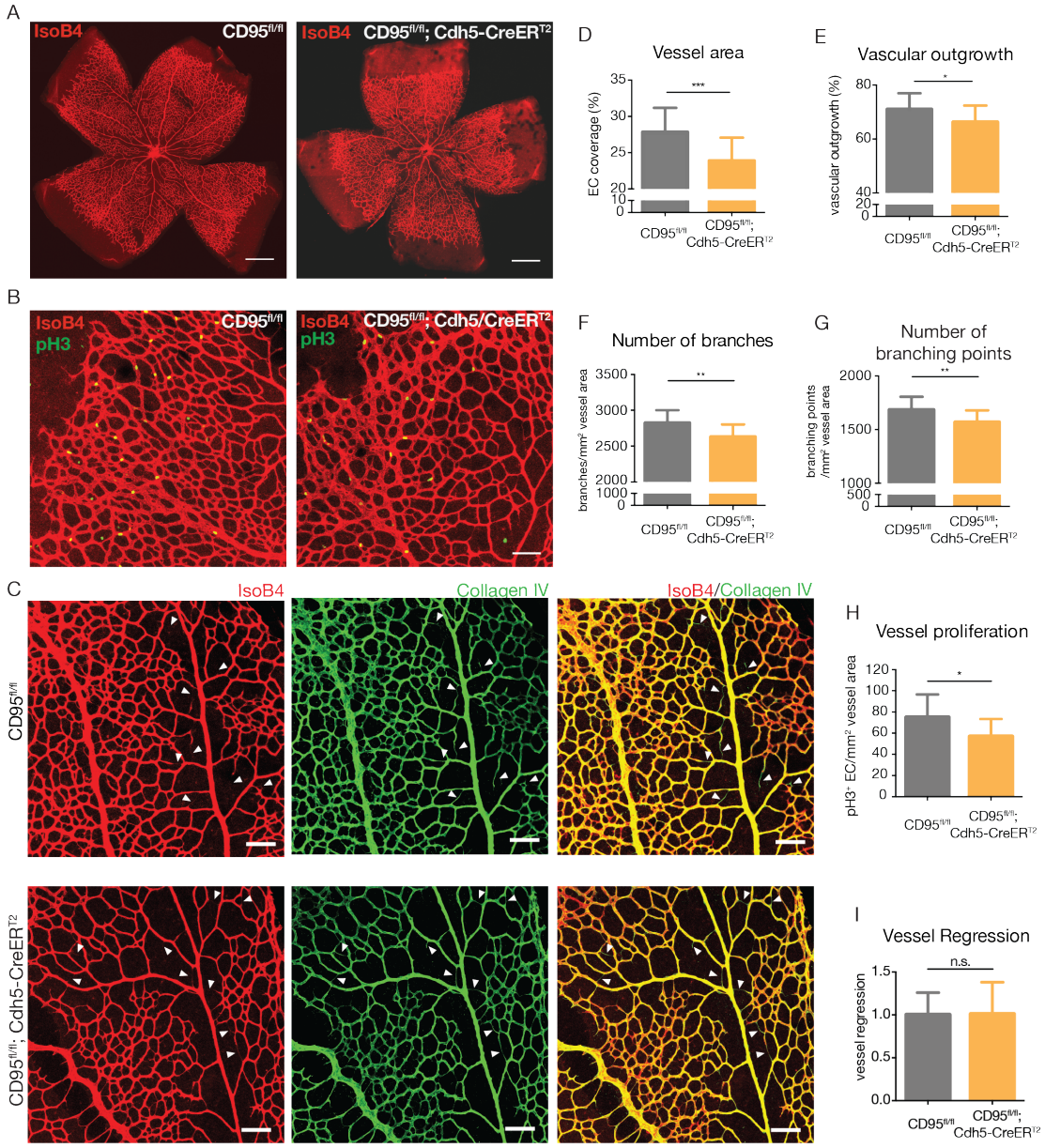


**Figure 3.6: Endothelial-specific CD95 deletion results in vessel defects in the retina.**
**A.** Representative images of CD95$^{fl/fl}$ and CD95$^{fl/fl}$;Cdh5-CreER$^{T2}$ retinas stained with IsoB4. Scale bars = 500 µm. **B.** Representative images of CD95$^{fl/fl}$ and CD95$^{fl/fl}$;Cdh5-CreER$^{T2}$ retinas stained with IsoB4 (red) and pH3 (green). Scale bars = 100 µm. **C.** Representative images of "collagen empty sleeves" as indicated by IsoB4 (red) negative and ColIV (green) positive stainings in CD95$^{fl/fl}$ and CD95$^{fl/fl}$ Cdh5-CreER$^{T2}$ mice. White arrowheads point to ColIV$^{+}$/IsoB4$^{-}$ empty sleeves. Scale bars = 100 µm. **D.** Quantification of the area covered by endothelial cells (Ctrl: n=19 vs. KO: n=32 retinas). Data are expressed as percentage of total retina area. **E.** Quantification of the vessel radial outgrowth to the periphery (Ctrl: n=16 vs. KO: n=28 retinas). Data are expressed as percentage of total lobe length. **F.-G.** Quantification of the nuber of branches (F) and branching points (G) (Ctrl: n=17 vs. KO: n=27 retinas). Data are expressed as number of branches/vessel area and number of branching points/vessel area, respectively. **H.** Quantification of proliferating (pH3$^{+}$) endothelial cells (Ctrl: n=12 vs. KO: n=17). Data are expressed as pH3$^{+}$/IsoB4$^{+}$ endothelial cells (EC)/vessel area. **I.** Quantification of vessel regression in retinas of CD95$^{fl/fl}$ and

$CD95^{fl/fl}$ Cdh5-$CreER^{T2}$ mice. (Ctrl: n= 7 vs. KO: n=15). Data expressed as number of $ColIV^+/IsoB4^-$ empty sleeves/vessel area.
Data are shown as mean± SD. *p<0.05, **p<0.01, ***p<0.001, n.s. not significant, unpaired two-tailed student's t-test. Data are produced in collaboration with Rosario Yerbes Cadenas.

Altogether, these data demonstrate that CD95 regulates developmental angiogenesis in the cortex and retina by promoting endothelial cell proliferation and branching, without affecting vessel regression.

### 3.1.4 CD95L is primarily expressed by microglia in the developing brain

The effect of CD95 on vessel morphology and proliferation should be a consequence of CD95 activation by its only known ligand - CD95L. Previous reports have shown that CD95L mRNA is expressed largely by glial cells in white matter and to a lesser extent in neurons of the adult brain (Shin et al., 2002). Where the source of CD95L lies in the developing brain, however, is unknown. To address this question, we again made use of FACS analysis of live cells to assess CD95L expression in different cell populations of the brain at E14.5 and P1. While $PSD95^+$ neurons and $CD133^+$ neural progenitors hardly express any CD95L (neurons MFI E14.5: 305.3 ± 46.3 & P1: 351.5 ± 11.4, p=0.1; $\%CD95L^+$ E14.5: 0.5% ± 0.2 & P1: 1.0% ± 0.3, p=0.04; neural progenitors (MFI E14.5: 196.0 ± 20.6 & P1: 284.8 ± 13.7, p=0.0003; % $CD95L^+$ E14.5: 1.1% ± 0.4 & P1: 4.7% ± 1.6, p=0.004) and $CD31^+$ endothelial cells express low levels of CD95L (MFI E14.5: 369.3 ± 80.2 & P1: 533.0 ± 62.4, p=0.02; % $CD95L^+$ E14.5: 3.0% ± 1.8 & P1: 7.0% ± 1.6, p=0.02), $CD45^{lo}CD11b^+$ microglia (Goldmann et al., 2013) exhibited the highest expression of CD95L and percentage of $CD95L^+$ cells (MFI E14.5: 16690.3 ± 2209.2 & P1: 16170.5 ± 3905.6, p=0.82; % $CD95L^+$ E14.5: 99.7% ± 0.1 & P1: 96.2% ± 7.3, p=0.38) (Figure 3.7 A, C-D). Notably, neural progenitors and endothelial cells upregulate CD95L expression during developmental progression from E14.5 to P1, although general expression levels are low (Figure 3.7 C-D). As astrocytes ($Glast^+$) and oligodendrocytes ($O4^+$) are just starting to be generated around birth, we assessed their expression of CD95L at P1 and P6. Both populations expressed barely detectable levels of CD95L (% $CD95L^+$ cells in $Glast^+$ population at P1: 0.08% ± 0.05 vs. P6: 0.22% ± 0.10, p=0.08; % $CD95L^+$ cells in $O4^+$ population at P1: 0.05% ± 0.01 vs. P6: 0.85% ± 0.13,

p=0.0004, Figure 3.7 B, E), thus they can be excluded from being a source of CD95L in early postnatal development.

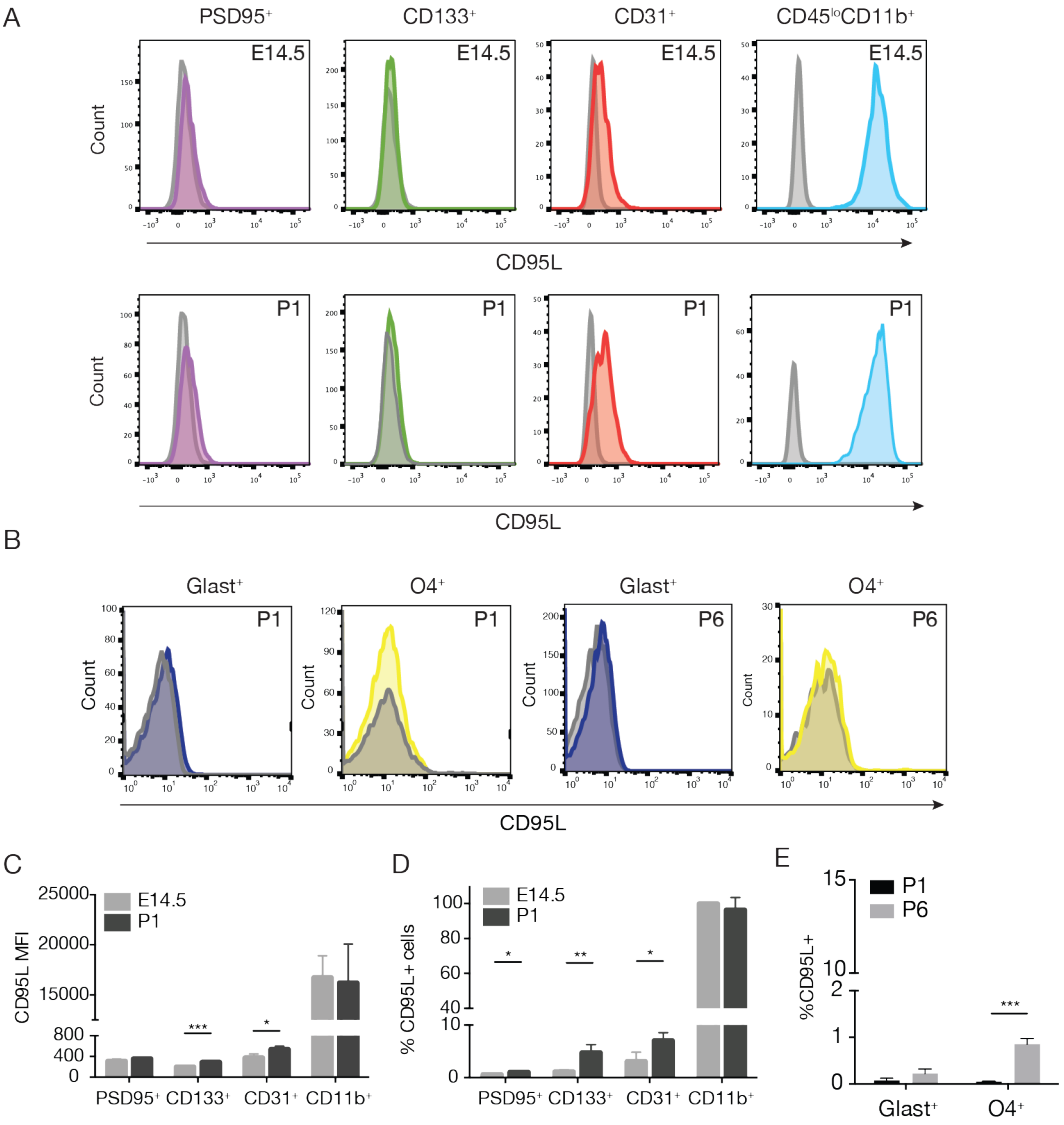


**Figure 3.7: CD95L is primarly expressed by microglia in the developing brain.**
**A.** FACS analysis of CD95L expression in E14.5 and P1 brains gated for neurons (PSD95$^+$), neural progenitors (CD133$^+$), endothelial cells (CD31$^+$) and microglia (CD45$^{lo}$CD11b$^+$). Representative FACS plots for CD95L of the different cell populations at P1 (unstained control in grey). **B.** FACS analysis of CD95L expression in P1 and P6 brains gated on astrocytes (Glast$^+$) and oligodendrocytes (O4$^+$). Representative FACS plots are shown (unstained control in grey). **C-D.** Normalized median fluorescence intensity (B) and percentage (C) of CD95L$^+$ cells for each cell population (E14.5: n=4 , P1: n= 4). **E.** Percentage of CD95L+ cells for astrocytes and oligodendrocytes (P1: n=3, P6: n=4). Data are shown as mean±SD, *p<0.05, **p<0.01, ***p<0.001, unpaired two-tailed student's t-test.

The high level of CD95L in microglia prompted us to hypothesize that microglia-derived CD95L might act in a paracrine manner to promote endothelial cell growth and proliferation. Thus, we further focused on the effect of microglial-derived CD95L in cortex and retina angiogenesis.

### 3.1.5 Microglia-derived CD95L regulates vessel morphology in the cortex

In order to test the effect of microglial-derived CD95L we generated microglia-specific knockout mice for CD95L. This was achieved by crossing LysM-Cre mice (Clausen et al., 1999) with CD95L$^{fl/fl}$ mice (Karray et al., 2004) to obtain CD95L$^{fl/fl}$;LysM-Cre mice (Figure 3.9 A). The LysM-Cre driver specifically recombines in monocytes, including microglia, but also in peripheral circulating monocytes (Clausen et al., 1999; Goldmann et al., 2013). To find out the recombination rate of the LysM-Cre driver in microglia, we made use of the LysM-Cre YFP mice that express YFP upon recombination and counted YFP$^+$ Iba$^+$ microglia. The number of double positive cells amounted to 31.5%, indicating that almost a third of microglia would recombine in the LysM-Cre line (Figure 3.8 A, B).

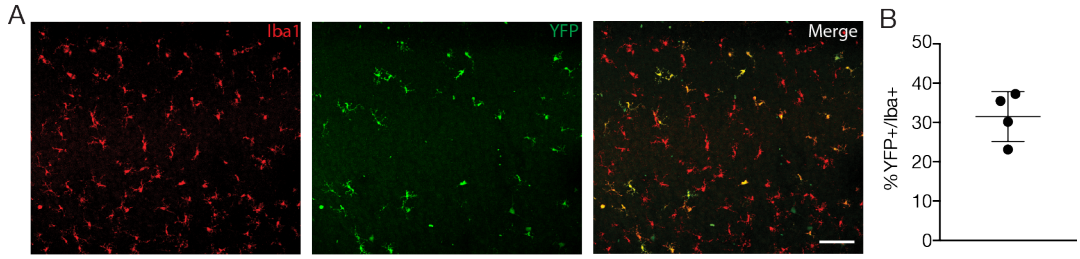


**Figure 3.8: Microglial-recombination with the LysM-Cre line.**
**A**. LysM-Cre YFP mice were killed at P6 and brains were stained with Iba1 and YFP to assess recombination efficiency in microglia. (**B**) Quantification of % of YFP$^+$/Iba1$^+$ double positive cells in the cortex (n=4).

Next, we confirmed deletion of CD95L in microglia by FACS analysis which showed significantly reduced levels of CD95L in CD45$^{lo}$CD11b$^+$ microglia of CD95L$^{fl/fl}$;LysM-Cre P1 pup brains compared to CD95L$^{fl/fl}$ controls (normalized MFI Ctrl: 113.1 ± 13.4 vs. KO: 85.9 ± 20.8, p=0.02, Figure 3.9 B-C).

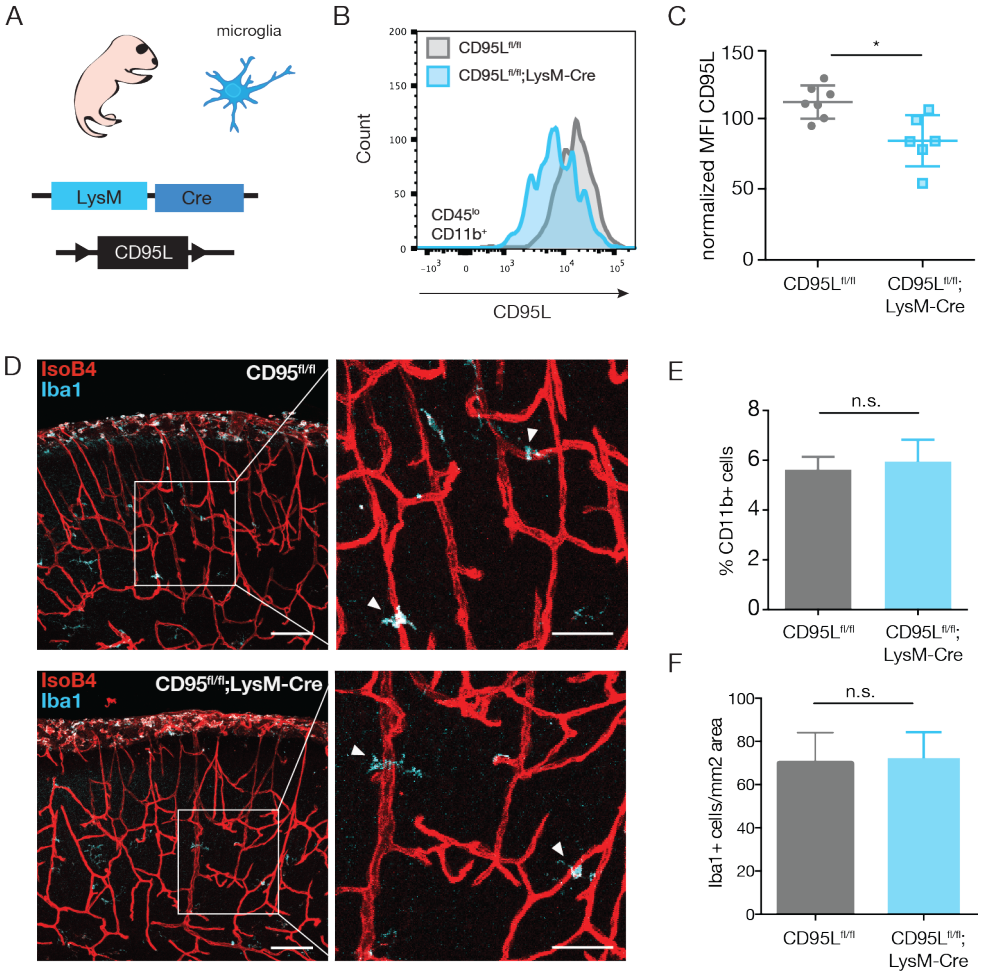


**Figure 3.9: Deletion of CD95L in microglia.**
**A.** LysM-Cre mice are crossed with CD95L$^{fl/fl}$ mice to delete CD95L in microglia. **B-C.** FACS analysis of brains of CD95L$^{fl/fl}$ and CD95L$^{fl/fl}$;LysM-Cre mice was performed for CD95L (Ctrl: n=7 vs. KO: n=6). FACS plot of CD95L gated on CD45$^{lo}$ CD11b$^{+}$ cells (B) and graph showing CD95L expression by normalized MFI (C). **D.** Representative images of CD95L$^{fl/fl}$ and CD95$^{fl/fl}$;LysM-Cre cortices stained with IsoB4 and Iba1. Arrows show Iba1$^{+}$ microglia are located closely to vessels. Scale bars = 100 µm, inlet = 50 µm. **E-F.** Quantification of microglia by FACS analysis for CD11b$^{+}$ cells (Ctrl: n=9 vs. KO: n=8) (E) or immunohistochemical staining for Iba1 (Ctrl: n=5 vs. KO: n=4) (F) in brains of CD95L$^{fl/fl}$ and CD95L$^{fl/fl}$;LysM-Cre mice. Data are shown as mean±SD, *p<0.05, n.s.=not significant, unpaired two-tailed student's t-test.

As CD95L may play a role in the recruitment of microglia to the brain during development, which would affect the outcome of CD95L deletion on vessel morphology, we wanted to rule out this possibility. Therefore, we further compared the number of microglia in the brain of CD95L$^{fl/fl}$;LysM-Cre knockout mice to CD95L$^{fl/fl}$ control mice by FACS (Ctrl: 5.6% ± 0.5 vs. KO: 5.9% ± 0.7, p=0.54) and by Iba1$^{+}$ immunostaining at P1 (Ctrl: 70 ± 14 vs. KO: 72 ± 12, p=0.71) (Figure 3.9

D-F). This showed comparable microglia numbers between control and knockout mice. Notably, Iba1$^{+}$ microglia are closely located to IsoB4 stained vessels (Figure 3.9 D), similar to previous reports of spatial association of tissue macrophages and sprouting vessels in early embryonic hindbrain and retina (Checchin et al., 2006; Fantin et al., 2013).

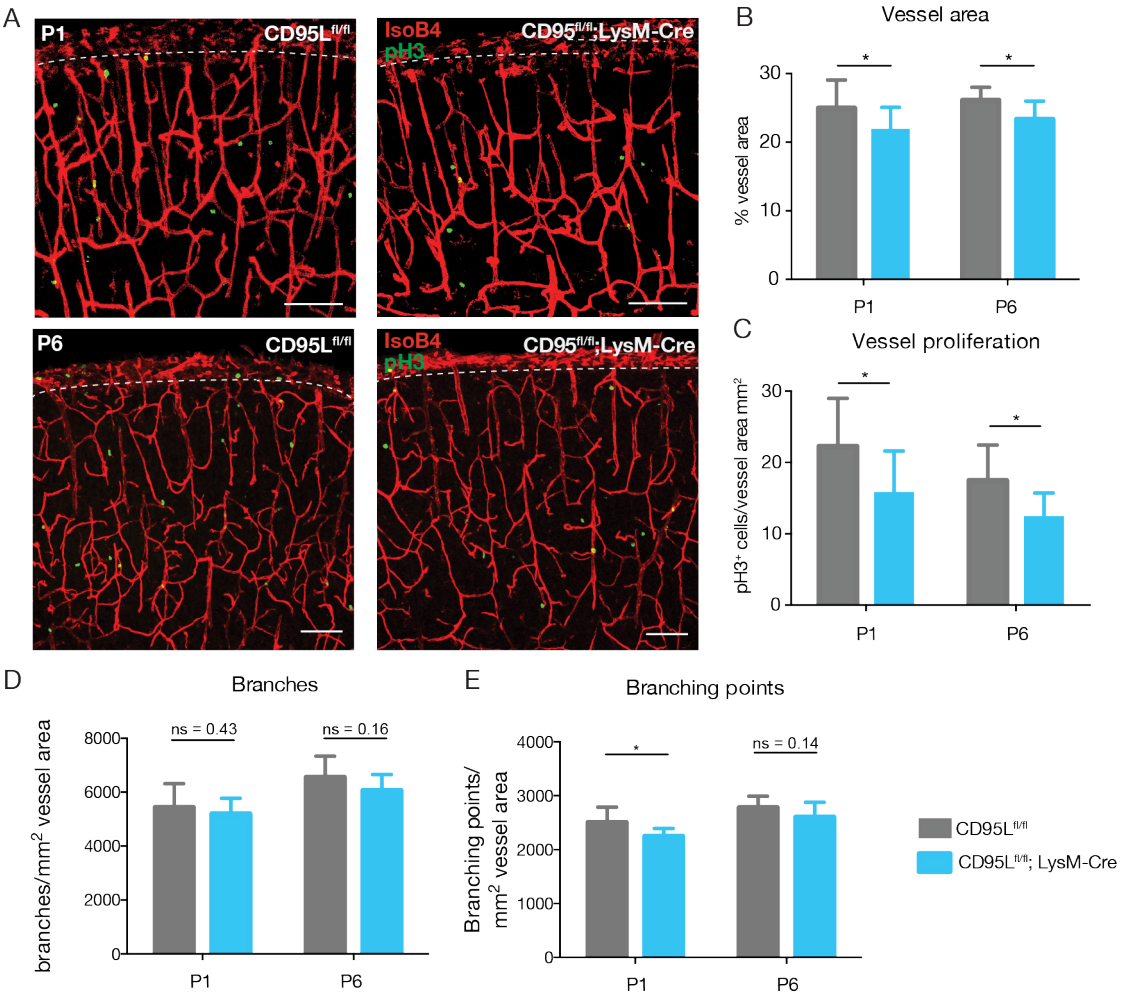


**Fig. 3.10: Microglial-deletion of CD95L impairs cortical vessel development.**
**A.** Representative images of CD95L$^{fl/fl}$ and CD95$^{fl/fl}$;LysM-Cre cortices stained with IsoB4 and pH3 at P1 and P6. Scale bar = 100 µm. **B-E.** Quantification of vessel area (Ctrl: n=13 vs. KO n=12) at P1, and P6 (Ctrl: n=14 vs. KO: n=7) (B), vessel proliferation P1 (Ctrl: n=10 vs. KO: n=9) and P6 (Ctrl: n=12 vs. KO: n=6) (C), number of branches (D) and number of branching points (E) (Ctrl: n=13 vs. KO n=12) at P1, and P6 (Ctrl: n=14 vs. KO: n=7). Data are shown as mean±SD, *p<0.05, unpaired two-tailed student's t-test.

To answer the question of whether paracrine signaling through microglial-CD95L would regulate vessel morphology, we quantified cortical vessels at P1 as well as P6 by staining for IsoB4. This revealed a significant reduction of area covered by vessels in

CD95L$^{fl/fl}$;LysM-Cre pups compared to CD95L$^{fl/fl}$ controls (P1 Ctrl: 25.0% ± 4.1 vs. KO: 21.8% ± 3.3, p=0.04; P6 Ctrl: 26.1% ± 1.9 vs. KO: 23.3% ± 2.7, p=0.01, Figure 3.10 A-B). Co-staining of IsoB4 and pH3 further showed a decrease in vessel proliferation in CD95L$^{fl/fl}$;LysM-Cre pups compared to CD95L$^{fl/fl}$ controls (P1 Ctrl: 22 ± 7 vs. KO: 16 ± 6 pH3$^{+}$IsoB4$^{+}$/mm$^2$ vessel area, p=0.04; P6 Ctrl: 17 ± 5 vs. KO: 12 ± 4 pH3$^{+}$IsoB4$^{+}$/mm$^2$ vessel area, p=0.04, Figure 3.10 A, C). The number of vessel branches and branching points was also assessed at P1 and P6. However, although there was a slight trend towards decreased branches and branching points in CD95L$^{fl/fl}$;LysM-Cre pups, statistical significance was only reached for branching points at P1 (branches: P1 Ctrl: 5432 ± 884/mm$^2$ vessel area vs. KO: 5194 ± 582/mm$^2$ vessel area, p=0.43; P6 Ctrl: 6547 ± 787/mm$^2$ vessel area vs. KO: 6057 ± 598/mm$^2$ vessel area, p=0.16; branching points: P1 Ctrl: 2503 ± 286/mm$^2$ vessel area vs. KO: 2245 ± 147/mm$^2$ vessel area, p=0.01; P6 Ctrl: 2775 ± 215/mm$^2$ vessel area vs. KO: 2600 ± 276/mm$^2$ vessel area, p=0.14; Figure 3.10 D-E).

We further took a look at IsoB4 stained retina whole-mounts and analysed vessel area, outgrowth, branching and proliferation. For all parameters no significant difference was observed between CD95L$^{fl/fl}$;LysM-Cre pups and CD95L$^{fl/fl}$ controls (Figure 3.11 A-D). (These data were produced in collaboration with Nathalie Tisch.)

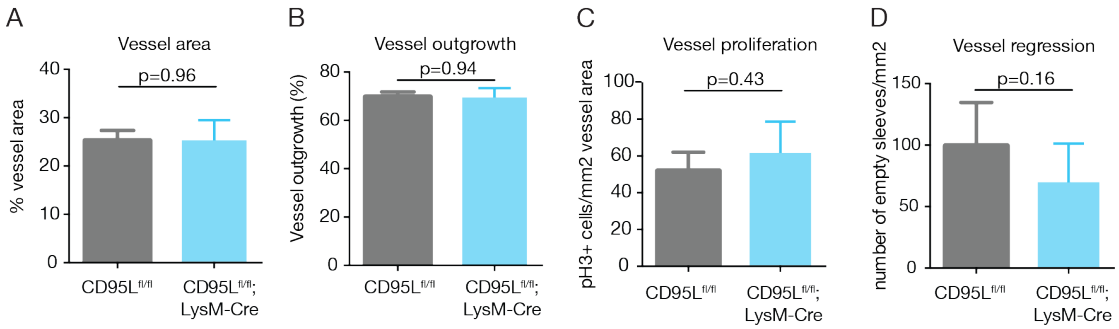


**Figure 3.11: Microglia-specific deletion of CD95L does not affect retina angiogenesis.**
**A-D.** Quantification of vessel area (A), vessel outgrowth (B) (Ctrl: n=5 vs. KO: n=9)., vessel proliferation (Ctrl: n=4 vs. KO: n=3). (C) and vessel regression (D) (Ctrl: n=5 vs. KO: n=9). of CD95L$^{fl/fl}$ and CD95$^{fl/fl}$;LysM-Cre wholemount retina stained with IsoB4 or IsoB4 and pH3. n.s=not significant, unpaired two-tailed student's t-test. Data produced in collaboration with Nathalie Tisch.

These results suggest that indeed microglia-derived CD95L is able to regulate overall vessel density as well as proliferation in the cortex, but does not give a definitive answer on its effect on vessel branching. Due to the incomplete recombination of the LysM-Cre line, CD95L expression may still be present in brain and retina, resulting in the absence of an observable effect.

### 3.1.6 Microglial-derived CD95L regulates neuronal branching in the cortex

Previous work in the lab has revealed that CD95 receptor activation on cortical and hippocampal neurons can promote neuronal branching during development, whereas CD95 deletion leads to the opposite effect (unpublished data). Consistent with this, it has been shown by Desbarats et al. that CD95 is involved in neurite outgrowth of dorsal root ganglion neurons (Desbarats et al., 2003).

Therefore, we wondered whether CD95 receptor in neurons may also be activated by microglia-derived CD95L, which presents the major source of CD95L in the developing brain as shown in (Figure 3.7 A, C-D). This would be in line with the theory of the neurovascular link where neurons and vessels are co-regulated by the same set of molecules and develop congruently with similar molecular and anatomical properties (Eichmann and Thomas, 2013; Segura et al., 2009).

To investigate the role of microglia-derived CD95L in cortical neuronal branching, we analysed neuron morphology of layer II/III neurons in CD95L$^{fl/fl}$;LysM-Cre pups at the age of P3, where CD95 expression was shown to be most intense (consistent with previous experiments on CD95's role in neuronal branching by Cecilia Zuliani and Hannes Hudalla). Single neurons were visualized using Golgi staining and branching morphology was quantified. This revealed an impairment in the neuronal branching of CD95L$^{fl/fl;}$LysM-Cre pups that was evident through a significant reduction in total branching length (Ctrl: 242.9 µm ± 76.8 vs. KO: 142.4 µm ± 43.0. $p<0.0001$), longest dendrite length (Ctrl: 97.4 µm ± 23.3 vs. KO: 67.0 µm ± 16.7, $p<0.0001$) and number of branching points (Ctrl: 8 ± 4 vs. KO: 5 ± 2, $p<0.0001$) compared to CD95L$^{fl/fl}$ controls (Figure 3.12 A-D). The number of primary dendrites was unchanged (Ctrl: 2 ± 1 vs. KO: 2 ± 1, $p=0.09$) (Figure 3.12 E), similar to previous data of CD95 receptor knockout (unpublished data by Cecilia Zuliani).

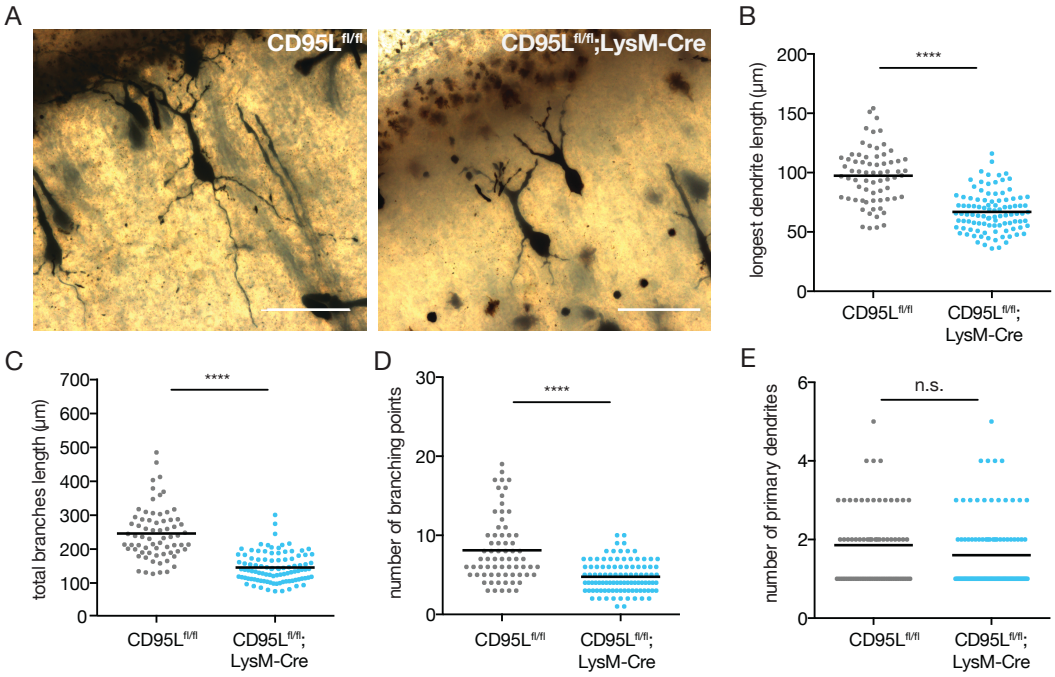


**Figure 3.12: Microglial-deletion of CD95L impairs cortical neuron branching.**
**A.** Representative images depicting Golgi-stained neurons in CD95L$^{fl/fl}$ and CD95$^{fl/fl}$;LysM-Cre cortices at P3. Scale bar = 50 µm. **B-E.** Quantification of longest dendrite length (B), total branches length (C), number of branching points (D) and number of primary dendrites (E) in CD95L$^{fl/fl}$ (n=69) and CD95$^{fl/fl}$;LysM-Cre neurons (n=100) from at least 7 different pups. Data are shown as mean±SD. ****p<0.0001, n.s=not significant, unpaired two-tailed student's t-test.

These data together with data from section 3.15 demonstrate that microglia can co-regulate neuron and vessel morphogenesis and that this is mediated by CD95/CD95L interaction.

### 3.1.7 CD95 interacts with Src-family kinases and p85 in endothelial cells

It has been previously shown that non-apoptotic functions of CD95 can be mediated by recruitment of SH2-containing proteins to the tyrosine residue Y283 lying within the YXXL motif of the mouse CD95 death domain (Sancho-Martinez and Martin-Villalba, 2009). Members of the Src-family kinase (SFK) can phosphorylate this residue allowing recruitment of different SH2-containing proteins that in turn lead to activation of diverse effectors such as PI3K, NFκB, Erk etc. (Martin-Villalba et al., 2013). CD95 therefore behaves similarly to a receptor tyrosine kinase.

During VEGF-mediated angiogenesis, PI3K and Erk activation are crucial to mediate endothelial cell proliferation, migration and growth (Gerber et al., 1998;

Somanath et al., 2006; Srinivasan et al., 2009), thus we hypothesized that CD95 may act in a similar manner as VEGF and use its tyrosine kinase receptor properties to activate PI3K and Erk.

We therefore examined a possible interaction of the SH2 kinases of the src family (SFK) as well as PI3K with CD95. First, antibody-mediated pulldown of CD95 from HUVEC lysates revealed binding of the regulatory subunit of PI3K, p85, to CD95 (Figure 3.12 A), although immunopreciptiation with an isotype control antibody also led to unspecific binding. In order to confirm this interaction of CD95 with p85 in endothelial cells, we further performed peptide pulldown assays with HUVEC lysates. For this purpose, we designed biotinylated, 15 amino acids long peptides that correspond to the YXXL motif of the human CD95 death domain. These contain either a scrambled sequence (Scr), an alanine mutant amino acid that substitutes Y291 of the human CD95 (A), a wildtype Y291 (Y), or a phosphorylated form of Y291 (pY) (Figure 3.12 B). While in the pulldown fraction of the pY peptide we could strongly detect p85, pulldown with the alanine mutant as well as the non-phosphorylated Y peptide resulted in much less enrichment of p85 and in the negative control binding was barely detectable (Figure 3.12 C). Furthermore, we also checked for binding of SFK to the peptides which showed a similar enrichment, with the highest binding found with the pY peptide. These data show that SFK and p85 can bind to the phosphorylated tyrosine of the death domain, and to a much lesser extent to the unphosphorylated one, which indicates that recruitment of SFK/p85 to CD95 is direct and requires prior phosphorylation presumably through binding of CD95L and CD95 receptor clustering. Consistent with this, there is a strong decrease of SKF and p85 signal in the flowthrough fraction of the pY pulldown (Figure 3.12 C). Together, these data indicate that the CD95 death domain is able to recruit SFK and p85 in endothelial cells.

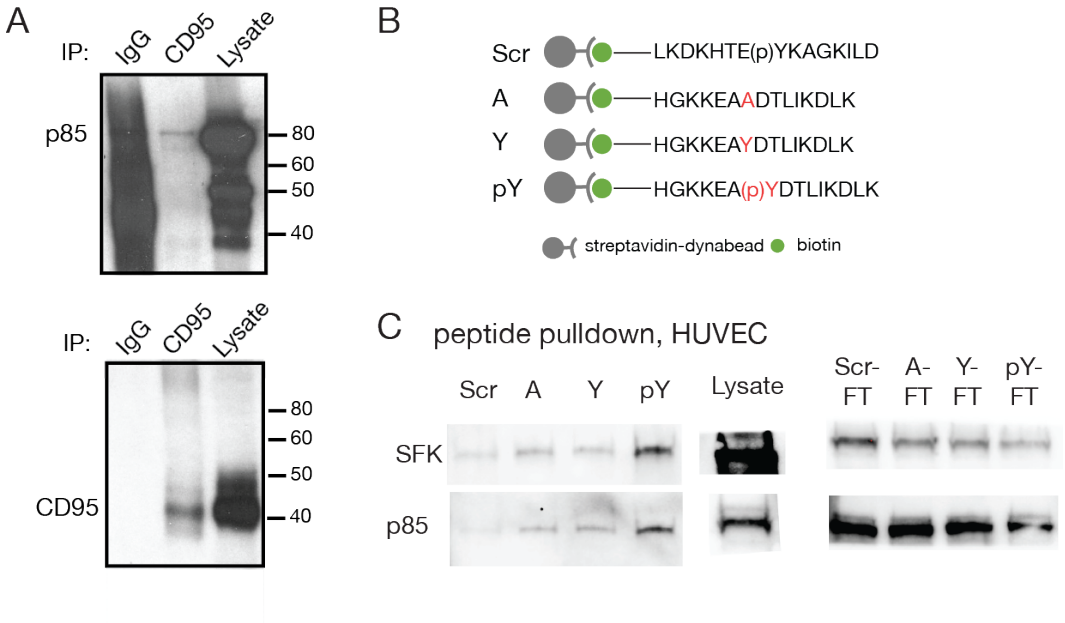


**Figure 3.13: CD95 death domain associates with SFK and p85 in endothelial cells.**
**A.** Immunopreciptation (IP) of HUVEC lysates with isotype control antibody or anti-CD95 antibody (Apo-1), and whole lysates. Shown are Western blots of IP fractions for p85 and CD95. **B.** Scheme of peptides used for peptide pulldown assay. C. Lysates of HUVEC cells were subjected to peptide pulldown with a CD95 death domain scrambled (Scr), alanin-mutant (A), wildtype tyrosine (Y) or phosphorylated tyrosin (pY) peptide. Peptide-bound fraction, whole lysate as well as flowthrough fraction (FT) were blottet for SFK and p85.

### 3.1.8 CD95L induces vessel growth through Akt and Erk activation

To further elucidate the signaling downstream of PI3K activation, we examined the downstream effectors of PI3K upon CD95 stimulation in HUVECs as well as a brain microvascular endothelial cell line bEnd.3. The canonical downstream target of PI3K is Akt which becomes phosphorylated either at Ser-473 or Thr-308, whereby Ser-473 phosphorylation leads to full activation of Akt (Hers et al., 2011). Upon treatment with trimerized T4-CD95L, Ser-473 phosphorylation of Akt, but not Thr-308 (not shown), was induced in HUVECs and bEnd.3 as shown by Western blot with the strongest activation 5 min after CD95L treatment (Figure 3.14 A-B).

Furthermore, Erk signaling can be activated downstream of SFK which also has also been shown for CD95 in other systems (Barnhart et al., 2004; McKay and Morrison, 2007; Wojtowicz et al., 2004). Thus, we also analysed phosphorylation of Erk1/2 (p44/42 MAPK). Erk1/2 also became phosphorylated after CD95L treatment, and exhibited the strongest phosphorylation at 20 min after treatment (Figure 3.14 A-B).

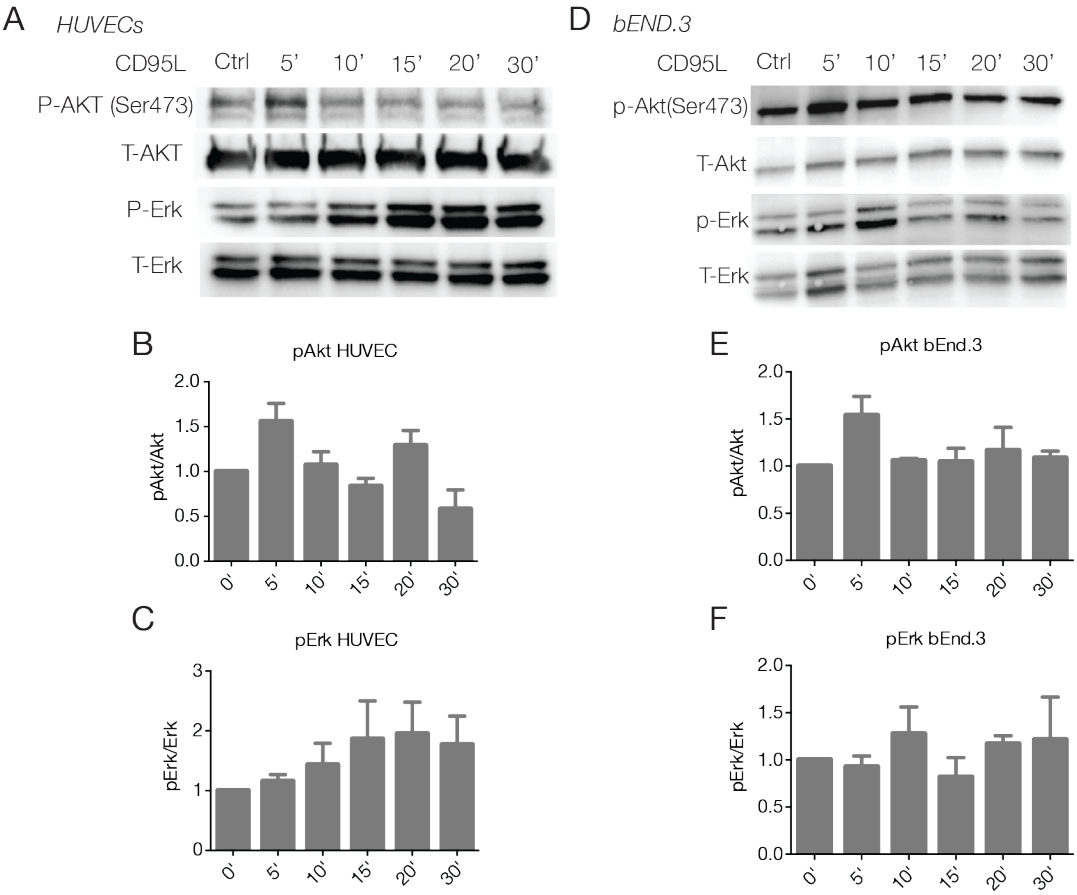


**Figure 3.14: CD95L activates Akt and Erk in endothelial cells.**
**A.** HUVECs were treated with 40 ng/ml CD95L for different time points and lysates were subjected to Western blot for Ser473 phosphorylated Akt (P-Akt (Ser473)), total Akt (T-Akt), phosphorylated Erk (P-Erk) and total Erk (T-Erk). **B-C.** Quantification of p-Akt (B) and p-Erk (C). C. bEnd.3 were treated with 40 ng/ml CD95L for different time points and lysates were subjected to Western blot for Ser473 phosphorylated Akt (P-Akt (Ser473)), total Akt (T-Akt), phosphorylated Erk (P-Erk) and total Erk (T-Erk). **D-E.** Quantification of p-Akt (D) and p-Erk (E).

Thus, Akt and Erk are two possible downstream effectors of PI3K activation that are responsible for the growth and proliferation of endothelial cells seen in the previous experiments.

To confirm that CD95 activates Akt and Erk to induce vessel growth on a functional level, we inhibited Akt signaling with a PI3K inhibitor LY294002 and Erk signaling with the Erk1/2 inhibitor PD98059 and assessed proliferation of HUVEC and bEnd.3 cells upon CD95L stimulation. Both LY294002 and PD98059 are effective at inhibiting Akt or Erk1/2 phosphorylation, respectively, already at low micromolar concentrations (Figure 3.15 A). 20 µM was chosen as it showed high effectiveness

with lower toxicity. CD95L stimulation resulted in increased Ki67 positivity in both HUVECs as well as bEnd.3 cells, which was significantly decreased upon additional inhibition of PI3K or Erk1/2 (Figure 3.15 B-E), indicating that endothelial cell proliferation upon CD95L treatment is dependent on PI3K/Akt and Erk1/2 signaling. Of note, Erk1/2 inhibition in HUVECs already leads to decreased proliferation by itself, possibly due to its toxicity in this primary cell line. (Figure 3.15 E).

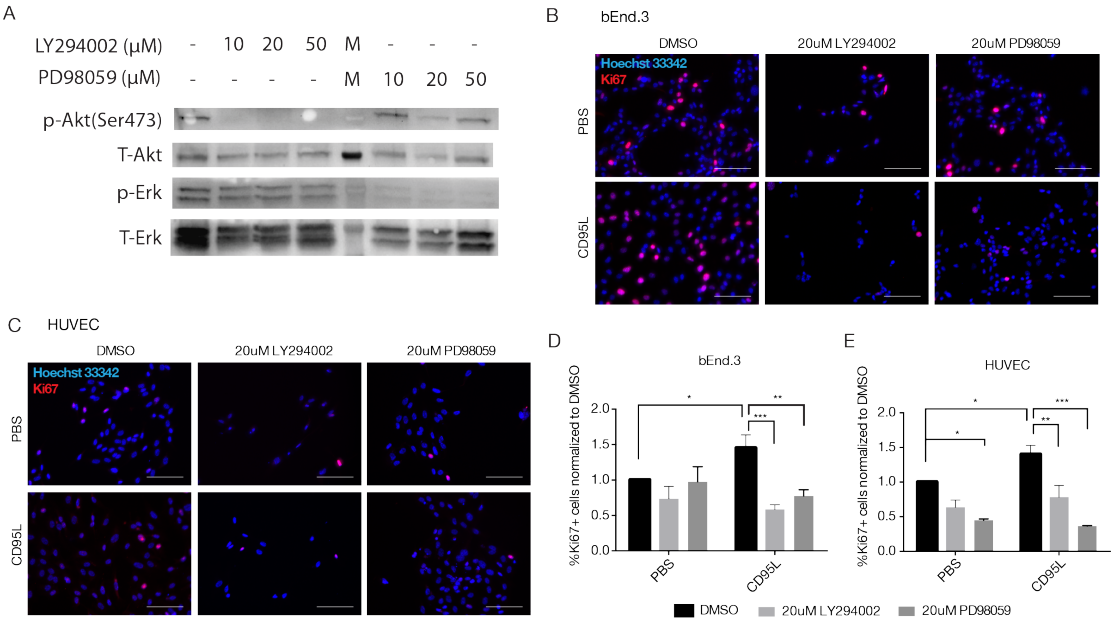


**Figure 3.15: Inhibition of Akt and Erk abrogates CD95L-induced endothelial cell proliferation.**

**A.** Western blot for p-Akt (Ser473), T-Akt, pErk1/2 and T-Erk of bEnd.3 cells treated with the PI3K inhibitor LY294002 and the Erk1/2 inhibitor PD98059 at different concentrations. **B-C.** Immunofluorescence staining for DAPI and Ki67 in bEND.3 (B) or HUVEC (C) cells treated with for 1h DMSO, 20 μM LY294002, 20 μM PD98059 in combination with PBS or 40 ng/ml CD95L. **D.** Quantification of $Ki67^{+}$ positive cells for B-C. Data are shown as mean±SD. *p<0.05, **p<0.01, ***p<0.001, statistical significance tested by ANOVA.

## 3.2 Investigation of CD95 function in glioblastoma angiogenesis

During development, angiogenesis occurs in a highly regulated manner to vascularize and support metabolic requirements of the tissue. These processes are exploited during tumor development, where angiogenesis is reactivated to support tumor cell growth and their nutrient demand (Weis and Cheresh, 2011). In fact, tumors are not able to grow above a certain size, if the "angiogenic switch" is not activated (Folkman, 1971).

One of the hallmarks of the most aggressive types of tumor in the brain, glioblastoma, is microvascular proliferation and angiogenesis (Dunn et al., 2012). Thus, we investigated the role of CD95 also during the process of glioblastoma angiogenesis.

### 3.2.1 Endothelial-specific deletion of CD95 does not significantly affect glioblastoma angiogenesis

In order to assess whether CD95 would also have an effect in glioblastoma angiogenesis, we again made use of the $CD95^{fl/fl}$;Cdh5-$CreER^{T2}$ mice and combined endothelial-specific CD95 deletion with an orthotopic tumor model. Deletion of CD95 was induced at adult age by tamoxifen injection for 5 days. After a break of 7 days during which tamoxifen could be cleared, SMA560 cells – a mouse syngeneic model of glioblastoma – were injected intracranially into the brain of $CD95^{fl/fl}$;Cdh5-$CreER^{T2}$ or $CD95^{fl/fl}$ control mice. Tumor as well as vessel growth were analysed two weeks after tumor cell implantation, when mice started to exhibit neurological symptoms due to tumor expansion (Figure 3.16 A). Tumor growth in $CD95^{fl/fl}$;Cdh5-$CreER^{T2}$ mice did not significantly differ from $CD95^{fl/fl}$, although a trend toward a decrease could be observed (Ctrl: 41.1 ± 24.2 $mm^3$ vs. KO: 25.3 ± 9.0 $mm^3$, p=0.08, Figure 3.16 C). The same was observed for vessel density, as assesed by percentage area calculations of CD31-positive staining within the tumor. Despite a tendency toward decreased vessel area, no significant change was observed in tumor vessels after deletion of CD95 in endothelial cells (Ctrl: 10.1 ± 2.9 %; KO: 7.8 ± 2.3 %, p=0.1, Figure 3.16 B-C).

(Data were generated together with Oguzhan Kaya.)

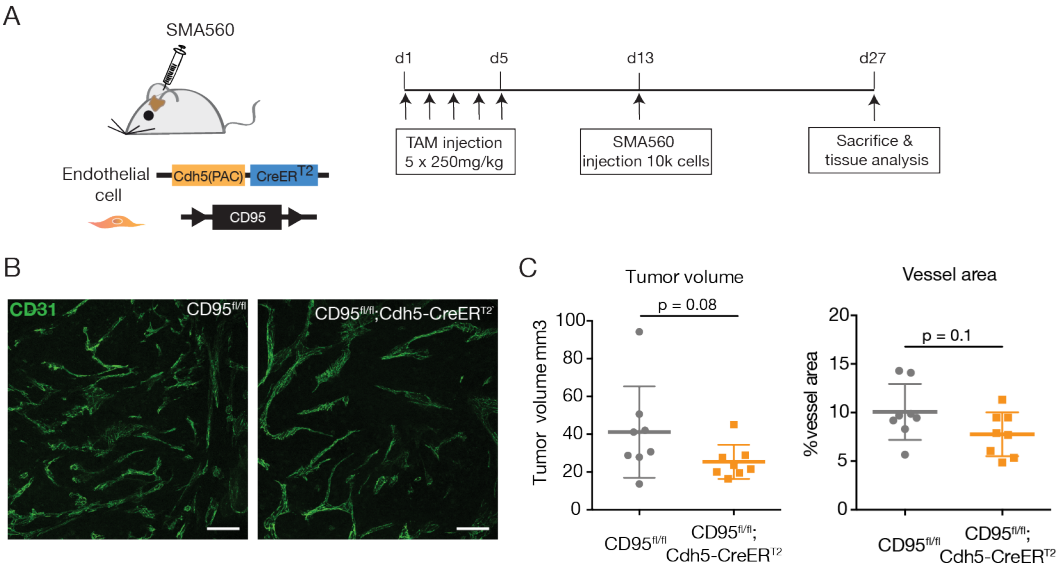


**Figure 3.16: Endothelial-specific deletion of CD95 does not significantly affect GBM growth and angiogenesis.**

**A.** Scheme of experimental design. Endothelial-cell specific deletion of CD95 was combined with a syngeneic model of glioblastoma – SMA560. Mice were first induced with tamoxifen for 5 days after which a break of 7 days was made. 10000 SMA560 were then intracranially injected into the mice and sacrificed 2 weeks later for tissue analysis. **B.** Representative images of tumor vessels in $CD95^{fl/fl}$ and $CD95^{fl/fl}$;Cdh5-$CreER^{T2}$ mice stained with anti-CD31. Scale bars: 100 µm. C. Quantification of tumor volume by stereologic analysis and percentage vessel area (Ctrl: n=8, KO: n=8).

Data are shown as mean±SD. Unpaired two-tailed student's t-test. (Data was generated together with Oguzhan Kaya.)

### 3.2.2 CD95 activation increases angiogenesis in a model of glioblastoma

To further study the effect CD95 activation may have on glioblastoma angiogenesis, we utilized a patient-derived xenografts (PDX) model and assessed whether CD95 activation by CD95L would increase tumor angiogenesis. PDX models have been increasingly accepted as the more relevant mouse model in preclinical cancer research as compared to syngeneic cell line models due to their higher applicability to the clinical situation.

Glioblastoma cells were isolated from a patient tumor (GBM39) and cultured *in vitro* under stem cell conditions before subcutaneous transplantation into immune-compromised SCID beige mice that lack T and B cells and have selective impairment in NK-cell functions. Eight weeks post transplantation, when small nodules first became visible, the mice were treated with either control- or CD95L-coated lipid beads by intravenous injection in order to assess the effect CD95 activation on tumor

vessels (Figure 3.17 A). Tumor growth was followed up and two weeks after treatment, the mice were sacrificed. When comparing the tumor size of CD95L- and control-treated mice, no significant difference was observed, although a trend toward increased tumor size was detected (Ctrl: 1281 ± 569 $mm^3$ vs. CD95L: 1991 ± 873 $mm^3$, p=0.07, Figure 3.17 B-C).

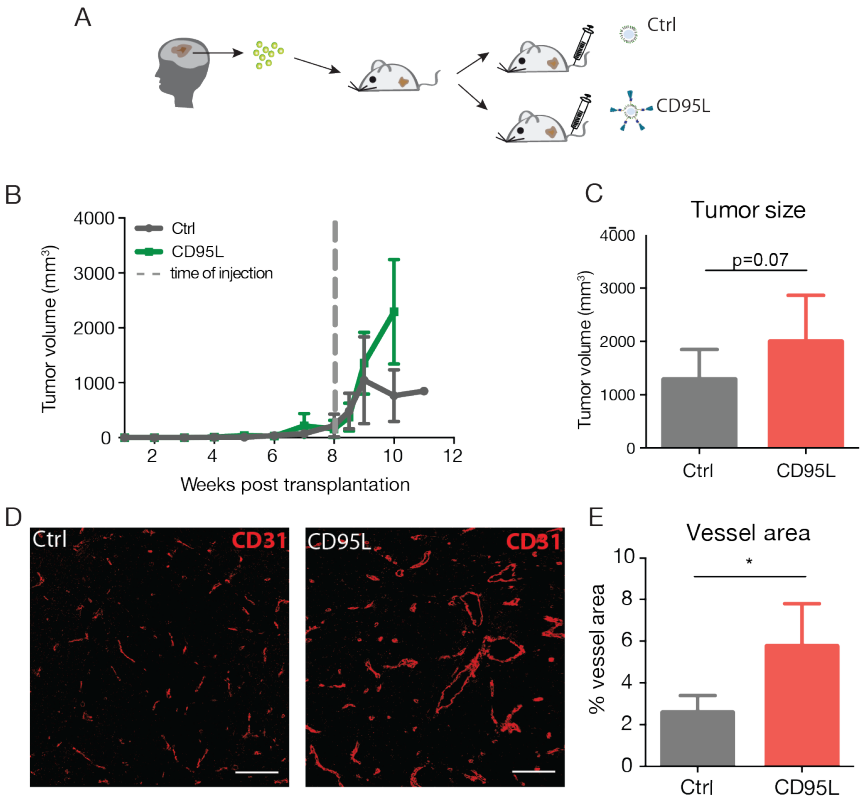


**Figure 3.17: CD95L stimulation increases tumor angiogenesis.**
**A.** Experimental scheme. Patient-derived glioblastoma cells were subcutaneously transplanted into SCID beige mice. Mice with established tumors were i.v. injected with Ctrl or CD95L-coated lipid bilayer beads. **B.** Development of tumor volume over time. **C.** Comparison of tumor size between control and CD95L-treated tumors at time of sacrifice (Ctrl: n=8 vs. CD95L: n=8). **D.** Representative images of CD31 stained tumors treated with control or CD95L. Scale bar = 100 µm. **E.** Quantification of vessel area (Ctrl: n=5 vs. CD95L: n=4). Data are shown as mean±SD. *p<0.05, unpaired two-tailed student's t-test.

Further, tumor vessels were quantified by immunohistochemical staining for CD31, which showed a significant increase in the percentage of tumor area covered by vessels in the CD95L-treated group compared to control-treated tumors (Ctrl: 2.6% ± 0.8 vs. CD95L: 5.7% ± 2.0, p=0.04) (Figure 3.17 D-E). This suggests that CD95L strongly promotes tumor vessel growth, either directly by acting on CD95 in endothelial cells

or indirectly by acting on CD95 in tumor cells that also express high levels of CD95 (Kleber et al., 2008).

### 3.2.2 Transcriptomic analysis reveals CD95L-induced upregulation of pro-angiogenic factors

To further explore the changes on GBM tumor upon CD95L treatment, we conducted RNA-sequencing experiments to assess transcriptomic differences. PolyA selected mRNA of three control-treated and three CD95L-treated tumors were isolated and libraries were prepared and sequenced. The quality of the RNA-sequencing experiment was controlled by spike-in RNAs of known concentrations, which strongly correlated with their reads detected (Figure 3.18 D). Moreover, the percentage of uniquely mapped reads was very high (~85%) which is indicative of low replicate reads (Figure 3.18 A) (These analyses were conducted by Sheng Zhao.)

Principal component analysis and hierarchical clustering of gene expression profiles of the single samples revealed a clear separation according to condition, except for the sample CD95L_3 which did not cluster to the appropriate group, possibly indicating non-responsiveness to CD95L or a technical error (Figure 3.18 B-C).

Next, we conducted differential expression analysis to investigate specific genes changing upon CD95L treatment. This revealed a total of 1119 genes to be differentially expressed between the two groups, among which 961 genes were upregulated and 150 were downregulated (cutoff: $p<0.05$, log2 fold change>0.5). To assess the functional relevance of the differentially expressed gene sets, we performed gene ontology functional enrichment analysis using the database for annotation, visualization and integrated discovery (DAVID) (Huang et al., 2008). This showed among the upregulated genes an overrepresentation of genes in several biological process categories involved in vessel development such as “angiogenesis”, “blood vessel development”, “blood vessel morphogenesis” as well as in related categories such as “response to hypoxia” and “extracellular matrix organisation” (Figure 3.19 A). Within the gene ontology category “blood vessel development”, various known, crucial drivers of angiogenesis were found, including VEGF, IL8, DLL4 etc. (Figure 3.19 B).

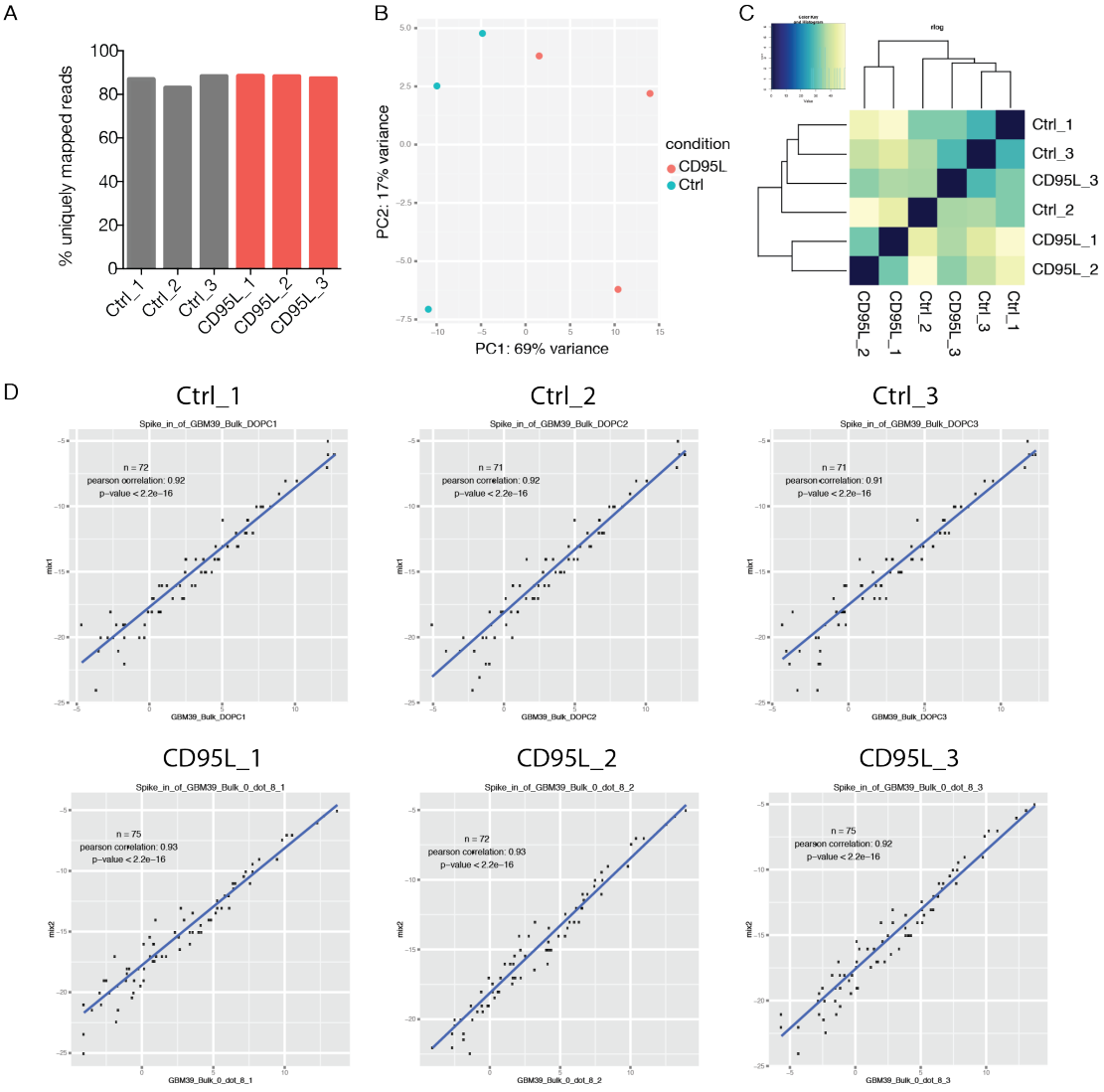


**Figure 3.18: Quality control of RNA-seq of Ctrl- and CD95L-treated tumors. A.** Percentage of reads uniquely mapped to the human genome (hg19). **B.** Principal component analysis of all six samples. **C.** Sample to sample heatmap. **D.** Correlation of reads detected and known concentration of spike-in RNAs. (Data from A. and D. are created by Sheng Zhao.)

Due to the fact that whole tumors were sequenced here without distinguishing between different cell types, it remains unclear whether CD95L induced the release of pro-angiogenic factors in tumor cells, endothelial cells, or other cell types. However, due to the majority of the cells within the tumor being GBM cells, it is mostly likely that CD95L binds CD95 on GBM cells to drive the production of pro-angiogenic factors.

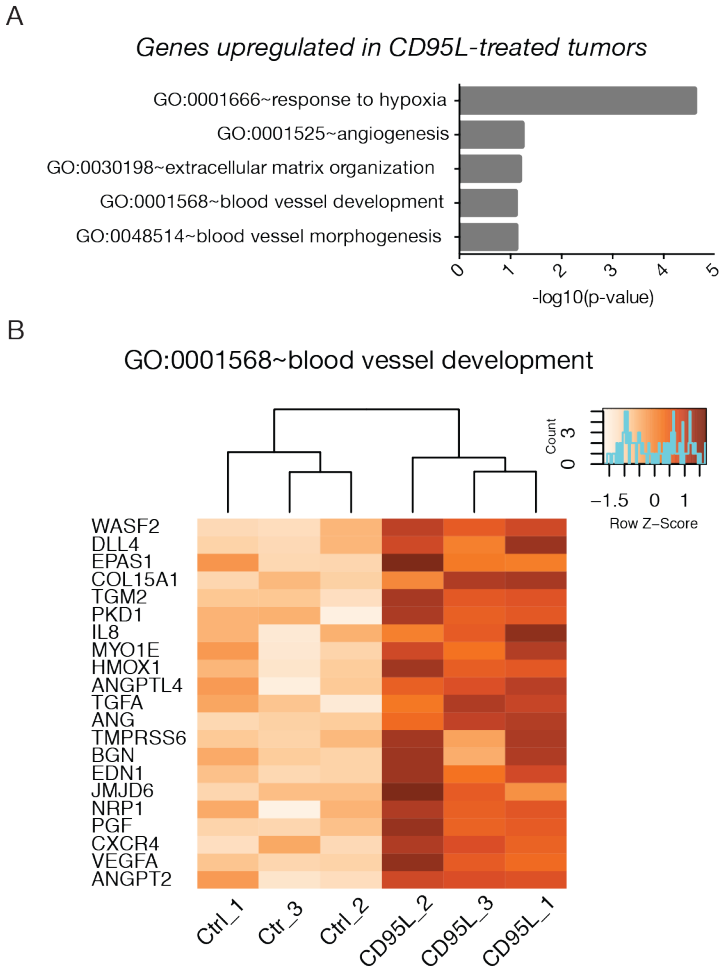


**Figure 3.19: Functional annotation of differentially expressed genes in Ctrl- vs. CD95L-treated tumors. A.** Selected gene ontologies and the statistical significance (shown as -log10 of Benjamini p-value) of the enrichment. **B.** Heatmap showing upregulated genes in CD95L-treated compared to control-treated tumors belonging to the gene ontology category blood vessel development. Color code represents z-score in a linear scale.

### 3.2.3 CD95L induces production of pro-angiogenic factors by GBM cells

In order to test whether indeed GBM cells are responsible for the increased vessel growth seen after CD95L treatment, we stimulated two human-derived GBM lines GBM39 and GBM48 *in vitro* on CD95L-membranes for 4 hours and collected conditioned media of the GBM cells 24 hours later (Figure 3.20 A).

The composition of the conditioned medium was subsequently analysed in regard to angiogenesis-related proteins using an angiogenesis antibody array (R&D Systems). This was composed of 55 antibodies for angiogenesis-related proteins spotted on a nitrocellulose membrane, thereby enabling simultaneous detection of various factors involved in angiogenesis. As expected, the conditioned media of both Ctrl- and

CD95L-stimulated GBM39 and GBM48 cells contained large, but equal amounts of EGF and bFGF, both of which were present in the GBM medium used for culturing GBM cells.

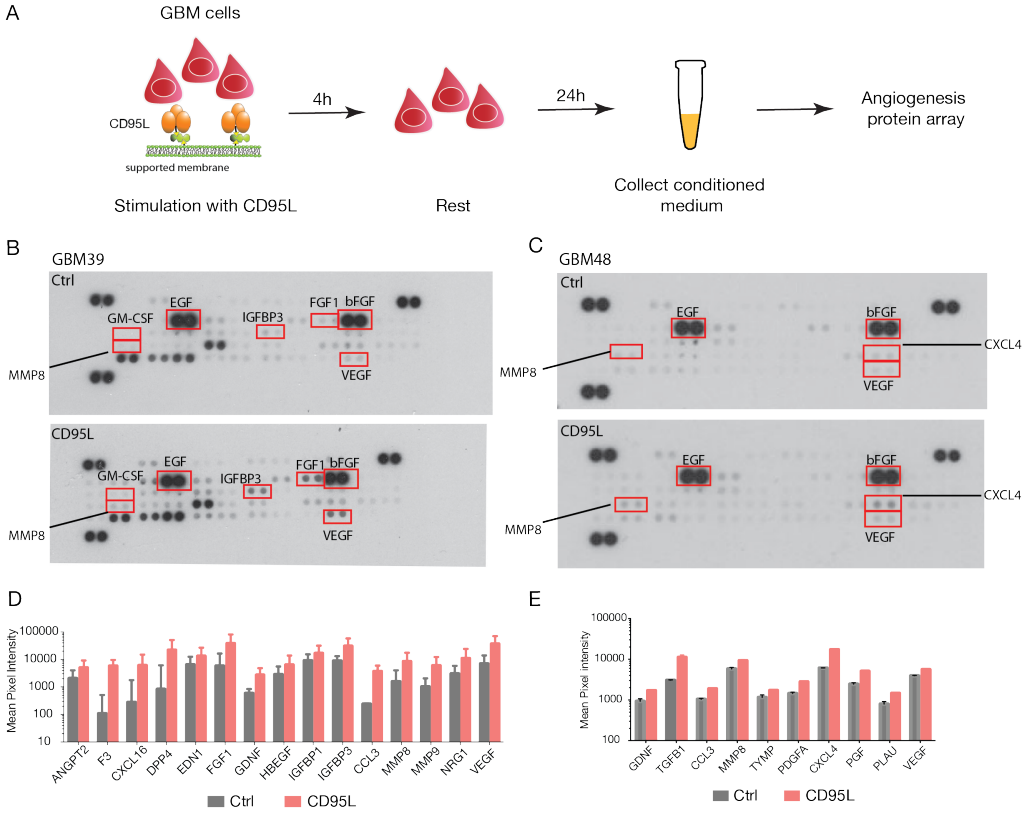


**Figure 3.20: Conditioned medium of CD95L-treated GBM cells contains pro-angiogenic factors.**
**A.** Experimental scheme. GBM cells were stimulated on CD95L membrane for 4 h and conditioned medium was collected 24 h later for angiogenesis protein array. **B-C.** Angiogenesis protein array blots for conditioned medium of GBM39 (B) and GBM48 (C) stimulated with control or CD95L membrane. Selected upregulated proteins are marked by red boxes. **D-E.** Mean pixel intensity plots for significantly upregulated proteins (fold change>2, p-value<0.05) for GBM39 (D) and GBM48 (E) conditioned medium.

Consistent with our hypothesis, the conditioned media of CD95L-treated cells contained much higher concentrations of various pro-angiogenic factors. These changes were cell-line-specific, with some factors only enriched upon stimulation in GBM39 cells and others in GBM48 cells (fold change>2, p-value<0.05) (Figure 3.20 B-E). VEGF-A, the most prominent pro-angiogenic factor, and the matrixmetalloprotease MMP8, were upregulated in both cell lines.

| Name | Gender | Age | Diagnosis | Treatment |
|---|---|---|---|---|
| GBM39 | female | 66 | Glioblastoma | Operation, concomitant radio- and chemotherapy |
| GBM47 | male | 18 | Glioblastoma | Operation, concomitant radio- and chemotherapy |
| GBM48 | Unknown | Unknown | Glioblastoma | unknown |

**Table 3.1: Clinical data of patients from whom GBM cells were derived.**

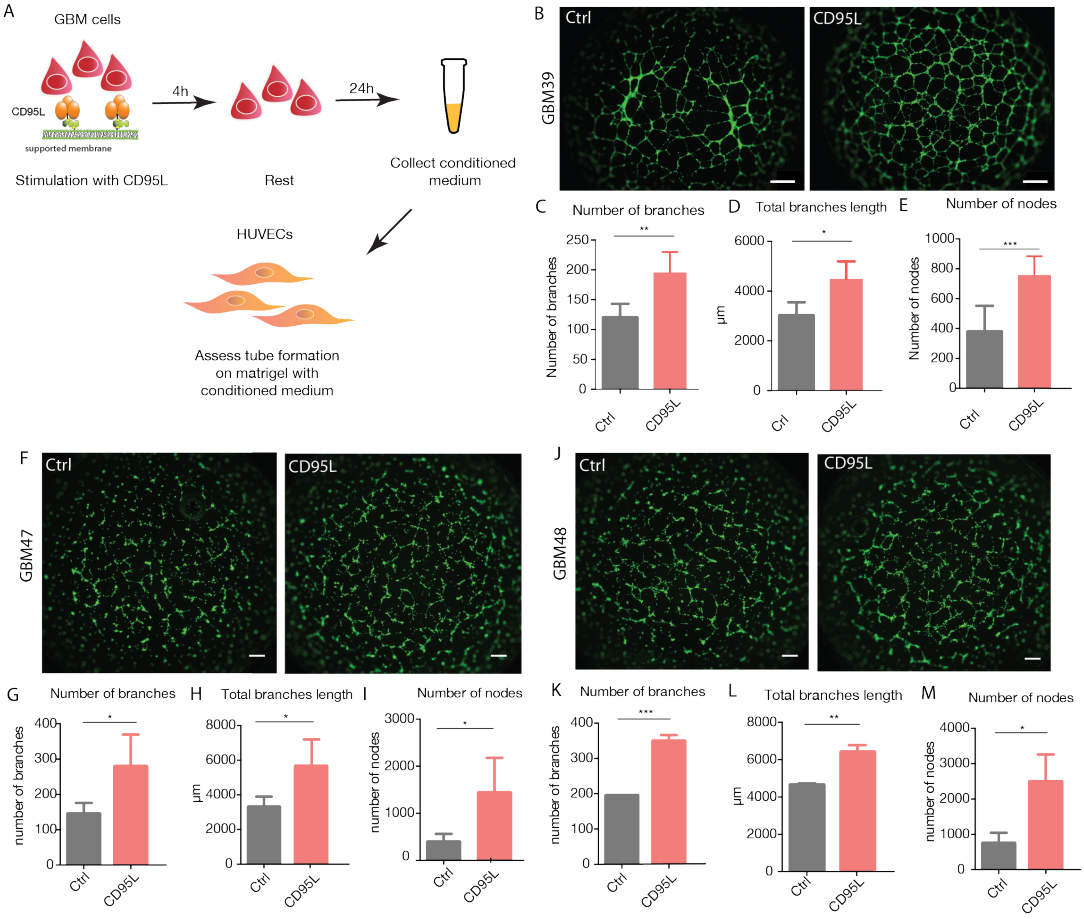


**Figure 3.21: Conditioned medium of CD95L-treated GBM cells increases tube formation in endothelial cells**

**A.** Experimental scheme. GBM cells were stimulated on CD95L membrane for 4 h, conditioned medium was collected 24 h later and given onto HUVEC cells in matrigel for tube formation assay. **B, F, J.** Representative images of endothelial tube formation with conditioned medium of control- or CD95L-treated GBM cells derived from three different patients. (n=3 for each patient) **C-E, G-I, K-M.** Quantification of B, F, J for number of branches, length and number of nodes. Unpaired two-tailed student's t-test.

To further test the functional effect of conditioned medium on angiogenesis, we added the GBM conditioned medium to HUVECs in matrigel and analysed their tube formation capacity (Figure 3.21 A). Conditioned medium from CD95L-treated

GBM cells resulted in a marked increase in the tube formation capacity of endothelial cells as compared to control-treated GBM cells, as evident through the number of tubes formed (GBM39: Ctrl: 119 ± 24 vs. CD95L: 196 ± 34, p=0.004; GBM47: Ctrl: 144 ± 32 vs. CD95L: 283 ± 42, p=0.01; GBM48: Ctrl: 194 ± 0 vs. CD95L: 349 ±18, p=0.007), their branching length (GBM39: Ctrl: 3010 ± 538 vs. CD95L: 4489 ± 702, p=0.006; GBM47: Ctrl: 3280 ± 617 vs. CD95L: 5775 ± 460, p=0.01; GBM48: Ctrl: 4635 ± 98 vs. CD95L: 6344 ± 435, p=0.003) and the number of nodes (GBM39: Ctrl: 376 ± 176 vs. CD95L: 756 ± 128, p=0.005; GBM47: Ctrl: 388 ± 175 vs. CD95L: 1757 ± 639, p=0.02; GBM48: Ctrl: 743 ± 302 vs. CD95L: 2486 ± 775, p=0.05) (Figure 3.21 B-M). This could not only been shown in the two primary cell lines GBM39 and GBM48 previously used to identify pro-angiogenic factors, but also in an additional primary cell line GBM47 (Table 3.1). In summary, this suggests that the pro-angiogenic factors contained in CD95L-treated tumor cell conditioned media indeed are functional and able to induce angiogenesis *in vitro*.

# 4. DISCUSSION

During development, a single cell is able through division and differentiation to make up a whole organism consisting of billions of cells. How a complex organ such as the brain is produced during this process is only slowly being comprehended in detail. Here, we uncovered a novel way of how cellular interactions during CNS development can contribute to the correct formation of cells within the brain and retina and demonstrate that the nervous and vascular systems are tightly connected during development.

The nervous and vascular systems follow similar growth patterns during development and are concomitantly regulated by a similar set of molecules. CD95 is a receptor that is expressed in both systems and has previously shown to promote neurite outgrowth and branching (Desbarats et al., 2003; Zuliani et al., 2006). We now demonstrate that CD95 is engaged in developmental angiogenesis in the cortex and retina, thus confirming our hypothesis that CD95 can act as an angioneurin during development.

Furthermore, we identify microglia, commonly known as the resident immune cells of the brain, as the main source of CD95L that interacts with its receptor CD95 on endothelial cells and neurons to induce their growth and branching. Thus, our data support an important novel role of microglia in the neurovascular development (Figure 4.1).

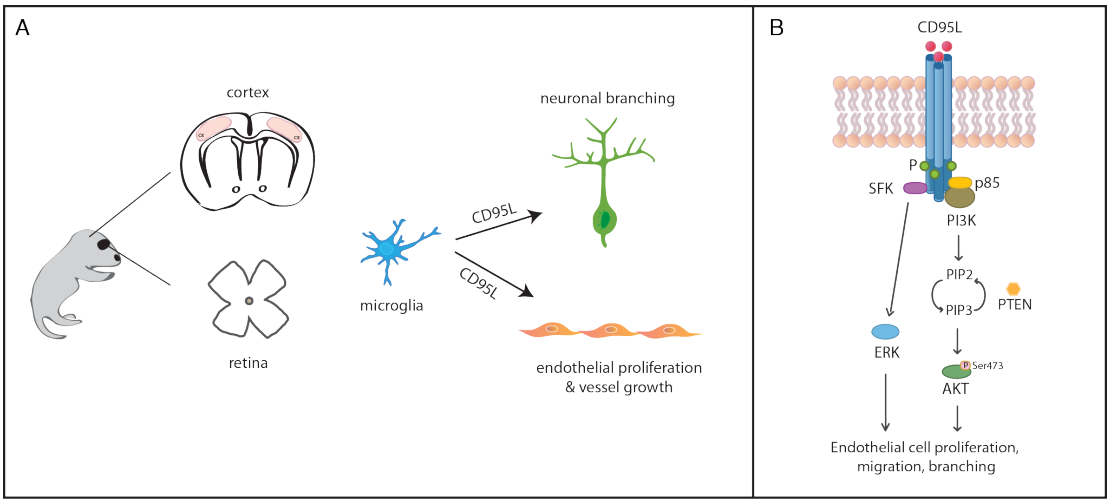


**Figure 4.1: Microglial-derived CD95L promotes neurovascular development. A.** Early postnatal development of vessels in the retina and neurons and vessels in the cortex are supported by microglial-derived CD95L that activates CD95 on neurons and endothelial cells. **B.** CD95 activation leads to recruitment of SFK and p85 to the CD95 death domain, resulting in activation of Erk and Akt signaling to promote endothelial cell proliferation, migration and branching.

Once development is completed, only little angiogenesis occurs. However, in tumors, the processes of development are often hijacked and exploited to drive tumor growth. Thus, we further examined the role of CD95 in glioblastoma angiogenesis. Unexpectedly, CD95 deletion in endothelial cells does not significantly affect vessel density in glioblastoma. This could be due to the nature of the highly proliferating syngeneic model used that might be independent of vessel supply. However, we found that CD95L stimulation of glioblastoma tumors indirectly promotes tumor vessel growth. As glioblastoma cells also express CD95, downstream signaling is elicited by CD95L stimulation in tumor cells that results in the production of pro-angiogenic factors. These are released by tumor cells into the their microenvironment in order to promote vessel growth (Figure 4.2).

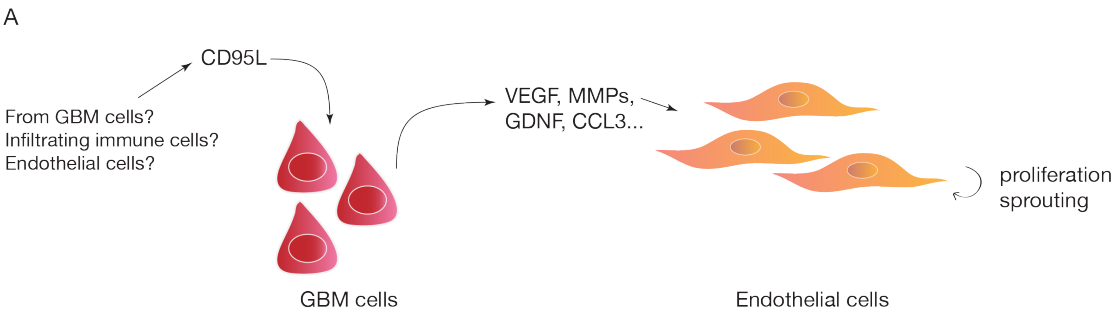


**Figure 4.2: Glioblastoma cells secrete pro-angiogenic factors upon CD95L stimulation. A.** CD95L possibly from the tumor microenvironment, e.g. from GBM cells themselves, infiltrating immune cells or endothelial cells activates CD95L on GBM cells resulting in the production of pro-angiogenic factors such as VEGF, MMPs etc. that promote endothelial cell growth and tumor angiogenesis.

By studying CD95 in development and disease we could show that it is both involved in angiogenesis of the developing CNS as well as in glioblastoma tumors.

## 4.1 CD95 in developmental angiogenesis of the CNS

By using *in vitro* models of angiogenesis and endothelial-cell specific deletion of CD95 *in vivo* we find that CD95 promotes endothelial cell proliferation and vessel branching during postnatal CNS development in the cortex and retina. When depleted of CD95, both vessels in culture as well as *in vivo* consistently display decreased branching and proliferation. In the retina, we further observed that the

increased branching is not due to a lack of pruning, but rather a direct effect on vessel growth. Consistent with this, no decrease in apoptotic endothelial cells is observed upon CD95 deletion.

Unlike in the retina, where angiogenesis starts postnatally and where the surface just becomes covered by vessels in the first 7 days after birth, the cortex is initially vascularized at E12.5 already. At the postnatal age of P6, when our analyses are conducted, the majority of the cortex vasculature is already existent, although endothelial cell proliferation and vessel branching is still taking place (Harb et al., 2012). The fact that CD95 seems to regulate both early and late angiogenesis in the retina and cortex hints at its versatile role. However, it would also be interesting to confirm CD95's role in early cortical angiogenesis at embryonic stages or in the early mouse hindbrain, another commonly used model for CNS angiogenesis due to the stereotypical ingrowth of vessels (Ruhrberg and Bautch, 2013). An early induction of CD95 deletion either using a Cdh5-cre line or tamoxifen administration to the pregnant mice would also give insights into the global phenotype of endothelial-cell CD95 deletion in embryonic development and its effect on embryonic survival. The drawback of the Cdh5-cre line however would be the unspecific targeting of hematopoietic cells (Alva et al., 2006) and tamoxifen induction in pregnant mice may cause toxic effects involving abortion or fetal death (Hayashi and McMahon, 2002; Higashi et al., 2009).

With the tamoxifen protocol applied for the mouse pups in this study, it was not possible to reach a 100% deletion of CD95. Based on the CD95 FACS data, a deletion of around 15% was reached. Thus, the effect sizes seen are not very pronounced with a decrease of vessel area of ca. 2-3% and of branching of ca. 5-10% after CD95 deletion. These numbers however are comparable with other molecules involved in developmental angiogenesis, such as another angioneurin Slit1/2 (Rama et al., 2015).

A number of proteins are implicated in developmental angiogenesis. Among those, VEGF-A and its main receptor VEGFR2 are the best studied. VEGF-A regulates various steps of developmental angiogenesis and exhibits a severe phenotype when deleted (Raab et al., 2004). CD95L thus is one of many players in angiogenesis and

may have overlapping functions with other growth factors. In fact, it has previously been demonstrated that HUVECs express an increased level of VEGF-A when stimulated by CD95L (Marx et al., 1999). It however also remains to be discovered whether the CD95L pathway can crosstalk with the VEGF-A pathway.

### 4.2 Controversial role of CD95 in angiogenesis

CD95 has not been described to promote angiogenic processes in development previously. Rather the opposite has been reported in that CD95 acts as a death receptor to induce apoptosis in endothelial cells upon CD95L exposure, in different pathological settings as well as during development, mainly in the retina (Barreiro et al., 2003; Davies et al., 2003; Ishida et al., 2003; Kaplan et al., 1999). These findings however stand in sharp contrast to studies that suggest endothelial-cell resistance to CD95-induced apoptosis (Aoudjit and Vuori, 2001; Bannerman et al., 2001; Limaye et al., 2005; Richardson et al., 1994; Sata et al., 2000; Suhara et al., 2001). Especially in situations of acute inflammation, the endothelium is protected against apoptotic signals from cytotoxic immune cells such as CD95L or TNFα (Al-Lamki et al., 2008), and rather exhibit increased growth (Biancone et al., 1997), indicating that CD95 signaling may confer endothelial cell survival.

The discrepancy may be a result of the different mouse models used. While previous studies were mainly conducted with the *lpr* or *gld* mice or systemic treatment that affect CD95 or CD95L expression globally in every cell, the model used in this study specifically targets deletion of CD95 in endothelial cells, thus pinning the observed effects down to the cell type of interest. Systemic effects of global deletions have masked CD95's function in other studies before. While it was thought that CD95 has a direct detrimental function on injured tissues of the CNS through induction of apoptosis (Broughton et al., 2009; Demjen et al., 2004), it was actually found that after spinal cord injury CD95 and its ligand participate in the recruitment of innate inflammatory mediators that are ultimately responsible for increased cell death (Letellier et al., 2010). Thus, cell-specific models may give more precise insights into the function of a protein. In both our *in vitro* as well as *in vivo* analyses no significant alterations to apoptosis rate were observed after modulating CD95.

In addition to CD95, other DD-containing receptors were also shown to be involved in angiogenesis. For instance, another member of the TNF receptor superfamily TNFR1 mediates TNFα-mediated tip cell induction and angiogenic sprouting (Sainson et al., 2008). Moreover, the DD-containing netrin receptor UNC5B is present in endothelial tip cells and modulates vascular morphogenesis through filopodial repulsion (Llambi et al., 2001; Lu et al., 2004). The presence of a DD therefore does not preclude from non-death functions of a receptor.

### 4.3 CD95 signaling elicits angiogenesis

CD95 is generally known as a cell death receptor. However, increasingly more studies underpin its functions in promoting cell survival, both in homeostasis as well as in disease (Brint et al., 2013). CD95's DD is known to be able to recruit alternative players beside cell death-inducing caspases to signal for proliferation, migration and growth (Sancho-Martinez and Martin-Villalba, 2009). As a cell surface receptor with adaptor-dependent intracellular kinase activity, CD95 is able to share the same signaling machinery with other receptor tyrosine kinases. The ability of the intracellular domain of CD95 to bind SH2-domain proteins (Sancho-Martinez and Martin-Villalba, 2009) therefore provides a signaling hub for proliferation, migration and branching.

Here, we find that CD95 engages Src family kinases and the PI3K regulatory subunit p85 specifically at the ITAM/ITIM-like domain with the YXXL motif in its DD and induces downstream phosphorylation of Erk and Akt in endothelial cells. In absence of Erk and Akt signaling through pharmacological inhibition, the proliferative effect of CD95 on endothelial cells is abrogated *in vitro*.

Thus, CD95 signaling inputs directly into major established pathways controlling vessel fate. PI3K and its main downstream target Akt play important roles in endothelial cell proliferation and migration (Gerber et al., 1998; Jiang et al., 2000; Somanath et al., 2006). Akt can phosphorylate the cell cycle inhibitor $p21^{Cip1}$ in endothelial cells, resulting in release of the replication protein PCNA and subsequent induction of endothelial cell proliferation (Rossig et al., 2001). Moreover, activation of the PI3K pathway via VEGFR2 has been shown before to trigger Rac/Rho as well as Grb2 and subsequently Cdc42, resulting in actin reorganization, filopodia

formation and cell migration in endothelial cells (Lamalice et al., 2004; Le Boeuf et al., 2004; Ruiz de Almodovar et al., 2009). In addition, CD95 may also support endothelial cell migration through activation of MMPs via a PI3K/Akt/GSK3β axis previously shown for glioblastoma cells (Kleber et al., 2008). Interestingly, CD95L can also mediate eNOS expression through Akt phosphorylation in order to regulate vascular tone and proliferation (Takemura et al., 2004).

Erk signaling overlaps in some aspects with the functions of PI3K signaling and can also induce endothelial cell proliferation as well as migration (Srinivasan et al., 2009). Deletion of Erk1/2 in endothelial cells results in embryonic lethality at E10.5 which is caused by decreased endothelial proliferation and migration as well as perturbed actin organization due to reduced levels of Paxilin and FAK (Srinivasan et al., 2009). Similar to VEGF-A, CD95 may induce Erk activity through Src and c-Raf activation (Hood et al., 2003).

The exact final effectors downstream of Erk and Akt that are ultimately responsible for the branching and proliferation phenotype elicited by CD95 activation remain to be elucidated.

Both the PI3K/Akt and Erk pathways can be activated downstream of SFKs (Lowell, 2011; McKay and Morrison, 2007; Rui et al., 1AD). SFKs are known to promote endothelial cell differentiation (Klint et al., 1999), survival (Wong et al., 1999), proliferation and angiogenesis (Eliceiri et al., 1999) and have been shown to be required for endothelial cell survival (Eliceiri et al., 1999) . The different members of SFKs such as Src, Yes and Fyn often have redundant functions and many have been shown to be involved in angiogenic processes. Major growth factors including VEGF-A and EGF signal through Src (Eliceiri et al., 1999; Thakker et al., 1999) to promote angiognesis.

To further validate whether PI3K and Erk are both activated by SFKs, SFK inhibition using the SFK inhibitor PP2 together with analysis of Akt and Erk phosphorylation upon CD95L stimulation can be conducted.

As neither Erk1/2 inhibition with PD98059 nor PI3K inhibition with LY294002 blocked proliferation of endothelial cells *in vitro* completely, CD95 may be mediating proliferation through multiple pathways. Concurrent inhibition of both PI3K and Er1/2 could provide insight into whether this is the case.

An open question remains which form of CD95L – the soluble or membrane bound – induces endothelial cell growth. In our *in vitro* tube formation experiments, we used trimerized CD95L bound to lipid membranes that resemble the membrane-bound form. This form of CD95L has been described to induce apoptosis, for instance in neurons, whereas the soluble form of CD95L antagonizes apoptosis (Gregory et al., 2011; Matsumoto et al., 2015; O' Reilly et al., 2009). However, the Western blot analyses also showed phosphorylation of downstream AKT and ERK upon stimulation of endothelial cells by soluble trimerized CD95L. Thus, it seems that endothelial cells are resistant to both membrane-bound as well as soluble forms of CD95L-induced apoptosis. This is likely also due to the elevated expression of the caspase-8 inhibitor c-FLIP (Suhara 2001). Which form(s) of CD95L is expressed by microglia *in vivo*, the main source of CD95L in the CNS, remains elusive. As microglia express matrixmetalloproteases during development that are required for CD95L cleavage from the membrane (Kierdorf et al., 2013), both forms of the ligand could potentially be present.

### 4.4 The angiogenic process: where does CD95 regulation fit?

Here, we report that CD95 is required for proper branching of vessels and proliferation of endothelial cells. How does this fit into the angiogenic process of tip/stalk cell selection, tip cell sprouting, stalk cell proliferation, guidance, anastomosis and vessel maturation?

As CD95 activates the Akt and Erk pathway, it potentially plays an important role in several steps. CD95 may be crucially involved in the first phase of angiogenesis through activation of MMPs via the PI3K/AKT/GSK3β pathway that has been previously described for glioblastoma cells (Kleber et al., 2008) MMP-mediated breakdown of the extracellular matrix is crucial for endothelial tip cells to begin the sprouting process (Potente et al., 2011). While the tip cells are sprouting, stalk cells proliferate to form the vessel lumen and CD95 seems to contribute to this process as well. At the same time, Erk and PI3K-induced cytoskeletal changes via FAK or Cdc42 respectively can lead to guidance-induced migration as well as increased branching.

In summary, we suggest that CD95 is involved in several steps of the angiogenic process, mainly promoting migration and proliferation of endothelial cells, two crucial processes during angiogenesis required for proper vessel formation.

### 4.5 CD95 in neuronal regulation

Beside CD95's role in vessel development, we further show that microglial-derived CD95L can affect dendrite branching of cortical neurons. Previous studies already described the involvement of CD95 in neurite branching of peripheral neurons as well as hippocampal neurons (Desbarats et al., 2003; Zuliani et al., 2006). Moreover, unpublished data from our laboratory show that neuron-specific deletion of CD95 by *in utero* electroporation results in decreased dendrite branching of layer II/III callosal projection neurons. However, the source of CD95L was not clear so far. By deleting CD95L specifically in microglia, the cell type in the brain that produces the largest amount of CD95L, we could see a similar decrease on callosal projection neuron branching, thus demonstrating that CD95L produced from microglia has the largest effect on neuron development.

Similar to endothelial cells, CD95 promotes dendritic branching via SFK and PI3K (unpublished data). Knockdown or pharmacological inhibition of SFK and PI3K abrogate CD95L-mediated neuronal branching. Further, unpublished data from our laboratory show that inhibition of PI3K in neurons abolishes CD95-dependent phosphorylation of GSK3β, a target effector of PI3K signaling important for the establishment and maintenance of neuronal polarity and neurite length (Jiang et al., 2005; Yoshimura et al., 2005). Moreover, GSK3β phosphorylation and therefore inactivation leads to dephosphorylation of Tau that promotes assembly and stabilization of microtubules important for regulation of neuronal morphology (Zuliani et al., 2006). As a regulator of GSK3β, CD95 thus can act as a determinant of neuronal polarity as well as promoter of branching.

A parallel pathway that has been described for CD95 in neurons is the recruitment of the adaptor protein ezrin and subsequent activation of Rac1, resulting in neurite growth in cortical neurons (Ruan et al., 2008).

Here, we merely describe CD95's role in dendritic branching. However, previous studies have also indicated CD95 in axonal branching of hippocampal neurons

(Zuliani et al., 2006). Thus, CD95 does neither seem to be a dedicated or a bimodal regulator but instead is involved in both axonal as well as dendritic branching, possibly at different developmental stages.

### 4.6 The connection of neural and vascular system and CD95

Previous studies have identified a number of growth factors and guidance molecules that are involved in the establishment of the neurovascular network (Segura et al., 2009). Similar to these molecules, we show that CD95/CD95L signaling promotes both neuronal branching and vessel growth to support congruent development of these two systems. In both neurons and endothelial cells, development is promoted by SFK and PI3K signalling via the CD95 death domain. We propose that by utilizing its tyrosine phosphorylation, CD95 acts as a growth factor receptor stimulating branching in neurons and proliferation in vessels.

An interesting question remains whether aberrant vessel growth in the $CD95^{fl/fl}$;Cdh5-(PAC)-$CreER^{T2}$ would affect neuron growth and function and conversely, whether neuronal branching defects associated with CD95 deletion would perturb vessel growth. Further studies are required to answer these questions related to the functional dependency of neurons and vessels.

As we have shown in the FACS experiments for CD95, neurons and endothelial cells are not the only populations expressing it. $CD133^{+}$ neural stem cells also exhibit high expression of CD95, thus it is likely that CD95 might also have a role in embryonic neural stem cell survival and differentiation, similar to the adult situation (Corsini and Martin-Villalba, 2010).

### 4.7 Novel functions of microglia

Extensive reciprocal interaction exist between different cell types of the CNS during development. We identify an important neuron/vessel/glia-interaction that is essential for proper neurovascular development. Traditionally, microglia have been mainly attributed the role of phagocyting apoptotic neurons (Bessis et al., 2007; Schlegelmilch et al., 2011). However, a plethora of studies have eluted to other functions of microglia beyond this. Microglia have been shown to have a variety of functions during brain development, including neuronal survival, vascularization, cell

differentiation as well as axon pathfinding and synaptogenesis (Aarum et al., 2003; Arnold and Betsholtz, 2013; Jonakait et al., 2000; Pont-Lezica et al., 2014; Ueno et al., 2013; Zhan et al., 2014). Interestingly, microglia can also promote neurite outgrowth and development in co-culture or conditioned media experiments, partially by releasing thrombospondin (Chamak et al., 1994; Pont-Lezica et al., 2014; Zhang and Fedoroff, 1996). In the brain and retina, microglia associate closely to vascular junctions in order to "bridge" vascular sprouts and depletion of microglia from the developing brain or retina reduces vessel density and branching (Checchin et al., 2006; Fantin et al., 2013; Rymo et al., 2011). The molecules responsible for microglia's ability to shape the neural and vascular system, however, have not been well studied so far. Our study provides evidence that CD95L is one of the players expressed by microglia that mediates both processes.

The CD95L$^{f/fl}$; LysMcre model used in this study to assess the effect of CD95L deletion on the neurovascular system, did not reach a 100% deletion of CD95L. This is partially due to the fact that the LysM promoter is expressed in ca. 30% of microglia. An underestimation of the effect of microglia-derived CD95L can therefore not be completely excluded, especially in regard to the observed tendency towards decreased vessel branching in CD95L deleted mice. The fact that a functional impairment in vessels and neurons was still observerd indicates that microglia-derived CD95L has a strong effect on both systems. An alternative to the LysM driver for the expression of cre-recombinase would be a Cx3cr1 driver which is expressed in nearly 100% of microglia (Goldmann et al., 2013) and can therefore lead to a higher level of deletion of the floxed gene. This line might also be helpful in detecting CD95L-dependent angiogenesis in the retina which was not possible using the LysM-cre line. LysM is also expressed in peripheral monocytes and macrophages and whether lack of CD95L in this cell types could affect the CNS development is unclear. With the blood-brain-barrier established at E13.5-E14.5 (Schneider 2015), it is however unlikely that peripheral cells enter the CNS without any perturbations in order to alter CNS development.

Moreover, as our FACS analysis showed, not only microglia express CD95L but also endothelial cells, although to a much lower extend. This is consistent with studies from literature, where CD95L was found to be expressed by human brain

microvascular endothelial cells (Bajou et al., 2008). Therefore, autocrine signaling in endothelial cells via self-produced CD95L cannot be ruled out and may also contribute to CD95-mediated vessel growth. To address this question, CD95Lfl/fl; Cdh5-(PAC)-CreER$^{T2}$ mice could be utilized.

One of the preferential localizations of microglia in the developing brain is areas of neuronal cell death which are associated with debris clearance (Cuadros et al., 1993; Peri and Nüsslein-Volhard, 2008). However, once clearance is completed, microglia might participate in reshaping surviving neurons, and concomittantly engaging the development of vessels to ensure their oxygen and nutrient support. Together, our study adds to the existing functions of microglia during development and establishes a link for neurovascular development by microglia through CD95L.

### 4.8 Implications on brain function and behavior

With CD95/CD95L deletion leading to impairments in neuronal and vessel branching that are crucial for the brain's function, it would be interesting to assess whether this would have a long-term functional effect on the brain.

Notably, early studies from the 90s using MRL *lpr* mice have already uncovered that loss of CD95 can induce a series of neurological symptoms. In these mice, global CD95 deficiency induced a number of behavioral and cognitive deficits at the age of 7-11 weeks that were assessed by standardized tests. The deficits included reduction in spontaneous activity, impaired exploration of the open field, increased anxiousness and disturbed emotionality (Sakić et al., 1992; 1994; Szechtman et al., 1997).

This phenotypes were attributed to a strong reduction of dendritic branching and loss of up to 20% of spines in pyramidal neurons in the parietal cortex and CA1 hippocampus at 5-14 weeks, induced by autoimmunity-associated CNS inflammation (Sakić et al., 1998). During development, however, when inflammation is not apparent yet in *lpr* mice, neuronal branching is still affected by CD95 deletion in hippocampal neurons (Zuliani et al., 2006), indicating that inflammation is not the main cause of the neuronal impairments. Thus, a lack of CD95 may directly influence behavioral and cognitive functions of the brain.

### 4.9 CD95 and glioblastoma angiogenesis

In different pathologies, angiogenesis plays an important role. Especially in cancer, angiogenesis is the major process by which new blood vessels are built to nourish tumor cell growth (Folkman, 1971). GBM is a type of cancer of the brain that is highly heterogenous, highly migratory and highly angiogenic.

As tumor vessels exhibit CD95 expression (Bhattacharya et al., 2016) we expected that CD95 also has a role during tumor angiogenesis. However, deletion of CD95 in endothelial cells did not affect the growth of tumor vessels in GBM in a syngeneic intracranial transplantation model. This may either be due to technical reasons whereby non-complete deletion of CD95 led to the preferred growth of WT endothelial cells in the tumor, or due to the fact that the syngeneic model represents a fast-growing tumor model that may not necessarily rely on tumor angiogenesis.

Surprisingly, treatment of subcutaneous tumor-bearing mice with the CD95L led to an increased vessel growth as well as a tendency of increased tumor growth. As GBM cells themselves are known to express CD95 and its activation has previously been shown to be vital for GBM migration and invasiveness as well as survival (Hadji et al., 2014; Kleber et al., 2008), we suspected an effect of CD95L on GBM cells that led to the increased angiogenesis. Indeed, GBM cells increased their expression of pro-angiogenic factors such as VEGF-A, IL-8 and DLL4 upon CD95L stimulation. Moreover, GBM culture conditioned medium also contain increased pro-angiogenic factors after CD95L treatment and the conditioned medium has a functional effect on endothelial cells as evident through increased tube formation in matrigel. Thus, it seems like that GBM cells do not only require CD95 for growth and migration, but also utilize it for tumor angiogenesis. In fact, it has been previously shown that CD95 activation in glioma cells can lead to production of chemokines such as MCP-1, IL-8 and IL-6 (Choi et al., 2001; 2002). Interestingly, GBM cells themselves as well as glioma-associated microglia produce CD95L (Badie et al., 2001; Kleber et al., 2008) that can potentially drive tumor angiogenesis in situ through activation of CD95 on tumor cells.

It remains elusive how CD95 activation on GBM cells results in expression of pro-angiogenic factors. However, VEGF-A expression for instance can be directly activated downstream of Erk signaling (Berra et al., 2000; Choi et al., 2001), a

pathway that is also activated by CD95 in tumor cells (Barnhart et al., 2004). Further experiments involving inhibition of the Erk pathway and its effect on pro-angiogenic factor release from CD95L stimulated GBM cells will provide answers to this question.

With CD95 involved in GBM migration, growth and angiogenesis, targeting CD95 signaling as a therapeutic intervention for GBM is an attractive avenue. APG101, a fusion protein of the extracellular domain of CD95 and the FC domain of IgG, has already been designed to block CD95L as a decoy receptor. In a phase II clinical trial, APG101 treatment has increased the percentage of patients reaching six months of progression-free survival in combination with radiotherapy (Bendszus et al., 2012).
CD95L was recently described to be expressed on the endothelium of different tumor entities with the function of inducing apoptosis of tumor invading cytotoxic T-cells, thus allowing immune evasion. The expression of CD95L on tumor endothelium was further found to be upregulated by tumor cell secreted IL-10, PGE2 and VEGF-A (Motz et al., 2014). Thus, blocking CD95L with a CD95-Fc such as the APG101 may act on different levels of tumor growth and serve as a multifunctional approach.

### 4.10 Conclusive remarks

In summary, the data from this study support an important role of microglia in neurovascular development and reveal an important function of the CD95/CD95L system in angiogenesis both during development and cancer. These results implicate that the CD95/CD95L system may be targeted to modulate neurovascular plasticity in the brain or angiogenesis in brain tumors.

# 5. APPENDIX

## 5.1 Fiji scripts

### 5.1.1 Macro for vessel area analysis

```
// choose folder with images to analyse
showMessage("Si, bitte wähle einen Ordner, dessen Inhalt bearbeitet
werden soll.");
dir = getDirectory("Choose a Directory ");
list = getFileList(dir);

// choose folder for analysed images
showMessage("Si, bitte wähle einen Ordner, in den die bearbeiteten
Bilder gespeichert werden sollen.");
folder = getDirectory("Choose a Directory");

// loop for each picture of the folder
// reset ROI manager after each loop run
for (i=0; i<list.length; i++) {
      roiManager("Reset");
      showProgress(i, list.length);
    open(dir+list[i]);

      title= getTitle();
      image= folder+title;

      //set scale for image, taken with 20x ojective SP5
      run("Set Scale...", "distance=1.3213 known=1 pixel=1 unit=um
      global");

      //background substraction and filter
      run("Subtract Background...", "rolling=10 sliding");
      run("Gaussian Blur...", "sigma=2");

      // Color Thresholder 2.0.0-rc-28/1.49q
      min=newArray(3);
      max=newArray(3);
      filter=newArray(3);
      a=getTitle();
      run("HSB Stack");
      run("Convert Stack to Images");
      selectWindow("Hue");
      rename("0");
      selectWindow("Saturation");
      rename("1");
      selectWindow("Brightness");
      rename("2");
      min[0]=0;
      max[0]=255;
      filter[0]="pass";
      min[1]=0;
      max[1]=255;
      filter[1]="pass";
      min[2]=38;
      max[2]=255;
      filter[2]="pass";
      for (j=0;j<3;j++){
            selectWindow(""+j);
            setThreshold(min[j], max[j]);
```

```
            run("Convert to Mask");
            if (filter[j]=="stop")  run("Invert");
            }
      imageCalculator("AND create", "0","1");
      imageCalculator("AND create", "Result of 0","2");
      for (j=0;j<3;j++){
            selectWindow(""+j);
            close();
            }
      selectWindow("Result of 0");
      close();
      selectWindow("Result of Result of 0");
      rename(a);
      // Colour Thresholding end

      //save thresholded picture
      saveAs ("Tiff", image+ " Threshold Mean");


      //measure area of all vessels, excluding particles smaller than
      400px
      run("Analyze Particles...", "size=400-Infinity show=Outlines
      display summarize add");

      //save image with outlines of analysed particles
      saveAs("PNG", image + "-outline.png");


      close();

      selectWindow(title+" Threshold Mean.tif");
      close();

      }
```

### 5.1.2 Macro for cortical vessel branching analysis

```
// choose folder with images to analyse, should be thresholded image
from the area analysis
showMessage("Si, bitte wähle einen Ordner, dessen Inhalt bearbeitet
werden soll.");
dir = getDirectory("Choose a Directory ");
list = getFileList(dir);

// choose folder for analysed images
showMessage("Si, bitte wähle einen Ordner, in den die bearbeiteten
Bilder gespeichert werden sollen.");
folder = getDirectory("Choose a Directory");


// loop for each picture of the folder
// reset ROI manager after each loop run
for (i=0; i<list.length; i++) {
      roiManager("Reset");
      showProgress(i, list.length);
     open(dir+list[i]);

      title= getTitle();
      image= folder+title;
```

```
//set scale for image, taken with 20x ojective SP5
run("Set Scale...", "distance=1.3213 known=1 pixel=1 unit=um
global");

//measure branches (number, branches)
run("Skeletonize");
run("Analyze Skeleton (2D/3D)", "prune=none calculate show
display");

//save table with info on number of branches and branching
points
selectWindow("Results");
saveAs("Measurements", image+ "_results.xls");
close();

//save table with info on branch lengths
selectWindow("Branch information");
saveAs("Measurements", image+ "_branch_length.xls");
close();

//save image of skeletonized vessels
selectWindow(title);
saveAs("Tiff", image+"_skeleton.tif");
close();

}
```

## 5.2 R scripts:

### 5.2.1 Interpolation of intracranial tumor volume

This script was created by Frederik Ziebell.

```
library(ggplot2)

# measured areas of the slides
y <- c(2,3,6,8,4,3)

# distances between slides
# Note: there need to be exactly n-1 distances to be specified
between the n slides
# dist[i] is the distance between slide i and slide i+1
dist=c(7,10,8,6,3)

x <- cumsum(append(dist,0,0))
d <- data.frame(x, y)
sfun <- splinefun(d,method="fmm")
area <- integrate(sfun,min(x),max(x))

ggplot(d,aes(x,y)) +
  geom_point() +
  stat_function(fun=sfun) +
  ggtitle(paste("Volume = ",format(area[1]))) +
  xlab("Distance from start of volume") +
  ylab("Area")
```

### 5.2.2 Differential expression analysis of RNA-Seq

```
Parts of the script were generated by Almut Lütge
##libraries
library("DESeq2")
library("biomaRt")
library("vsn")
library("RColorBrewer")
library("gplots")
library("ggplot2")
library("clusterProfiler")
library("pathview")

# DEseq2 package used for differential expression analysis
###define DE functions
##1.
#function to load raw count data and analyse by DESeq2 to find
differetially expressed genes
mydeseq <- function(counttable, condition){

  coldata <- data.frame(row.names = colnames(counttable), condition =
condition )
  countDS <- DESeqDataSetFromMatrix(countData = counttable, colData =
coldata, design = ~condition)

  dds <- DESeq(countDS)
  res <- results(dds)

  resordered <- res[order(res$padj),]
  dtab <- as.data.frame(resordered)
  desall <- list(deseqtable = dtab, deseq = dds, resordered =
resordered)
  return(desall)
}


##2.
#function to add further informations using BiomaRt
mybiomart <- function(deseqtable){
  ensembl <- useMart("ensembl", dataset = "hsapiens_gene_ensembl")
  selfilters <- c("ensembl_gene_id")
  attr <- c("ensembl_gene_id", "external_gene_name", "entrezgene",
"chromosome_name", "gene_biotype")
  #further interesting attributes: "go_id", "name_1006",
"definition_1006"
  val <- c(rownames(deseqtable))
  BMtable <- getBM(attributes = attr, filters = selfilters, values =
val, mart=ensembl)
  return(BMtable)
}


#function to merge all informations in one table
myresulttable <- function(deseqtable, BMtable, resfile){
  restable <- merge(deseqtable, BMtable, by.x = "row.names", by.y =
"ensembl_gene_id")
  write.table(restable, file = paste(resfile, "tsv", sep = "."), sep=
"\t", eol = "\r", row.names = F)
  return(restable)
}
```

```
#comparison DOPC vs CD95L

counttable <- read.table(file =
paste("/Users/schen/Documents/Data/Human tumor sequencing
project/GBM39_RNAseq_CD95L_beads_vs_DOPC_01_06_2013_Si/Raw_counts/raw
_count_renamed.txt", sep=""), header=T)

condition <- c(rep("DOPC", 3), rep("CD95L",3))

resfile <- paste("DOPC_vs_CD95L", sep ="")
desall <- mydeseq(counttable, condition)

BMtable <- mybiomart(desall$deseqtable)
resulttable <- myresulttable(desall$deseqtable, BMtable, resfile)
```

### 5.2.3 Principal component analysis and sample-to-sample heatmap of RNA-Seq

```
counttable <- read.table(file =
paste("/Users/schen/Documents/Data/Human tumor sequencing
project/GBM39_RNAseq_CD95L_beads_vs_DOPC_01_06_2013_Si/Raw_counts/raw
_count_renamed.txt", sep=""), header=T)
condition <- c(rep("DOPC", 3), rep("CD95L",3))

coldata <- data.frame(row.names = colnames(counttable), condition =
condition)
countDS <- DESeqDataSetFromMatrix(countData = counttable, colData =
coldata, design = ~condition)

dds <- DESeq(countDS)

# two types of transformation of the data for normalization
rld <- rlogTransformation(dds)
vsd <- varianceStabilizingTransformation(dds)

# generate png and pdf of PCA with rld transformed data
png("PCA_CD95L_rld.png")
pdf("PCA_CD95L_rld.pdf")
rldpca <- plotPCA(rld, intgroup=c("condition"), returnData=TRUE)
percentVar <- round(100 * attr(rldpca, "percentVar"))
ggplot(rldpca, aes(PC1, PC2, color=condition)) +
  geom_point(size=4) +
  xlab(paste0("PC1: ",percentVar[1],"% variance")) +
  ylab(paste0("PC2: ",percentVar[2],"% variance")) +
  scale_shape_manual(values=c(4,3,25,10,19,17,8))
dev.off()

# generate png and pdf of PCA with rld transformed data
png("PCA_CD95L_vsd.png")
pdf("PCA_CD95L_vsd.pdf")
vsdpca <- plotPCA(vsd, intgroup=c("condition"), returnData=TRUE)
percentVar <- round(100 * attr(vsdpca, "percentVar"))
ggplot(vsdpca, aes(PC1, PC2, color=condition)) +
  geom_point(size=4) +
  xlab(paste0("PC1: ",percentVar[1],"% variance")) +
  ylab(paste0("PC2: ",percentVar[2],"% variance")) +
  scale_shape_manual(values=c(4,3,25,10,19,17,8))
dev.off()

# generate sample-to-sample heatmap with rld transformed data
```

```
rldmat <- as.matrix(dist(t(assay(rld))))

# define colors
hmcol <- colorRampPalette(brewer.pal(9,"YlGnBu"))(100)

png("StoS_heatmap_CD95L_rld.png", w=1500, h=1500, pointsize=20)
heatmap.2(rldmat, trace = "none", col = rev(hmcol), margin =
c(17,17), main = "rlog")
dev.off()

pdf("StoS_heatmap_CD95L_rld.pdf")
heatmap.2(rldmat_2, trace = "none", col = rev(hmcol), margin =
c(18,18))
dev.off()
```

### 5.2.4 Heatmap generation of differentially expressed genes

```
#load data, GO categories of DE genes and tpm values
BVD <- read.table(file = paste("/Users/schen/Documents/Data/Human
tumor sequencing
project/GBM39_RNAseq_CD95L_beads_vs_DOPC_01_06_2013_Si/R_analysis/GO_
blood vessel development_genes_ensembl.txt", sep=""), header=F)
BVD_vector <- as.vector(BVD)
tpm <- read.table(file = paste("/Users/schen/Documents/Data/Human
tumor sequencing
project/GBM39_RNAseq_CD95L_beads_vs_DOPC_01_06_2013_Si/TPM/All_genes.
TPM_renamed.txt", sep=""), header=T)

#transform tpm values to log2(tpm+1)
log2_1_tpm <- log2(tpm[,1:6]+1)

#select genes that are in GO blood vessel development
log2_1_tpm_BVD <- subset(log2_1_tpm, rownames(log2_1_tpm) %in%
c("ENSG00000128917",
"ENSG00000112715",
"ENSG00000100292",
"ENSG00000214274",
"ENSG00000070495",
"ENSG00000204291",
"ENSG00000008710",
"ENSG00000198959",
"ENSG00000163235",
"ENSG00000119630",
"ENSG00000182492",
"ENSG00000099250",
"ENSG00000121966",
"ENSG00000158195",
"ENSG00000091879",
"ENSG00000167772",

"ENSG00000157483",
"ENSG00000187045",
"ENSG00000169429",
"ENSG00000078401",
"ENSG00000116016"))

#translate ensemble ID to gene symbol
rownames(log2_1_tpm_BVD) <- c("DLL4",
                              "VEGFA",
                              "HMOX1",
```

```
                                    "ANG",
                                    "JMJD6",
                                    "COL15A1",
                                    "PKD1",
                                    "TGM2",
                                    "TGFA",
                                    "PGF",
                                    "BGN",
                                    "NRP1",
                                    "CXCR4",
                                    "WASF2",
                                    "ANGPT2",
                                    "ANGPTL4",
                                    "MYO1E",
                                    "TMPRSS6",
                                    "IL8",
                                    "EDN1",
                                    "EPAS1")

#define colors
hmcol <- colorRampPalette(brewer.pal(9,"Oranges"))(100)


#generate heatmap
png("Heatmap_blood_vesseL_dev.png", w=2000, h=2000, pointsize=20)
heatmap.2(as.matrix(log2_1_tpm_BVD), dendrogram = "column", trace =
"none", col = hmcol, margin = c(20,20), cexRow=2, cexCol=1.8,
srtCol=45, scale="row", key=T, keysize=1)
dev.off()

pdf("Heatmap_blood_vesseL_dev.pdf")
heatmap.2(as.matrix(log2_1_tpm_BVD), dendrogram = "column", trace =
"none", col = hmcol, margin = c(15,15), cexRow=1, cexCol=0.8,
srtCol=45, scale="row", key=T, keysize=1)
dev.off()
```

## 6. References


Aarum, J., Sandberg, K., Haeberlein, S.L.B., and Persson, M.A.A. (2003). Migration and differentiation of neural precursor cells can be directed by microglia. Proc Natl Acad Sci USA *100*, 15983–15988.

Adams, R.H., and Eichmann, A. (2010). Axon Guidance Molecules in Vascular Patterning. Cold Spring Harbor Perspectives in Biology *2*, a001875–a001875.

Ajami, B., Bennett, J.L., Krieger, C., Tetzlaff, W., and Rossi, F.M.V. (2007). Local self-renewal can sustain CNS microglia maintenance and function throughout adult life. Nat Neurosci *10*, 1538–1543.

Al-Lamki, R.S., Bradley, J.R., and Pober, J.S. (2008). Endothelial Cells in Allograft Rejection. Transplantation *86*, 1340–1348.

Alderson, M.R., Armitage, R.J., Maraskovsky, E., Tough, T.W., Roux, E., Schooley, K., Ramsdell, F., and Lynch, D.H. (1993). Alderson_Lynch_1993_Fas Transduces Activation Signals in Normal Human T Lymphocytes. J Exp Med *178*, 2231–2235.

Alderson, M.R., Tough, T.W., Davis-Smith, T., Braddy, S., Falk, B., Schooley, K.A., Goodwin, R.G., Smith, C.A., Ramsdell, F., and Lynch, D.H. (1995). Fas ligand mediates activation-induced cell death in human T lymphocytes. J Exp Med *181*, 71–77.

Alliot, F., Godin, I., and Pessac, B. (1999). Microglia derive from progenitors, originating from the yolk sac, and which proliferate in the brain. Brain Res. Dev. Brain Res. *117*, 145–152.

Alva, J.A., Zovein, A.C., Monvoisin, A., Murphy, T., Salazar, A., Harvey, N.L., Carmeliet, P., and Iruela-Arispe, M.L. (2006). VE-Cadherin-Cre-recombinase transgenic mouse: A tool for lineage analysis and gene deletion in endothelial cells. Dev. Dyn. *235*, 759–767.

Aoudjit, F., and Vuori, K. (2001). Matrix Attachment Regulates Fas-induced Apoptosis in Endothelial Cells A Role for c-Flip and Implications for Anoikis. J Cell Biol *152*, 633–643.

Araujo, D.M., and Cotman, C.W. (1992). Basic FGF in astroglial, microglial, and neuronal cultures: characterization of binding sites and modulation of release by lymphokines and trophic factors. J Neurosci *12*, 1668–1678.

Arnaoutova, I., George, J., Kleinman, H.K., and Benton, G. (2009). The endothelial cell tube formation assay on basement membrane turns 20: state of the science and the art. Angiogenesis *12*, 267–274.

Arnold, T., and Betsholtz, C. (2013). The importance of microglia in the development of the vasculature in the central nervous system. Vascular Cell *5*, 1–1.

Arroyo, A.G., and Iruela-Arispe, M.L. (2010). Extracellular matrix, inflammation, and the angiogenic response. Cardiovascular Research *86*, 226–235.

Ashwell, K. (1990). Microglia and cell death in the developing mouse cerebellum. Brain Res. Dev. Brain Res. *55*, 219–230.

Azevedo, F.A.C., Carvalho, L.R.B., Grinberg, L.T., Farfel, J.M., Ferretti, R.E.L., Leite, R.E.P., Filho, W.J., Lent, R., and Herculano-Houzel, S. (2009). Equal numbers of neuronal

and nonneuronal cells make the human brain an isometrically scaled-up primate brain. J. Comp. Neurol. *513*, 532–541.

Badie, B., Schartner, J., Prabakaran, S., Paul, J., and Vorpahl, J. (2001). Expression of Fas ligand by microglia: possible role in glioma immune evasion. J. Neuroimmunol. 19–24.

Bajou, K., Peng, H., Laug, W.E., Maillard, C., Noel, A., Foidart, J.M., Martial, J.A., and DeClerck, Y.A. (2008). Plasminogen Activator Inhibitor-1 Protects Endothelial Cells from FasL-Mediated Apoptosis. Cancer Cell *14*, 324–334.

Bannerman, D.D., Tupper, J.C., Ricketts, W.A., Bennett, C.F., Winn, R.K., and Harlan, J.M. (2001). A Constitutive Cytoprotective Pathway Protects Endothelial Cells from Lipopolysaccharide-induced Apoptosis. J Biol Chem *276*, 14924–14932.

Barnhart, B.C., Legembre, P., Pietras, E., Bubici, C., Franzoso, G., and Peter, M.E. (2004). CD95 ligand induces motility and invasiveness of apoptosis-resistant tumor cells. Embo J. *23*, 3175–3185.

Barreiro, R., Schadlu, R., Herndon, J., Kaplan, H.J., and Ferguson, T.A. (2003). The Role of Fas-FasL in the Development and Treatment of Ischemic Retinopathy. Invest. Ophthalmol. Vis. Sci. *44*, 1282.

Beattie, E.C., Stellwagen, D., and Morishita, W. (2002). Control of synaptic strength by glial TNFα. Science (New York, N.Y.) *295*, 2282–2285.

Behin, A., Hoang-Xuan, K., Carpentier, A.F., and Delattre, J.-Y. (2003). Primary brain tumours in adults. The Lancet *361*, 323–331.

Bendszus, M., Debus, J., Wick, W., Kobyakov, G., Martens, T., Heese, O., Pichler, J., Stupp, R., Kunz, C., and Fricke, H. (2012). APG101_CD_002: A phase II, randomized, open-label, multicenter study of weekly APG101 plus reirradiation versus reirradiation in the treatment of patients with recurrent glioblastoma. ASCO Annual Meeting Abstract.

Berke, G. (1995). The CTL's kiss of death. Cell *81*, 9–12.

Berra, E., Pages, G., and Pouyssegur, J. (2000). MAP kinases and hypoxia in the control of VEGF expression. Cancer Metastasis Rev. *19*, 139–145.

Bessis, A., Béchade, C., Bernard, D., and Roumier, A. (2007). Microglial control of neuronal death and synaptic properties. Glia *55*, 233–238.

Bhattacharya, D., Singh, M.K., Chaudhuri, S., Datta, A., and Chaudhuri, S. (2016). T11TS Treatment Augments Apoptosis of Glioma Associated Brain Endothelial Cells, Hint towards Anti-Angiogenic Action in Glioma. J. Cell. Physiol. 1–14.

Biancone, L., De Martino, A., Orlandi, V., Conaldi, P.G., Toniolo, A., and Camussi, G. (1997). Development of inflammatory angiogenesis by local stimulation of Fas in vivo. J Exp Med *186*, 147–152.

Black, J.E., Isaacs, K.R., Anderson, B.J., Alcantara, A., and Greenough, T. (1990). Learning causes synaptogenesis, whereas motor activity causes angiogenesis, in cerebellar cortex of adult rats. pp. 5568–5572.

Bodmer, J.-L., Schneider, P., and Tschopp, J. (2002). The molecular architecture of the TNF

superfamily. Trends Biochem. Sci. *27*, 19–26.

Brandenburg, S., Müller, A., Turkowski, K., Radev, Y.T., Rot, S., Schmidt, C., Bungert, A.D., Acker, G., Schorr, A., Hippe, A., et al. (2015). Resident microglia rather than peripheral macrophages promote vascularization in brain tumors and are source of alternative pro-angiogenic factors. Acta Neuropathol. *131*, 365–378.

Breier, G., Albrecht, U., Sterrer, S., and Risau, W. (1992). Expression of vascular endothelial growth factor during embryonic angiogenesis and endothelial cell differentiation. Development *114*, 521–532.

Brem, S., Cotran, R., and Folkman, J. (1972). Tumor Angiogenesis: A Quantitative Method for Histologic Grading. JNCI Journal of the National Cancer Institute *48*, 347–356.

Brint, E., O'Callaghan, G., and Houston, A. (2013). Life in the Fas lane: differential outcomes of Fas signaling. Cell. Mol. Life Sci. *70*, 4085–4099.

Broughton, B.R.S., Reutens, D.C., and Sobey, C.G. (2009). Apoptotic Mechanisms After Cerebral Ischemia. Stroke *40*, e331–e339.

Brunner, T., Mogil, R.J., LaFace, D., Yoo, N.J., Mahboubi, A., Echeverri, F., Martin, S.J., Force, W.R., Lynch, D.H., and Ware, C.F. (1995). Cell-autonomous Fas (CD95)/Fas-ligand interaction mediates activation-induced apoptosis in T-cell hybridomas. Nature *373*, 441–444.

Calabrese, C., Poppleton, H., Kocak, M., Hogg, T.L., Fuller, C., Hamner, B., Oh, E.Y., Gaber, M.W., Finklestein, D., Allen, M., et al. (2007). A Perivascular Niche for Brain Tumor Stem Cells. Cancer Cell *11*, 69–82.

Calderó, J., Brunet, N., Ciutat, D., Hereu, M., and Esquerda, J.E. (2009). Development of microglia in the chick embryo spinal cord: Implications in the regulation of motoneuronal survival and death. J Neurosci Res *87*, 2447–2466.

Cardier, J.E., Schulte, T., Kammer, H., Kwak, J., and Cardier, M. (1999). Fas (CD95, APO-1) antigen expression and function in murine liver endothelial cells: implications for the regulation of apoptosis in liver endothelial cells. Faseb J. *13*, 1950–1960.

Carmeliet, P., and Jain, R.K. (2000). Angiogenesis in cancer and other diseases. Nature *407*, 249–257.

Carmeliet, P., and Jain, R.K. (2011). PERSPECTIVES. Nat Rev Drug Discov *10*, 1–11.

Carmeliet, P., and Tessier-Lavigne, M. (2005). Common mechanisms of nerve and blood vessel wiring. Nat Cell Biol *436*, 193–200.

Casano, A.M., and Peri, F. (2015). Microglia: multitasking specialists of the brain. Developmental Cell *32*, 469–477.

Casano, A.M., Albert, M., and Peri, F. (2016). Developmental Apoptosis Mediates Entry and Positioning of Microglia in the Zebrafish Brain. Cell Reports *16*, 897–906.

Cavallaro, U., and Dejana, E. (2011). Adhesion molecule signalling: not always a sticky business. Nat Rev Mol Cell Biol *12*, 189–197.

Chamak, B., Morandi, V., and Mallat, M. (1994). Brain macrophages stimulate neurite growth and regeneration by secreting thrombospondin. J Neurosci Res *38*, 221–233.

Checchin, D., Sennlaub, F., Levavasseur, E., Leduc, M., and Chemtob, S. (2006). Potential role of microglia in retinal blood vessel formation. Invest. Ophthalmol. Vis. Sci. *47*, 3595–3602.

Cheema, Z.F., Cheema, Z.F., Wade, S.B., Wade, S.B., Sata, M., Sata, M., Walsh, K., Walsh, K., Sohrabji, F., Sohrabji, F., et al. (1999). Fas/Apo [apoptosis]-1 and associated proteins in the differentiating cerebral cortex: induction of caspase-dependent cell death and activation of NF-kappaB. J Neurosci *19*, 1754–1770.

Chen, L., Park, S.-M., Tumanov, A.V., Hau, A., Sawada, K., Feig, C., Turner, J.R., Fu, Y.-X., Romero, I.L., Lengyel, E., et al. (2010a). CD95 promotes tumour growth. Nature *465*, 492–496.

Chen, S.-K., Tvrdik, P., Peden, E., Cho, S., Wu, Sen, Spangrude, G., and Capecchi, M.R. (2010b). Hematopoietic Origin of Pathological Grooming in Hoxb8 Mutant Mice. Cell *141*, 775–785.

Cheng, P.-L., and Poo, M.-M. (2012). Early Events in Axon/Dendrite Polarization. Annu. Rev. Neurosci. *35*, 181–201.

Chinot, O.L., Wick, W., Mason, W., Henriksson, R., Saran, F., Nishikawa, R., Carpentier, A.F., Hoang-Xuan, K., Kavan, P., Cernea, D., et al. (2014). Bevacizumab plus Radiotherapy–Temozolomide for Newly Diagnosed Glioblastoma. N Engl J Med *370*, 709–722.

Choi, C., Xu, X., Oh, J.W., Lee, S.J., Gillespie, G.Y., Park, H., Jo, H., and Benveniste, E.N. (2001). Fas-induced expression of chemokines in human glioma cells: involvement of extracellular signal-regulated kinase 1/2 and p38 mitogen-activated protein kinase. Cancer Research *61*, 3084–3091.

Choi, C., Gillespie, G.Y., Van Wagoner, N.J., and Benveniste, E.N. (2002). Fas engagement increases expression of interleukin-6 in human glioma cells. J. Neurooncol. *56*, 13–19.

Clausen, B.E., Burkhardt, C., Reith, W., Renkawitz, R., and Förster, I. (1999). Conditional gene targeting in macrophages and granulocytes using LysMcre mice. Transgenic Res. *8*, 265–277.

Corsini, N.S., and Martin-Villalba, A. (2010). Integrin Alpha 6:Anchors Away for Glioma Stem Cells. Cell Stem Cell *6*, 403–404.

Corsini, N.S., Corsini, N.S., Sancho-Martinez, I., Sancho-Martinez, I., Laudenklos, S., Laudenklos, S., Glagow, D., Glagow, D., Kumar, S., Kumar, S., et al. (2009). The death receptor CD95 activates adult neural stem cells for working memory formation and brain repair. Cell Stem Cell *5*, 178–190.

Cuadros, M.A., and Navascués, J. (1998). The origin and differentiation of microglial cells during development. Progress in Neurobiology *56*, 173–189.

Cuadros, M.A., Martin, C., Coltey, P., Almendros, A., and Navascués, J. (1993). First appearance, distribution, and origin of macrophages in the early development of the avian central nervous system. J. Comp. Neurol. *330*, 113–129.

Cuadros, M.A., Moujahid, A., Martin-Partido, G., and Navascués, J. (1992). Microglia in the mature and developing quail brain as revealed by a monoclonal antibody recognizing hemopoietic cells. Neuroscience Letters *148*, 11–14.

Cubelos, B., Sebastián-Serrano, A., Beccari, L., Calcagnotto, M.E., Cisneros, E., Kim, S., Dopazo, A., Alvarez-Dolado, M., Redondo, J.M., Bovolenta, P., et al. (2010). Cux1 and Cux2 Regulate Dendritic Branching, Spine Morphology, and Synapses of the Upper Layer Neurons of the Cortex. Neuron *66*, 523–535.

Cunningham, C.L., Martínez-Cerdeño, V., and Noctor, S.C. (2013). Microglia regulate the number of neural precursor cells in the developing cerebral cortex. J Neurosci *33*, 4216–4233.

Dalmau, I., Finsen, B., Tønder, N., Zimmer, J., González, B., and Castellano, B. (1997). Development of microglia in the prenatal rat hippocampus. J. Comp. Neurol. *377*, 70–84.

Damon, D.H., teRiele, J.A., and Marko, S.B. (2007). Vascular-derived artemin: a determinant of vascular sympathetic innervation? AJP: Heart and Circulatory Physiology *293*, H266–H273.

Daneman, R., Agalliu, D., Zhou, L., Kuhnert, F., Kuo, C.J., and Barres, B.A. (2009). Wnt/beta-catenin signaling is required for CNS, but not non-CNS, angiogenesis. Proc Natl Acad Sci USA *106*, 641–646.

Davalos, D., Grutzendler, J., Yang, G., Kim, J.V., Zuo, Y., Jung, S., Littman, D.R., Dustin, M.L., and Gan, W.-B. (2005). ATP mediates rapid microglial response to local brain injury in vivo. Nat Neurosci *8*, 752–758.

Davies, M.H., Eubanks, J.P., and Powers, M.R. (2003). Increased Retinal Neovascularization in Fas Ligand–Deficient Mice. Invest. Ophthalmol. Vis. Sci. *44*, 3202.

De Smet, F., Segura, I., De Bock, K., Hohensinner, P.J., and Carmeliet, P. (2009). Mechanisms of Vessel Branching: Filopodia on Endothelial Tip Cells Lead the Way. Arteriosclerosis, Thrombosis, and Vascular Biology *29*, 639–649.

Demjen, D., Klussmann, S., Kleber, S., Zuliani, C., Stieltjes, B., Metzger, C., Hirt, U.A., Walczak, H., Falk, W., Essig, M., et al. (2004). Neutralization of CD95 ligand promotes regeneration and functional recovery after spinal cord injury. Nat Med *10*, 389–395.

Desbarats, J., and Newell, M.K. (2000). Fas engagement accelerates liver regeneration after partial hepatectomy. Nat Med *6*, 920–923.

Desbarats, J., Wade, T., and Wade, W.F. (1999). Dichotomy between naive and memory CD4+ T cell responses to Fas engagement. pp. 8104–8109.

Desbarats, J., Birge, R.B., Mimouni-Rongy, M., Weinstein, D.E., Palerme, J.-S., and Newell, M.K. (2003). Fas engagement induces neurite growth through ERK activation and p35 upregulation. Nat Cell Biol *5*, 118–125.

Dickens, L.S., Boyd, R.S., Jukes-Jones, R., Hughes, M.A., Robinson, G.L., Fairall, L., Schwabe, J.W.R., Cain, K., and MacFarlane, M. (2012). A Death Effector Domain Chain DISC Model Reveals a Crucial Role for Caspase-8 Chain Assembly in Mediating Apoptotic Cell Death. Molecular Cell *47*, 291–305.

Dobin, A., Davis, C.A., Schlesinger, F., Drenkow, J., Zaleski, C., Jha, S., Batut, P.,

Chaisson, M., and Gingeras, T.R. (2012). STAR: ultrafast universal RNA-seq aligner. Bioinformatics *29*, 15–21.

Drachman, D.A. (2005). Do we have brain to spare? Neurology *64*, 2004–2005.

Drachsler, M., Kleber, S., Mateos, A., Volk, K., Mohr, N., Chen, S., Cirovic, B., ttenberg, J.T.U., Gieffers, C., Sykora, J., et al. (2016). CD95 maintains stem cell-like and non-classical EMT programs in primary human glioblastoma cells. Cell Death and Disease *7*, e2209–e2211.

Dunn, G.P., Rinne, M.L., Wykosky, J., Genovese, G., Quayle, S.N., Dunn, I.F., Agarwalla, P.K., Chheda, M.G., Campos, B., Wang, A., et al. (2012). Emerging insights into the molecular and cellular basis of glioblastoma. Genes & Development *26*, 756–784.

Eble, J.A., and Niland, S. (2009). The extracellular matrix of blood vessels. Curr. Pharm. Des. *15*, 1385–1400.

Eichmann, A., and Thomas, J.L. (2013). Molecular Parallels between Neural and Vascular Development. Cold Spring Harbor Perspectives in Medicine *3*, a006551–a006551.

Eilken, H.M., and Adams, R.H. (2010). Dynamics of endothelial cell behavior in sprouting angiogenesis. Current Opinion in Cell Biology *22*, 617–625.

Eliceiri, B.P., Paul, R., Schwartzberg, P.L., Hood, J.D., Leng, J., and Cheresh, D.A. (1999). Selective requirement for Src kinases during VEGF-induced angiogenesis and vascular permeability. Molecular Cell *4*, 915–924.

Erskine, L., Reijntjes, S., Pratt, T., Denti, L., Schwarz, Q., Vieira, J.M., Alakakone, B., Shewan, D., and Ruhrberg, C. (2011). VEGF Signaling through Neuropilin 1 Guides Commissural Axon Crossing at the Optic Chiasm. Neuron *70*, 951–965.

Fantin, A., Vieira, J.M., Gestri, G., Denti, L., Schwarz, Q., Prykhozhij, S., Peri, F., Wilson, S.W., and Ruhrberg, C. (2010). Tissue macrophages act as cellular chaperones for vascular anastomosis downstream of VEGF-mediated endothelial tip cell induction. Blood *116*, 829–840.

Fantin, A., Vieira, J.M., Plein, A., Maden, C.H., and Ruhrberg, C. (2013). The embryonic mouse hindbrain as a qualitative andquantitative model for studying the molecular andcellular mechanisms of angiogenesis. Nature Protocols *8*, 418–429.

Fidler, I.J., Yano, S., Zhang, R.-D., Fujimaki, T., and Bucana, C.D. (2002). The seed and soil hypothesis: vascularisation and brain metastases. Lancet Oncol. *3*, 53–57.

Flamme, I., Frölich, T., and Risau, W. (1997). Molecular mechanisms of vasculogenesis and embryonic angiogenesis. J. Cell. Physiol. *173*, 206–210.

Folkman, J. (1971). Tumor angiogenesis: therapeutic implications. N Engl J Med *285*, 1182–1186.

Folkman, J. (1972). Anti-angiogenesis: new concept for therapy of solid tumors. Ann. Surg. *175*, 409–416.

Frankel, B., Longo, S.L., and Ryken, T.C. (1999). Co-expression of Fas and Fas ligand in human non-astrocytic glial tumors. Acta Neuropathol. *98*, 363–366.

Freiberg, R.A., Spencer, D.M., Choate, K.A., Duh, H.J., Schreiber, S.L., Crabtree, G.R., and Khavari, P.A. (1997). Fas Signal Transduction Triggers Either Proliferation. Journal of Investigative Dermatology *108*, 215–219.

French, L.E., French, L.E., Hahne, M., Hahne, M., Viard, I., Viard, I., Radlgruber, G., Radlgruber, G., Zanone, R., Zanone, R., et al. (1996). Fas and Fas ligand in embryos and adult mice: ligand expression in several immune-privileged tissues and coexpression in adult tissues characterized by apoptotic cell turnover. J Cell Biol *133*, 335–343.

Fruttiger, M. (2007). Development of the retinal vasculature. Angiogenesis *10*, 77–88.

Fukumura, D., Xu, L., Chen, Y., Gohongi, T., Seed, B., and Jain, R.K. (2001). Hypoxia and acidosis independently up-regulate vascular endothelial growth factor transcription in brain tumors in vivo. Cancer Research *61*, 6020–6024.

Furnari, F.B., Fenton, T., Bachoo, R.M., Mukasa, A., Stommel, J.M., Stegh, A., Hahn, W.C., Ligon, K.L., Louis, D.N., Brennan, C., et al. (2007). Malignant astrocytic glioma: genetics, biology, and paths to treatment. Genes & Development *21*, 2683–2710.

Gaudillière, B., Konishi, Y., la Iglesia, de, N., Yao, G.L., and Bonni, A. (2004). A CaMKII-NeuroD signaling pathway specifies dendritic morphogenesis. Neuron *41*, 229–241.

Gerber, H.P., McMurtrey, A., Kowalski, J., Yan, M., Keyt, B.A., Dixit, V., and Ferrara, N. (1998). Vascular endothelial growth factor regulates endothelial cell survival through the phosphatidylinositol 3'-kinase/Akt signal transduction pathway. Requirement for Flk-1/KDR activation. J Biol Chem *273*, 30336–30343.

Gerhardt, H., Golding, M., Fruttiger, M., Ruhrberg, C., Lundkvist, A., Abramsson, A., Jeltsch, M., Mitchell, C., Alitalo, K., Shima, D., et al. (2003). VEGF guides angiogenic sprouting utilizing endothelial tip cell filopodia. J Cell Biol *161*, 1163–1177.

Gilbert, M.R., Dignam, J.J., Armstrong, T.S., Wefel, J.S., Blumenthal, D.T., Vogelbaum, M.A., Colman, H., Chakravarti, A., Pugh, S., Won, M., et al. (2014). A Randomized Trial of Bevacizumab for Newly Diagnosed Glioblastoma. N Engl J Med *370*, 699–708.

Ginhoux, F., Greter, M., Leboeuf, M., Nandi, S., See, P., Gokhan, S., Mehler, M.F., Conway, S.J., Ng, L.G., R, S.E., et al. (2010). Fate mapping analysis reveals that adult microglia derive from primitive macrophages. Science (New York, N.Y.) *330*, 841–845.

Goldmann, T., Wieghofer, P., Müller, P.F., Wolf, Y., Varol, D., Yona, S., Brendecke, S.M., Kierdorf, K., Staszewski, O., Datta, M., et al. (2013). A new type of microglia gene targeting shows TAK1 to be pivotal in CNS autoimmune inflammation. Nat Neurosci *16*, 1618–1626.

Götz, M., and Barde, Y.-A. (2005). Radial Glial Cells. Neuron *46*, 369–372.

Gratas, C., Tohma, Y., Van Meir, E.G., Klein, M., Tenan, M., Ishii, N., Tachibana, O., Kleihues, P., and Ohgaki, H. (1997). Fas ligand expression in glioblastoma cell lines and primary astrocytic brain tumors. Brain Pathol. *7*, 863–869.

Greenberg, D.A., and Jin, K. (2005). From angiogenesis to neuropathology. Nat Cell Biol *438*, 954–959.

Gregory, M.S., Hackett, C.G., Abernathy, E.F., Lee, K.S., Saff, R.R., Hohlbaum, A.M., Moody, K.-S.L., Hobson, M.W., Jones, A., Kolovou, P., et al. (2011). Opposing Roles for

Membrane Bound and Soluble Fas Ligand in Glaucoma-Associated Retinal Ganglion Cell Death. PLoS ONE *6*, e17659.

Greig, L.C., Woodworth, M.B., Galazo, M.J., Padmanabhan, H., and Macklis, J.D. (2013). Molecular logic of neocortical projection neuron specification, development and diversity. Nat Rev Neurosci *14*, 755–769.

Griffith, T.S., Yu, X., Herndon, J.M., Green, D.R., and Ferguson, T.A. (1996). CD95-induced apoptosis of lymphocytes in an immune privileged site induces immunological tolerance. Immunity.

Grossmann, R., Stence, N., Carr, J., Fuller, L., Waite, M., and Dailey, M.E. (2002). Juxtavascular microglia migrate along brain microvessels following activation during early postnatal development. Glia *37*, 229–240.

Guo, P., Hu, B., Gu, W., Xu, L., Wang, D., Huang, H.-J.S., Cavenee, W.K., and Cheng, S.-Y. (2010). Platelet-Derived Growth Factor-B Enhances Glioma Angiogenesis by Stimulating Vascular Endothelial Growth Factor Expression in Tumor Endothelia and by Promoting Pericyte Recruitment. The American Journal of Pathology *162*, 1083–1093.

Hadji, A., Ceppi, P., Murmann, A.E., Brockway, S., Pattanayak, A., Bhinder, B., Hau, A., De Chant, S., Parimi, V., Kolesza, P., et al. (2014). Death induced by CD95 or CD95 ligand elimination. Cell Reports *7*, 208–222.

Hanayama, R., Tanaka, M., Miwa, K., Shinohara, A., Iwamatsu, A., and Nagata, S. (2002). Identification of a factor that links apoptotic cells to phagocytes. Nature *417*, 182–187.

Hao, Z., Hampel, B., Yagita, H., and Rajewsky, K. (2004). T Cell–specific Ablation of Fas Leads to Fas Ligand–mediated Lymphocyte Depletion and Inflammatory Pulmonary Fibrosis. J Exp Med *199*, 1355–1365.

Harb, R., Whiteus, C., Freitas, C., and Grutzendler, J. (2012). In vivo imaging of cerebral microvascular plasticity from birth to death. Journal of Cerebral Blood Flow &Amp; Metabolism *33*, 146–156.

Hardee, M.E., and Zagzag, D. (2012). Mechanisms of Glioma-Associated Neovascularization. The American Journal of Pathology *181*, 1126–1141.

Harik, N., Harik, S.I., Kuo, N.T., Sakai, K., Przybylski, R.J., and LaManna, J.C. (1996). Time-course and reversibility of the hypoxia-induced alterations in cerebral vascularity and cerebral capillary glucose transporter density. Brain Res. *737*, 335–338.

Hatanaka, Y., and Murakami, F. (2002). In vitro analysis of the origin, migratory behavior, and maturation of cortical pyramidal cells. J. Comp. Neurol. *454*, 1–14.

Hayashi, S., and McMahon, A.P. (2002). Efficient Recombination in Diverse Tissues by a Tamoxifen-Inducible Form of Cre: A Tool for Temporally Regulated Gene Activation/Inactivation in the Mouse. Developmental Biology *244*, 305–318.

Herbert, S.P., and Stainier, D.Y.R. (2011). Molecular control of endothelialcell behaviour during blood vesselmorphogenesis. Nat Rev Mol Cell Biol *12*, 551–564.

Herbomel, P., Thisse, B., and Thisse, C. (2001). Zebrafish Early Macrophages Colonize Cephalic Mesenchyme and Developing Brain, Retina, and Epidermis through a M-CSF

Receptor-Dependent Invasive Process. Developmental Biology *238*, 274–288.

Hers, I., Vincent, E.E., and Tavaré, J.M. (2011). Cellular Signalling. Cellular Signalling *23*, 1515–1527.

Higashi, A.Y., Ikawa, T., Muramatsu, M., Economides, A.N., Niwa, A., Okuda, T., Murphy, A.J., Rojas, J., Heike, T., Nakahata, T., et al. (2009). Direct Hematological Toxicity and Illegitimate Chromosomal Recombination Caused by the Systemic Activation of CreERT2. The Journal of Immunology *182*, 5633–5640.

Hobbs, S.K., Monsky, W.L., Yuan, F., Roberts, W.G., Griffith, L., Torchilin, V.P., and Jain, R.K. (1998). Regulation of transport pathways in tumor vessels: role of tumor type and microenvironment. Proc Natl Acad Sci USA *95*, 4607–4612.

Hogan, K.A. (2004). The neural tube patterns vessels developmentally using the VEGF signaling pathway. Development *131*, 1503–1513.

Holash, J., Maisonpierre, P.C., Compton, D., Boland, P., Alexander, C.R., Zagzag, D., Yancopoulos, G.D., and Wiegand, S.J. (1999). Vessel cooption, regression, and growth in tumors mediated by angiopoietins and VEGF. Science (New York, N.Y.) *284*, 1994–1998.

Hood, J.D., Frausto, R., Kiosses, W.B., Schwartz, M.A., and Cheresh, D.A. (2003). Differential αv integrin–mediated Ras-ERK signaling during two pathways of angiogenesis. J Cell Biol *162*, 933–943.

Huang, D.W., Sherman, B.T., and Lempicki, R.A. (2008). Systematic and integrative analysis of large gene lists using DAVID bioinformatics resources. Nature Protocols *4*, 44–57.

Igney, F.H., and Krammer, P.H. (2002). Death and anti-death: tumour resistance to apoptosis. Nat. Rev. Cancer *2*, 277–288.

Innocenti, G.M., Clarke, S., and Koppel, H. (1983). Transitory macrophages in the white matter of the developing visual cortex. II. Development and relations with axonal pathways. Developmental Brain Research *11*, 55–66.

Irmler, M., Thome, M., Hahne, M., Schneider, P., Hofmann, K., Steiner, V., Bodmer, J.L., Schröter, M., Burns, K., Mattmann, C., et al. (1997). Inhibition of death receptor signals by cellular FLIP. Nature *388*, 190–195.

Ishida, S., Yamashiro, K., Usui, T., Kaji, Y., Ogura, Y., Hida, T., Honda, Y., Oguchi, Y., and Adamis, A.P. (2003). Leukocytes mediate retinal vascular remodeling during development and vaso-obliteration in disease. Nat Med *9*, 781–788.

Iwata, T., and Hevner, R.F. (2009). Fibroblast growth factor signaling in development of the cerebral cortex. Development, Growth & Differentiation *51*, 299–323.

Jain, R.K. (2003). Molecular regulation of vessel maturation. Nat Med *9*, 685–693.

Jemal, A., Siegel, R., Ward, E., Hao, Y., Xu, J., and Thun, M.J. (2009). Cancer Statistics, 2009. CA: a Cancer Journal for Clinicians *59*, 225–249.

Jiang, B.H., Zheng, J.Z., and Aoki, M. (2000). Phosphatidylinositol 3-kinase signaling mediates angiogenesis and expression of vascular endothelial growth factor in endothelial cells. pp. 1749–1753.

Jiang, H., Guo, W., Liang, X., and Rao, Y. (2005). Both the Establishment and the Maintenance of Neuronal Polarity Require Active Mechanisms. Cell *120*, 123–135.

Jonakait, G.M., Wen, Y., Wan, Y., and Ni, L. (2000). Macrophage cell-conditioned medium promotes cholinergic differentiation of undifferentiated progenitors and synergizes with nerve growth factor action in the developing basal forebrain. Exp Neurol *161*, 285–296.

Kaindl, T., Rieger, H., Kaschel, L.-M., Engel, U., Schmaus, A., Sleeman, J., and Tanaka, M. (2012). Spatio-Temporal Patterns of Pancreatic Cancer Cells Expressing CD44 Isoforms on Supported Membranes Displaying Hyaluronic Acid Oligomers Arrays. PLoS ONE *7*, e42991.

Kanamori, T., Kanai, M.I., Dairyo, Y., and Yasunaga, K. (2013). Compartmentalized calcium transients trigger dendrite pruning in Drosophila sensory neurons. Science (New York, N.Y.) *240*, 1475–1478.

Kaplan, H.J., Leibole, M.A., Tezel, T., and Ferguson, T.A. (1999). Fas ligand (CD95 ligand) controls angiogenesis beneath the retina. Nat Med *5*, 292–297.

Karray, S., Kress, C., Cuvellier, S., Hue-Beauvais, C., Damotte, D., Babinet, C., and Levi-Strauss, M. (2004). Complete Loss of Fas Ligand Gene Causes Massive Lymphoproliferation and Early Death, Indicating a Residual Activity of gld Allele. The Journal of Immunology *172*, 2118–2125.

Kayagaki, N., Kawasaki, A., and Ebata, T. (1995). Metalloproteinase-mediated release of human Fas ligand. J Exp Med *182*, 1777–1783.

Kern, W., and Puotinen, D.A. (1970). Cleaning solutions based on hydrogen peroxide for use in silicon semiconductor technology. RCA Rev *31*, 187–206.

Kettenmann, H., Hanisch, U.K., Noda, M., and Verkhratsky, A. (2011). Physiology of Microglia. Physiological Reviews *91*, 461–553.

Kierdorf, K., Erny, D., Goldmann, T., Sander, V., Schulz, C., Perdiguero, E.G., Wieghofer, P., Heinrich, A., Riemke, P., Hölscher, C., et al. (2013). Microglia emerge from erythromyeloid precursors via Pu.1- and Irf8-dependent pathways. Nat Neurosci *16*, 273–280.

Kim, A.H., Puram, S.V., Bilimoria, P.M., Ikeuchi, Y., Keough, S., Wong, M., Rowitch, D., and Bonni, A. (2009). A Centrosomal Cdc20-APC Pathway Controls Dendrite Morphogenesisin Postmitotic Neurons. Cell *136*, 322–336.

Kim, Y.T., Hur, E.-M., Snider, W.D., and Zhou, F.-Q. (2011). Role of GSK3 Signaling in Neuronal Morphogenesis. Front Mol Neurosci *4*, 48.

Kischkel, F.C., Hellbardt, S., Behrmann, I., Germer, M., Pawlita, M., Krammer, P.H., and Peter, M.E. (1995). Cytotoxicity-dependent APO-1 (Fas/CD95)-associated proteins form a death-inducing signaling complex (DISC) with the receptor. Embo J. *14*, 5579–5588.

Kleber, S., Sancho-Martinez, I., Wiestler, B., Beisel, A., Gieffers, C., Hill, O., Thiemann, M., Mueller, W., Sykora, J., Kuhn, A., et al. (2008). Yes and PI3K Bind CD95 to Signal Invasion of Glioblastoma. Cancer Cell *13*, 235–248.

Klint, P., Kanda, S., Kloog, Y., and Claesson-Welsh, L. (1999). Contribution of Src and Ras

pathways in FGF-2 induced endothelial cell differentiation. Oncogene *18*, 3354–3364.

Kong, Y. (2011). Btrim: A fast, lightweight adapter and quality trimming program for next-generation sequencing technologies. Genomics *98*, 152–153.

Koushik, S.V., Wang, J., Rogers, R., Moskophidis, D., Lambert, N.A., Creazzo, T.L., and Conway, S.J. (2001). Targeted inactivation of the sodium-calcium exchanger (Ncx1) results in the lack of a heartbeat and abnormal myofibrillar organization. The FASEB Journal *15*, 1209–1211.

Kriegstein, A., and Alvarez-Buylla, A. (2009). The Glial Nature of Embryonic and Adult Neural Stem Cells. Annu. Rev. Neurosci. *32*, 149–184.

Kubota, Y., Takubo, K., Shimizu, T., Ohno, H., Kishi, K., Shibuya, M., Saya, H., and Suda, T. (2009). M-CSF inhibition selectively targets pathological angiogenesis and lymphangiogenesis. J Exp Med *206*, 1089–1102.

Kuhnert, F., Mancuso, M.R., Shamloo, A., Wang, H.T., Choksi, V., Florek, M., Su, H., Fruttiger, M., Young, W.L., Heilshorn, S.C., et al. (2010). Essential Regulation of CNS Angiogenesis by the Orphan G Protein-Coupled Receptor GPR124. Science (New York, N.Y.) *330*, 985–989.

Kuida, K., Haydar, T.F., Kuan, C.Y., Gu, Y., Taya, C., Karasuyama, H., Su, M.S., Rakic, P., and Flavell, R.A. (1998). Reduced apoptosis and cytochrome c-mediated caspase activation in mice lacking caspase 9. Cell *94*, 325–337.

Kurz, H., and Christ, B. (1998). Embryonic CNS macrophages and microglia do not stem from circulating, but from extravascular precursors. Glia *22*, 98–102.

la Rosa, de, E.J., and de Pablo, F. (2000). Cell death in early neural development: beyond the neurotrophic theory. Trends Neurosci *23*, 454–458.

Lacoste, B., Comin, C.H., Ben-Zvi, A., Kaeser, P.S., Xu, X., Costa, L.D.F., and Gu, C. (2014). Sensory-Related Neural Activity Regulates the Structure of Vascular Networks in the Cerebral Cortex. Neuron *83*, 1117–1130.

Lai, Y.J., Lin, V.T.G., Zheng, Y., Benveniste, E.N., and Lin, F.T. (2010). The Adaptor Protein TRIP6 Antagonizes Fas-Induced Apoptosis but Promotes Its Effect on Cell Migration. Mol Cell Biol *30*, 5582–5596.

Lamalice, L., Houle, F., Jourdan, G., and Huot, J. (2004). Phosphorylation of tyrosine 1214 on VEGFR2 is required for VEGF-induced activation of Cdc42 upstream of SAPK2/p38. Oncogene *23*, 434–445.

Lassmann, H., Zimprich, F., Vass, K., and Hickey, W.F. (1991). Microglial cells are a component of the perivascular glia limitans. J Neurosci Res *28*, 236–243.

Lavrik, I.N., and Krammer, P.H. (2011). Regulation of CD95/Fas signaling at the DISC. Cell Death and Differentiation *19*, 36–41.

Lavrik, I.N., Golks, A., Riess, D., Bentele, M., Eils, R., and Krammer, P.H. (2007). Analysis of CD95 threshold signaling: triggering of CD95 (FAS/APO-1) at low concentrations primarily results in survival signaling. J Biol Chem *282*, 13664–13671.

Le Boeuf, F., Houle, F., and Huot, J. (2004). Regulation of Vascular Endothelial Growth Factor Receptor 2-mediated Phosphorylation of Focal Adhesion Kinase by Heat Shock Protein 90 and Src Kinase Activities. J Biol Chem *279*, 39175–39185.

Le-Niculescu, H., Bonfoco, E., Kasuya, Y., Claret, F.X., Green, D.R., and Karin, M. (1999). Withdrawal of survival factors results in activation of the JNK pathway in neuronal cells leading to Fas ligand induction and cell death. Mol Cell Biol *19*, 751–763.

Letellier, E., Kumar, S., Sancho-Martinez, I., Krauth, S., Funke-Kaiser, A., Laudenklos, S., Konecki, K., Klussmann, S., Corsini, N.S., Kleber, S., et al. (2010). CD95-Ligand on Peripheral Myeloid Cells Activates Syk Kinase to Trigger Their Recruitment to the Inflammatory Site. Immunity *32*, 240–252.

Li, B., and Dewey, C.N. (2011). RSEM: accurate transcript quantification from RNA-Seq data with or without a reference genome. BMC Bioinformatics *12*, 323.

Li, M., and Ransohoff, R.M. (2009). The roles of chemokine CXCL12 in embryonic and brain tumor angiogenesis. Seminars in Cancer Biology *19*, 111–115.

Li, N., Zhao, C.-T., Wang, Y., and Yuan, X.-B. (2010). The Transcription Factor Cux1 Regulates Dendritic Morphology of Cortical Pyramidal Neurons. PLoS ONE *5*, e10596.

Limaye, V., Li, X., Hahn, C., Xia, P., Berndt, M.C., Vadas, M.A., and Gamble, J.R. (2005). Sphingosine kinase-1 enhances endothelial cell survival through a PECAM-1-dependent activation of PI-3K/Akt and regulation of Bcl-2 family members. Blood *105*, 3169–3177.

Lindahl, P., Johansson, B.R., Levéen, P., and Betsholtz, C. (1997). Pericyte loss and microaneurysm formation in PDGF-B-deficient mice. Science (New York, N.Y.) *277*, 242–245.

Llambi, F., Causeret, F., and Gallego, E.B. (2001). Netrin-1 acts as a survival factor via its receptors UNC5H and DCC. Embo J. *20*, 2715–2722.

Locksley, R.M., Killeen, N., and Lenardo, M.J. (2001). The TNF and TNF receptor superfamilies: integrating mammalian biology. Cell *104*, 487–501.

Louis, D.N., Perry, A., Reifenberger, G., Deimling, A., Figarella-Branger, D., Cavenee, W.K., Ohgaki, H., Wiestler, O.D., Kleihues, P., and Ellison, D.W. (2016). The 2016 World Health Organization Classi cation of Tumors of the Central Nervous System: a summary. Acta Neuropathol. *131*, 803–820.

Love, M.I., Huber, W., and Anders, S. (2014). Moderated estimation of fold change and dispersion for RNA-seq data with DESeq2. Genome Biology *15*.

Lowell, C.A. (2011). Src-family and Syk Kinases in Activating and Inhibitory Pathways in Innate Immune Cells: Signaling Cross Talk. Cold Spring Harbor Perspectives in Biology *3*, a002352–a002352.

Lowin, B., Hahne, M., Mattmann, C., and Tschopp, J. (1994). Cytolytic T-cell cytotoxicity is mediated through perforin and Fas lytic pathways. Nature *370*, 650–652.

Lu, X., Le Noble, F., Yuan, L., Jiang, Q., and De Lafarge, B. (2004). The netrin receptor UNC5B mediates guidance events controlling morphogenesis of the vascular system. Nature *432*, 179–186.

Lucin, K.M., and Wyss-Coray, T. (2009). Immune Activation in Brain Aging and Neurodegeneration: Too Much or Too Little? Neuron *64*, 110–122.

Lui, H., Zhang, J., Makinson, S.R., Cahill, M.K., Kelley, K.W., Huang, H.-Y., Shang, Y., Oldham, M.C., Martens, L.H., Gao, F., et al. (2016). Progranulin Deficiency Promotes Circuit-Specific Synaptic Pruning by Microglia via Complement Activation. Cell *165*, 921–935.

Luo, L., Hensch, T.K., Ackerman, L., Barbel, S., Jan, L.Y., and Jan, Y.N. (1996). Differential effects of the Rac GTPase on Purkinje cell axons and dendritic trunks and spines. Nature *379*, 837–840.

Lyck, L., Santamaria, I.D., Pakkenberg, B., Chemnitz, J., Schrøder, H.D., Finsen, B., and Gundersen, H.J.G. (2009). An empirical analysis of the precision of estimating the numbers of neurons and glia in human neocortex using a fractionator-design with sub-sampling. Journal of Neuroscience Methods *182*, 143–156.

Ma, S., Kwon, H.J., and Huang, Z. (2012). A Functional Requirement for Astroglia in Promoting Blood Vessel Development in the Early Postnatal Brain. PLoS ONE *7*, e48001.

Makita, T., Sucov, H.M., Gariepy, C.E., Yanagisawa, M., and Ginty, D.D. (2008). Endothelins are vascular-derived axonal guidance cues for developing sympathetic neurons. Nature *452*, 759–763.

Mancuso, M.R., Kuhnert, F., and Kuo, C.J. (2008). Developmental Angiogenesis of the Central Nervous System. Lymphatic Research and Biology *6*, 173–180.

Martin-Villalba, A., Llorens-Bobadilla, E., and Wollny, D. (2013). CD95 in cancer: tool or target? Trends Mol Med *19*, 329–335.

Marx, P., Mulder, A.B., Van Den Bergh, F., Haanen, O.C., and Vermes, I. (1999). Apoptosis inducers endotoxin and Fas-ligation enhance the expression of vascular endothelial growth factor in human endothelial cells. Endothelium *6*, 335–340.

Matsumoto, H., Murakami, Y., Kataoka, K., Notomi, S., Mantopoulos, D., Trichonas, G., Miller, J.W., Gregory, M.S., Ksander, B.R., Marshak-Rothstein, A., et al. (2015). Membrane-bound and soluble Fas ligands have opposite functions in photoreceptor cell death following separation from the retinal pigment epithelium. Cell Death and Disease *6*, e1986–e1989.

Matsumoto, T., and Mugishima, H. (2006). Signal transduction via vascular endothelial growth factor (VEGF) receptors and their roles in atherogenesis. J. Atheroscler. Thromb. *13*, 130–135.

McAllister, A.K. (2000). Cellular and molecular mechanisms of dendrite growth. Cereb. Cortex *10*, 963–973.

McCarty, J.H. (2004). Selective ablation of  v integrins in the central nervous system leads to cerebral hemorrhage, seizures, axonal degeneration and premature death. Development *132*, 165–176.

McKay, M.M., and Morrison, D.K. (2007). Integrating signals from RTKs to ERK/MAPK. Oncogene *26*, 3113–3121.

Meyer, C., and Köhn, M. (2011). Efficient Scaled-Up Synthesis of N-α-Fmoc-4-Phosphono(difluoromethyl)-l-phenylalanine and Its Incorporation into Peptides. Synthesis *2011*, 3255–3260.

Michaelson, M.D., Bieri, P.L., Mehler, M.F., Xu, H., Arezzo, J.C., Pollard, J.W., and Kessler, J.A. (1996). CSF-1 deficiency in mice results in abnormal brain development. Development *122*, 2661–2672.

Milde, F., Lauw, S., Koumoutsakos, P., and Iruela-Arispe, M.L. (2013). The mouse retina in 3D: quantification of vascular growth and remodeling. Integr. Biol. *5*, 1426.

Mildner, A., Schmidt, H., Nitsche, M., Merkler, D., Hanisch, U.-K., Mack, M., Heikenwalder, M., Brück, W., Priller, J., and Prinz, M. (2007). Microglia in the adult brain arise from Ly-6ChiCCR2+ monocytes only under defined host conditions. Nat Neurosci *10*, 1544–1553.

Monier, A., Adle-Biassette, H., Delezoide, A.-L., Evrard, P., Gressens, P., and Verney, C. (2007). Entry and distribution of microglial cells in human embryonic and fetal cerebral cortex. J. Neuropathol. Exp. Neurol. *66*, 372–382.

Morgan, S.C., Taylor, D.L., and Pocock, J.M. (2004). Microglia release activators of neuronal proliferation mediated by activation of mitogen-activated protein kinase, phosphatidylinositol-3-kinase/Akt and delta-Notch signalling cascades. J Neurochem *90*, 89–101.

Motz, G.T., Santoro, S.P., Wang, L.-P., Garrabrant, T., Lastra, R.R., Hagemann, I.S., Lal, P., Feldman, M.D., Benencia, F., and Coukos, G. (2014). Tumor endothelium FasL establishes a selective immune barrier promoting tolerance in tumors. Nat Med *20*, 607–615.

Moya, I.M., Umans, L., Maas, E., Pereira, P.N.G., Beets, K., Francis, A., Sents, W., Robertson, E.J., Mummery, C.L., Huylebroeck, D., et al. (2012). Stalk Cell Phenotype Depends on Integration of Notch and Smad1/5 Signaling Cascades. Developmental Cell *22*, 501–514.

Nagata, K., Nakajima, K., Takemoto, N., Saito, H., and Kohsaka, S. (1993). Microglia-derived plasminogen enhances neurite outgrowth from explant cultures of rat brain. Int. J. Dev. Neurosci. *11*, 227–237.

Nagata, S. (1997). Apoptosis by death factor. Cell *88*, 355–365.

Nakajima, K., Honda, S., Tohyama, Y., Imai, Y., Kohsaka, S., and Kurihara, T. (2001). Neurotrophin secretion from cultured microglia. J Neurosci Res *65*, 322–331.

Nakayama, A.Y., Harms, M.B., and Luo, L. (2000). Small GTPases Rac and Rho in the maintenance of dendritic spines and branches in hippocampal pyramidal neurons. J Neurosci *20*, 5329–5338.

Nayak, D., Roth, T.L., and McGavern, D.B. (2014). Microglia development and function. Annu. Rev. Immunol. *32*, 367–402.

Nimmerjahn, A., Kirchhoff, F., and Helmchen, F. (2005). Resting microglial cells are highly dynamic surveillants of brain parenchyma in vivo. Science (New York, N.Y.) *308*, 1314–1318.

O' Reilly, L.A., O' Reilly, L.A., Tai, L., Tai, L., Lee, L., Lee, L., Kruse, E.A., Kruse, E.A.,

Grabow, S., Grabow, S., et al. (2009). Membrane-bound Fas ligand only is essential for Fas-induced apoptosis. Nature *461*, 659–663.

Ogasawara, J., Watanabe-Fukunaga, R., Adachi, M., Matsuzawa, A., Kasugai, T., Kitamura, Y., Itoh, N., Suda, T., and Nagata, S. (1993). Lethal effect of the anti-Fas antibody in mice. Nature *364*, 806–809.

Okabe, K., Kobayashi, S., Yamada, T., Kurihara, T., Tai-Nagara, I., Miyamoto, T., Mukouyama, Y.-S., Sato, T.N., Suda, T., Ema, M., et al. (2014). Neurons Limit Angiogenesis by Titrating VEGF in Retina. Cell *159*, 584–596.

Oppenheim, R.W. (1991). Cell death during development of the nervous system. Annu. Rev. Neurosci. *14*, 453–501.

Orłowski, D., Sołtys, Z., and Janeczko, K. (2003). Morphological development of microglia in the postnatal rat brain. International Journal of Developmental Neuroscience *21*, 445–450.

Osterberg, N., Ferrara, N., Vacher, J., Gaedicke, S., Niedermann, G., Weyerbrock, A., Doostkam, S., Schaefer, H.-E., Plate, K.H., and Machein, M.R. (2016). Decrease of VEGF-A in myeloid cells attenuates glioma progression and prolongs survival in an experimental glioma model. Neuro-Oncology *18*, 939–949.

Paez-Ribes, M., Allen, E., Hudock, J., Takeda, T., Okuyama, H., ViNals, F., Inoue, M., Bergers, G., Hanahan, D., and Casanovas, O. (2009). Antiangiogenic Therapy ElicitsMalignant Progression of Tumorsto Increased Local Invasion and Distant Metastasis. Cancer Cell *15*, 220–231.

Paolicelli, R.C., Bolasco, G., Pagani, F., Maggi, L., Scianni, M., Panzanelli, P., Giustetto, M., Ferreira, T.A., Guiducci, E., Dumas, L., et al. (2011). Synaptic pruning by microglia is necessary for normal brain development. Science (New York, NY) *333*, 1456–1458.

Paridaen, J.T., and Huttner, W.B. (2014). Neurogenesis during development of the vertebrate central nervous system. EMBO Reports *15*, 351–364.

Park, C., Park, C., Sakamaki, K., Sakamaki, K., Tachibana, O., Tachibana, O., Yamashima, T., Yamashima, T., Yamashita, J., Yamashita, J., et al. (1998). Expression of fas antigen in the normal mouse brain. Biochem Biophys Res Commun *252*, 623–628.

Pelvig, D.P., Pakkenberg, H., Stark, A.K., and Pakkenberg, B. (2008). Neocortical glial cell numbers in human brains. Neurobiology of Aging *29*, 1754–1762.

Perdiguero, E.G., Klapproth, K., Schulz, C., Busch, K., Azzoni, E., Crozet, L., Garner, H., Trouillet, C., de Bruijn, M.F., Geissmann, F., et al. (2015). Tissue-resident macrophages originate from yolk-sac-derived erythro-myeloid progenitors. Nature *518*, 547–551.

Peri, F., and Nüsslein-Volhard, C. (2008). Live imaging of neuronal degradation by microglia reveals a role for v0-ATPase a1 in phagosomal fusion in vivo. Cell *133*, 916–927.

Peter, M.E., and Krammer, P.H. (2003). The CD95(APO-1/Fas) DISC and beyond. Cell Death and Differentiation *10*, 26–35.

Peter, M.E., Hadji, A., Murmann, A.E., Brockway, S., Putzbach, W., Pattanayak, A., and Ceppi, P. (2015). The role of CD95 and CD95 ligand in cancer. *22*, 549–559.

Pfenninger, C.V., Roschupkina, T., Hertwig, F., Kottwitz, D., Englund, E., Bengzon, J., Jacobsen, S.E., and Nuber, U.A. (2007). CD133 Is Not Present on Neurogenic Astrocytes in the Adult Subventricular Zone, but on Embryonic Neural Stem Cells, Ependymal Cells, and Glioblastoma Cells. Cancer Research *67*, 5727–5736.

Phng, L.K., and Gerhardt, H. (2009). Angiogenesis: A Team Effort Coordinated by Notch. Developmental Cell *16*, 196–208.

Pitulescu, M.E., Schmidt, I., Benedito, R., and Adams, R.H. (2010). Inducible gene targeting in the neonatal vasculatureand analysis of retinal angiogenesis in mice. Nature Protocols *5*, 1518–1534.

Polleux, F., Morrow, T., and Ghosh, A. (2000). Semaphorin 3A is a chemoattractant for cortical apical dendrites. Nature 567–573.

Pont-Lezica, L., Beumer, W., Colasse, S., Drexhage, H., Versnel, M., and Bessis, A. (2014). Microglia shape corpus callosum axon tract fasciculation: functional impact of prenatal inflammation. Eur. J. Neurosci. *39*, 1551–1557.

Pont-Lezica, L., Béchade, C., Belarif-Cantaut, Y., Pascual, O., and Bessis, A. (2011). Physiological roles of microglia during development. J Neurochem *119*, 901–908.

Porter, K., Komiyama, N.H., Vitalis, T., Kind, P.C., and Grant, S.G.N. (2005). Differential expression of two NMDA receptor interacting proteins, PSD-95 and SynGAP during mouse development. European Journal of Neuroscience *21*, 351–362.

Potente, M., Gerhardt, H., and Carmeliet, P. (2011). Basic and Therapeutic Aspects of Angiogenesis. Cell *146*, 873–887.

Proctor, J.M. (2005). Vascular Development of the Brain Requires  8 Integrin Expression in the Neuroepithelium. Journal of Neuroscience *25*, 9940–9948.

Puram, S.V., and Bonni, A. (2013). Cell-intrinsic drivers of dendrite morphogenesis. Development *140*, 4657–4671.

Quaegebeur, A., Lange, C., and Carmeliet, P. (2011). The Neurovascular Link in Health and Disease: Molecular Mechanisms and Therapeutic Implications. Neuron *71*, 406–424.

Raab, S., Beck, H., Gaumann, A., Yüce, A., Gerber, H.-P., Plate, K., Hammes, H.-P., Ferrara, N., and Breier, G. (2004). Impaired brain angiogenesis and neuronal apoptosis induced by conditional homozygous inactivation of vascular endothelial growth factor. Thromb. Haemost. *91*, 595–605.

Rama, N., Dubrac, A., Mathivet, T., Ní Chárthaigh, R.-A., Genet, G., Cristofaro, B., Pibouin-Fragner, L., Ma, L., Eichmann, A., and Chédotal, A. (2015). Slit2 signaling through Robo1 and Robo2 is required for retinal neovascularization. Nat Med *21*, 483–491.

Reinehr, R., Sommerfeld, A., and Häussinger, D. (2008). CD95 Ligand Is a Proliferative and Antiapoptotic Signal in Quiescent Hepatic Stellate Cells. Gastroenterology *134*, 1494–1506.e1497.

Ricci-Vitiani, L., Pallini, R., Biffoni, M., Todaro, M., Invernici, G., Cenci, T., Maira, G., Parati, E.A., Stassi, G., Larocca, L.M., et al. (2010). Tumour vascularization via endothelial differentiation of glioblastoma stem-like cells. Nature *468*, 824–828.

Richardson, B.C., Lalwani, N.D., Johnson, K.J., and Marks, R.M. (1994). Fas ligation triggers apoptosis in macrophages but not endothelial cells. Eur. J. Immunol. *24*, 2640–2645.

Riffkin, C.D., Gray, A.Z., Hawkins, C.J., Chow, C.W., and Ashley, D.M. (2001). Ex vivo pediatric brain tumors express Fas (CD95) and FasL (CD95L) and are resistant to apoptosis induction. Neuro-Oncology *3*, 229–240.

Rigato, C., Buckinx, R., Le-Corronc, H., Rigo, J.M., and Legendre, P. (2011). Pattern of invasion of the embryonic mouse spinal cord by microglial cells at the time of the onset of functional neuronal networks. Glia *59*, 675–695.

Robson, A., Allinson, K.R., Anderson, R.H., Henderson, D.J., and Arthur, H.M. (2010). The TGFβ type II receptor plays a critical role in the endothelial cells during cardiac development. Dev. Dyn. *239*, 2435–2442.

Rossig, L., Jadidi, A.S., Urbich, C., Badorff, C., Zeiher, A.M., and Dimmeler, S. (2001). Akt-Dependent Phosphorylation of p21Cip1 Regulates PCNA Binding and Proliferation of Endothelial Cells. Mol Cell Biol *21*, 5644–5657.

Ruan, W., Lee, C.T., and Desbarats, J. (2008). A novel juxtamembrane domain in tumor necrosis factor receptor superfamily molecules activates Rac1 and controls neurite growth. Mol Biol Cell *19*, 3192–3202.

Ruhrberg, C., and Bautch, V.L. (2013). Neurovascular development and links to disease. Cell. Mol. Life Sci. *70*, 1675–1684.

Rui, Y., Myers, K.R., Yu, K., Wise, A., De Blas, A.L., Hartzell, H.C., and Zheng, J.Q. (1AD). Activity-dependent regulation of dendritic growth and maintenance by glycogen synthase kinase 3. Nature Communications *4*, 1–13.

Ruiz de Almodovar, C., Coulon, C., Salin, P.A., Knevels, E., Chounlamountri, N., Poesen, K., Hermans, K., Lambrechts, D., Van Geyte, K., Dhondt, J., et al. (2010). Matrix-Binding Vascular Endothelial Growth Factor (VEGF) Isoforms Guide Granule Cell Migration in the Cerebellum via VEGF Receptor Flk1. J Neurosci *30*, 15052–15066.

Ruiz de Almodovar, C., Lambrechts, D., Mazzone, M., and Carmeliet, P. (2009). Role and Therapeutic Potential of VEGF in the Nervous System. Physiological Reviews *89*, 607–648.

Rymo, S.F., Gerhardt, H., Wolfhagen Sand, F., Lang, R., Uv, A., and Betsholtz, C. (2011). A two-way communication between microglial cells and angiogenic sprouts regulates angiogenesis in aortic ring cultures. PLoS ONE *6*, e15846.

Sainson, R.C.A., Johnston, D.A., Chu, H.C., Holderfield, M.T., Nakatsu, M.N., Crampton, S.P., Davis, J., Conn, E., and Hughes, C.C.W. (2008). TNF primes endothelial cells for angiogenic sprouting by inducing a tip cell phenotype. Blood *111*, 4997–5007.

Sakić, B., Szechtman, H., Denburg, J.A., Gorny, G., Kolb, B., and Whishaw, I.Q. (1998). Progressive atrophy of pyramidal neuron dendrites in autoimmune MRL-lpr mice. J. Neuroimmunol. *87*, 162–170.

Sakić, B., Szechtman, H., Keffer, M., and Talangbayan, H. (1992). A behavioral profile of autoimmune lupus-prone MRL mice. Brain *6*, 265–285.

Sakić, B., Szechtman, H., Talangbayan, H., Denburg, S., Carbotte, R., and Denburg, J.A.

(1994). Behavior and immune status of MRL mice in the postweaning period. Brain Behavior and Immunity *8*, 1–13.

Salmaggi, A., Eoli, M., Frigerio, S., Silvani, A., Gelati, M., Corsini, E., Broggi, G., and Boiardi, A. (2003). Intracavitary VEGF, bFGF, IL-8, IL-12 levels in primary and recurrent malignant glioma. J. Neurooncol. *62*, 297–303.

Sancho-Martinez, I., and Martin-Villalba, A. (2009). Tyrosine phosphorylation and CD95: a FAScinating switch. Cell Cycle *8*, 838–842.

Santos, A.M., Calvente, R., Tassi, M., Carrasco, M.-C., Martín-Oliva, D., Marín-Teva, J.L., Navascués, J., and Cuadros, M.A. (2008). Embryonic and postnatal development of microglial cells in the mouse retina. J. Comp. Neurol. *506*, 224–239.

Sata, M., and Walsh, K. (1998). TNFalpha regulation of Fas ligand expression on the vascular endothelium modulates leukocyte extravasation. Nat Med *4*, 415–420.

Sata, M., Suhara, T., and Walsh, K. (2000). Vascular Endothelial Cells and Smooth Muscle Cells Differ in Expression of Fas and Fas Ligand and in Sensitivity to Fas Ligand-Induced Cell Death : Implications for Vascular Disease and Therapy. Arteriosclerosis, Thrombosis, and Vascular Biology *20*, 309–316.

Sánchez-López, A., Cuadros, M.A., Calvente, R., Tassi, M., Marín-Teva, J.L., and Navascués, J. (2004). Radial migration of developing microglial cells in quail retina: A confocal microscopy study. Glia *46*, 261–273.

Schafer, D.P., Lehrman, E.K., and Stevens, B. (2012). The "quad-partite" synapse: Microglia-synapse interactions in the developing and mature CNS. Glia *61*, 24–36.

Schlegelmilch, T., Henke, K., and Peri, F. (2011). Microglia in the developing brain: from immunity to behaviour. Curr. Opin. Neurobiol. *21*, 5–10.

Schleich, K., Warnken, U., Fricker, N., Öztürk, S., Richter, P., Kammerer, K., Schnölzer, M., Krammer, P.H., and Lavrik, I.N. (2012). Stoichiometry of the CD95 Death-Inducing Signaling Complex: Experimental and Modeling Evidence for a Death Effector Domain Chain Model. Molecular Cell *47*, 306–319.

Schlottmann, K.E., Gulbins, E., Lau, S.M., and Coggeshall, K.M. (1996). Activation of Src-family tyrosine kinases during Fas-induced apoptosis. J. Leukoc. Biol. *60*, 546–554.

Schmidt, N.O., Westphal, M., and Hagel, C. (1999). Levels of vascular endothelial growth factor, hepatocyte growth factor/scatter factor and basic fibroblast growth factor in human gliomas and their relation to …. Intl J Cancer *84*, 10–18.

Schulz, C., Perdiguero, E.G., and Chorro, L. (2012). A lineage of myeloid cells independent of Myb and hematopoietic stem cells. Science (New York, N.Y.) *336*, 86–90.

Scott, A., Powner, M.B., Gandhi, P., Clarkin, C., Gutmann, D.H., Johnson, R.S., Ferrara, N., and Fruttiger, M. (2010). Astrocyte-Derived Vascular Endothelial Growth Factor Stabilizes Vessels in the Developing Retinal Vasculature. PLoS ONE *5*, e11863.

Scott, E.K., and Luo, L. (2001). How do dendrites take their shape? Nat Neurosci *4*, 359–365.

Scott, F.L., Stec, B., Pop, C., Dobaczewska, M.K., Lee, J.J., Monosov, E., Robinson, H., Salvesen, G.S., Schwarzenbacher, R., and Riedl, S.J. (2009). FADD death domain complex structure unravels signalling by receptor clustering. Nature *457*, 1019–1022.

Segura, I., De Smet, F., Hohensinner, P.J., Almodovar, C.R. de, and Carmeliet, P. (2009). The neurovascular link in health and disease: an update. Trends Mol Med *15*, 439–451.

Shelly, M., Lim, B.K., Cancedda, L., Heilshorn, S.C., Gao, H., and Poo, M. (2011a). Local and long-range reciprocal regulation of cAMP and cGMP in axon/dendrite formation. Science (New York, N.Y.) *327*, 547–552.

Shelly, M., Cancedda, L., Lim, B.K., Popescu, A.T., Cheng, P.-L., Gao, H., and Poo, M.-M. (2011b). Semaphorin3A Regulates Neuronal Polarization by Suppressing Axon Formation and Promoting Dendrite Growth. Neuron *71*, 433–446.

Shen, Q., Goderie, S.K., Jin, L., Karanth, N., and Sun, Y. (2004). Endothelial cells stimulate self-renewal and expand neurogenesis of neural stem cells. Science (New York, N.Y.) *304*, 1338–1340.

Shin, D.H., Lee, E., Kim, H.J., Kim, S., Cho, S.S., Chang, K.Y., and Lee, W.J. (2002). Fas ligand mRNA expression in the mouse central nervous system. J. Neuroimmunol. *123*, 50–57.

Sierra, A., Encinas, J.M., Deudero, J.J.P., Chancey, J.H., Enikolopov, G., Overstreet-Wadiche, L.S., Tsirka, S.E., and Maletic-Savatic, M. (2010). Microglia Shape Adult Hippocampal Neurogenesis through Apoptosis-Coupled Phagocytosis. Cell Stem Cell *7*, 483–495.

Silverman, W.F., Krum, J.M., Mani, N., and Rosenstein, J.M. (1999). Vascular, glial and neuronal effects of vascular endothelial growth factor in mesencephalic explant cultures. Neuroscience *90*, 1529–1541.

Soda, Y., Myskiw, C., Rommel, A., and Verma, I.M. (2013). Mechanisms of neovascularization and resistance to anti-angiogenic therapies in glioblastoma multiforme. J Mol Med *91*, 439–448.

Somanath, P.R., Razorenova, O.V., Chen, J., and Byzova, T.V. (2006). Akt1 in endothelial cell and angiogenesis. Cell Cycle *5*, 512–518.

Sondell, M., Lundborg, G., and Kanje, M. (1999). Vascular endothelial growth factor has neurotrophic activity and stimulates axonal outgrowth, enhancing cell survival and Schwann cell proliferation in the peripheral nervous system. Journal of Neuroscience *19*, 5731–5740.

Sorensen, I., Adams, R.H., and Gossler, A. (2009). DLL1-mediated Notch activation regulates endothelial identity in mouse fetal arteries. Blood *113*, 5680–5688.

Sorokin, S.P., McNelly, N.A., and Hoyt, R.F. (1992). Macrophage development: IV. Effects of blood factors on macrophages from prenatal rat lung cultures. Anat. Rec. *233*, 415–428.

Sridurongrit, S., Larsson, J., Schwartz, R., Ruiz-Lozano, P., and Kaartinen, V. (2008). Signaling via the Tgf-β type I receptor Alk5 in heart development. Developmental Biology *322*, 208–218.

Srinivasan, R., Zabuawala, T., Huang, H., Zhang, J., Gulati, P., Fernandez, S., Karlo, J.C., Landreth, G.E., Leone, G., and Ostrowski, M.C. (2009). Erk1 and Erk2 Regulate

Endothelial Cell Proliferation and Migration during Mouse Embryonic Angiogenesis. PLoS ONE *4*, e8283.

Stence, N., Waite, M., and Dailey, M.E. (2001). Dynamics of microglial activation: A confocal time-lapse analysis in hippocampal slices. Glia *33*, 256–266.

Stenman, J.M., Rajagopal, J., Carroll, T.J., and Ishibashi, M. (2008). Canonical Wnt signaling regulates organ-specific assembly and differentiation of CNS vasculature. Sceince *322*, 1247–1250.

Stevens, B., Allen, N.J., Vazquez, L.E., Howell, G.R., Christopherson, K.S., Nouri, N., Micheva, K.D., Mehalow, A.K., Huberman, A.D., Stafford, B., et al. (2007). The Classical Complement Cascade Mediates CNS Synapse Elimination. Cell *131*, 1164–1178.

Stiles, J., and Jernigan, T.L. (2010). The Basics of Brain Development. Neuropsychol Rev *20*, 327–348.

Strilic, B., Kučera, T., Eglinger, J., Hughes, M.R., McNagny, K.M., Tsukita, S., Dejana, E., Ferrara, N., and Lammert, E. (2009). The Molecular Basis of Vascular Lumen Formation in the Developing Mouse Aorta. Developmental Cell *17*, 505–515.

Stubbs, D., DeProto, J., Nie, K., Englund, C., Mahmud, I., Hevner, R., and Molnar, Z. (2009). Neurovascular Congruence during Cerebral Cortical Development. Cerebral Cortex *19*, i32–i41.

Stupp, R., Mason, W.P., Van Den Bent, M.J., Weller, M., Fisher, B., Taphoorn, M.J.B., Belanger, K., Brandes, A.A., Marosi, C., Bogdahn, U., et al. (2005). Radiotherapy plus concomitant and adjuvant temozolomide for glioblastoma. N Engl J Med *325*, 987–996.

Suhara, T., Mano, T., Oliveira, B.E., and Walsh, K. (2001). Phosphatidylinositol 3-Kinase/Akt Signaling Controls Endothelial Cell Sensitivity to Fas-Mediated Apoptosis via Regulation of FLICE-Inhibitory Protein (FLIP). Circulation Research *89*, 13–19.

Szechtman, H., Sakić, B., and Denburg, J.A. (1997). Behaviour of MRL mice: an animal model of disturbed behaviour in systemic autoimmune disease. Lupus *6*, 223–229.

Tachibana, O., Lampe, J., Kleihues, P., and Ohgaki, H. (1996). Preferential expression of Fas/APO1 (CD95) and apoptotic cell death in perinecrotic cells of glioblastoma multiforme. Acta Neuropathol. *92*, 431–434.

Takahashi, T., Tanaka, M., Brannan, C.I., Jenkins, N.A., Copeland, N.G., Suda, T., and Nagata, S. (1994). Generalized lymphoproliferative disease in mice, caused by a point mutation in the Fas ligand. Cell *76*, 969–976.

Takemura, Y., Fukuo, K., Yasuda, O., Inoue, T., Inomata, N., Yokoi, T., Kawamoto, H., Suhara, T., and Ogihara, T. (2004). Fas Signaling Induces Akt Activation and Upregulation of Endothelial Nitric Oxide Synthase Expression. Hypertension *43*, 880–884.

Tanaka, M., Itai, T., Adachi, M., and Nagata, S. (1998). Downregulation of Fas ligand by shedding. Nat Med *4*, 31–36.

Tessier-Lavigne, M., and Goodman, C.S. (1996). The molecular biology of axon guidance. Science (New York, N.Y.) *274*, 1123–1133.

Thakker, G.D., Hajjar, D.P., Muller, W.A., and Rosengart, T.K. (1999). The role of phosphatidylinositol 3-kinase in vascular endothelial growth factor signaling. J Biol Chem *274*, 10002–10007.

Trauth, B.C., Klas, C., Peters, A.M., Matzku, S., Moller, P., Falk, W., Debatin, K.M., and Krammer, P.H. (1989). Monoclonal antibody-mediated tumor regression by induction of apoptosis. Science (New York, N.Y.) *245*, 301–305.

Tremblay, M.-È., Lowery, R.L., and Majewska, A.K. (2010). Microglial Interactions with Synapses Are Modulated by Visual Experience. PLoS Biol *8*, e1000527.

Ueno, M., Fujita, Y., Tanaka, T., Nakamura, Y., Kikuta, J., Ishii, M., and Yamashita, T. (2013). Layer V cortical neurons require microglial support for survival during postnatal development. Nature Publishing Group *16*, 543–551.

Vallon, M., Chang, J., Zhang, H., and Kuo, C.J. (2014). Developmental and pathological angiogenesis in the central nervous system. Cell. Mol. Life Sci. *71*, 3489–3506.

Valnegri, P., Puram, S.V., and Bonni, A. (2015). Regulation of dendrite morphogenesis by extrinsic cues. Trends Neurosci *38*, 439–447.

Vasudevan, A., and Bhide, P.G. (2014). Angiogenesis in the embryonic CNS. Cell Adhesion & Migration *2*, 167–169.

Verney, C., Monier, A., Fallet-Bianco, C., and Gressens, P. (2010). Early microglial colonization of the human forebrain and possible involvement in periventricular white-matter injury of preterm infants. Journal of Anatomy *217*, 436–448.

Volpert, O.V., Zaichuk, T., Zhou, W., Reiher, F., Ferguson, T.A., Stuart, P.M., Amin, M., and Bouck, N.P. (2002). Inducer-stimulated Fas targets activated endothelium for destruction by anti-angiogenic thrombospondin-1 and pigment epithelium-derived factor. Nat Med *8*, 349–357.

Vredenburgh, J.J., Desjardins, A., Herndon, J.E., Dowell, J.M., Reardon, D.A., Quinn, J.A., Rich, J.N., Sathornsumetee, S., Gururangan, S., Wagner, M., et al. (2007). Phase II Trial of Bevacizumab and Irinotecan in Recurrent Malignant Glioma. Clinical Cancer Research *13*, 1253–1259.

Wake, H., Moorhouse, A.J., Jinno, S., Kohsaka, S., and Nabekura, J. (2009). Resting Microglia Directly Monitor the Functional State of Synapses In Vivo and Determine the Fate of Ischemic Terminals. J Neurosci *29*, 3974–3980.

Wakselman, S., Bechade, C., Roumier, A., Bernard, D., Triller, A., and Bessis, A. (2008). Developmental Neuronal Death in Hippocampus Requires the Microglial CD11b Integrin and DAP12 Immunoreceptor. J Neurosci *28*, 8138–8143.

Wang, R., Chadalavada, K., Wilshire, J., Kowalik, U., Hovinga, K.E., Geber, A., Fligelman, B., Leversha, M., Brennan, C., and Tabar, V. (2010). Glioblastoma stem-like cells give rise to tumour endothelium. Nature *468*, 829–833.

Wang, X., Sterne, G.R., and Ye, B. (2014). Regulatory mechanisms underlying the differential growth of dendrites and axons. Neurosci. Bull. *30*, 557–568.

Watanabe-Fukunaga, R., Watanabe-Fukunaga, R., Brannan, C.I., Brannan, C.I., Itoh, N.,

Itoh, N., Yonehara, S., Yonehara, S., Copeland, N.G., Copeland, N.G., et al. (1992). The cDNA structure, expression, and chromosomal assignment of the mouse Fas antigen. J Immunol *148*, 1274–1279.

Weis, S.M., and Cheresh, D.A. (2011). Tumor angiogenesis: molecular pathways and therapeutic targets. Nat Med *17*, 1359–1370.

Weller, M., Frei, K., Groscurth, P., Krammer, P.H., Yonekawa, Y., and Fontana, A. (1994). Anti-Fas/APO-1 antibody-mediated apoptosis of cultured human glioma cells. Induction and modulation of sensitivity by cytokines. J. Clin. Invest. *94*, 954–964.

Winkler, F., Kozin, S.V., Tong, R.T., Chae, S.-S., Booth, M.F., Garkavtsev, I., Xu, L., Hicklin, D.J., Fukumura, D., di Tomaso, E., et al. (2004). Kinetics of vascular normalization by VEGFR2 blockade governs brain tumor response to radiation: role of oxygenation, angiopoietin-1, and matrix metalloproteinases. Cancer Cell *6*, 553–563.

Winter, C.G., Wang, B., Ballew, A., Royou, A., Karess, R., Axelrod, J.D., and Luo, L. (2001). Drosophila Rho-associated kinase (Drok) links Frizzled-mediated planar cell polarity signaling to the actin cytoskeleton. Cell *105*, 81–91.

Wojtowicz, W.M., Flanagan, J.J., Millard, S.S., Zipursky, S.L., and Clemens, J.C. (2004). Alternative splicing of Drosophila Dscam generates axon guidance receptors that exhibit isoform-specific homophilic binding. Cell *118*, 619–633.

Wong, B.R., Besser, D., Kim, N., Arron, J.R., Vologodskaia, M., Hanafusa, H., and Choi, Y. (1999). TRANCE, a TNF family member, activates Akt/PKB through a signaling complex involving TRAF6 and c-Src. Molecular Cell *4*, 1041–1049.

Yamagata, T., Muroya, K., Mukasa, T., Igarashi, H., Momoi, M., Tsukahara, T., Arahata, K., Kumagai, H., and Momoi, T. (1995). Hepatocyte growth factor specifically expressed in microglia activated Ras in the neurons, similar to the action of neurotrophic factors. Biochem Biophys Res Commun *210*, 231–237.

Yonehara, S., Ishii, A.I., and Yonehara, M. (1989). A cell-killing monoclonal antibody (anti-Fas) to a cell surface antigen co-downregulated with the receptor of tumor necrosis factor. J Exp Med *169*, 1747–1756.

Yoshimura, T., Kawano, Y., Arimura, N., Kawabata, S., Kikuchi, A., and Kaibuchi, K. (2005). GSK-3β Regulates Phosphorylation of CRMP-2 and Neuronal Polarity. Cell *120*, 137–149.

Yue, W.Y. (2005). Does Vasculogenic Mimicry Exist in Astrocytoma? Journal of Histochemistry and Cytochemistry *53*, 997–1002.

Yurchenko, M., Shlapatska, L.M., and Sidorenko, S.P. (2012). The multilevel regulation of CD95 signaling outcome. Exp. Oncol. *34*, 153–159.

Zacchigna, S., Almodovar, C.R. de, and Carmeliet, P. (2007). Similarities Between Angiogenesis and Neural Development: What Small Animal Models Can Tell Us. *80*, 1–55.

Zagzag, D., Amirnovin, R., Greco, M.A., Yee, H., Holash, J., Wiegand, S.J., Zabski, S., Yancopoulos, G.D., and Grumet, M. (2000). Vascular apoptosis and involution in gliomas precede neovascularization: a novel concept for glioma growth and angiogenesis. Lab. Invest. *80*, 837–849.

Zeeb, M., Strilic, B., and Lammert, E. (2010). Resolving cell. Current Opinion in Cell Biology *22*, 626–632.

Zhan, Y., Paolicelli, R.C., Sforazzini, F., Weinhard, L., Bolasco, G., Pagani, F., Vyssotski, A.L., Bifone, A., Gozzi, A., Ragozzino, D., et al. (2014). Deficient neuron-microglia signaling results in impaired functional brain connectivity and social behavior. Nat Neurosci *17*, 400–406.

Zhang, S.C., and Fedoroff, S. (1996). Neuron-microglia interactions in vitro. Acta Neuropathol. *91*, 385–395.

Zhong, Y., Zhou, L.-J., Ren, W.-J., Xin, W.-J., Li, Y.-Y., Zhang, T., and Liu, X.-G. (2010). Brain, Behavior, and Immunity. Brain Behavior and Immunity *24*, 874–880.

Zuliani, C., Kleber, S., Klussmann, S., Wenger, T., Kenzelmann, M., Schreglmann, N., Martinez, A., del Rio, J.A., Soriano, E., Vodrazka, P., et al. (2006). Control of neuronal branching by the death receptor CD95 (Fas/Apo-1). Cell Death and Differentiation *13*, 31–40.